The Dynamics and Mass Budget of Arctic Glaciers

Extended abstracts

**Workshop and GLACIODYN (IPY) meeting,
29 - 31 January 2008, Obergurgl (Austria)**

IASC Working group on Arctic Glaciology

IMAU Institute for Marine and
Atmospheric research Utrecht

**Institute for Marine and Atmospheric Research Utrecht
Utrecht University, The Netherlands**

The Dynamics and Mass Budget of Arctic Glaciers

Extended abstracts

**Workshop and GLACIODYN (IPY) Meeting,
29 - 31 January 2008, Obergurgl (Austria)**

IASC Working Group on Arctic Glaciology

Organized by J. Oerlemans and C.H. Tijm-Reijmer

Institute for Marine and Atmospheric Research Utrecht
Utrecht University, The Netherlands

CONTENTS

PREFACE

The 2008 annual workshop of the Working Group on Arctic Glaciology was combined again with a GLACIODYN workshop. It was held in Obergurgl, Austria, 29-31 January 2008.

GLACIODYN is a lead IPY project dealing with Arctic glaciers. It comprises an internationally-coordinated effort to study the dynamics of Arctic glaciers and to develop better tools to predict the response of these glaciers to climate warming. The key elements of this effort are (i) to *make better use of observational techniques* to assess the detailed dynamics of a key set of glaciers, and (ii) to *develop models* that can be used to aggregate data and that are sufficiently robust to have predictive power. A set of target glaciers have been identified for intensive observations (in situ and from space) for the period 2007-2010. This set covers a wide range of climatic/geographical settings and takes maximum advantage of prior long-term studies.

Over 58 participants presented 36 oral contributions and 16 posters on a wide range of subjects. Previous reports of the workshop appear to be very popular, so it was decided to make a book of extended abstracts once more. A considerable number of the workshop presentations are summarized here, and I want to thank the contributors for their efforts to produce clear and well-illustrated texts.

Hopefully, the long series of workshops we had until now will be continued in the future. The next workshop is scheduled for February 2009, and will be hosted by the Canadian GLACIODYN partners. General information about past and future meetings can be found at:
http://www.phys.uu.nl/%7Ewwwimau/research/ice_climate/iasc_wag/

Once more, Carleen Tijm-Reijmer has been the key person in the organization of the workshop and the production of the abstract book. Carleen, thank you very much for all the work you have done to make these workshops a success!

Johannes Oerlemans
Coordinator of GLACIODYN

PROGRAM

Chair: Johannes Oerlemans

- 09:00 – 09:10   *Johannes Oerlemans*: Welcome
- 09:10 – 09.30   *Douglas Mair*: The mass balance of the Prince of Wales Icefield, Ellesmere Island, Canada
- 09.30 – 09:50   *David Burgess*: Monitoring the mass balance of ice caps and glaciers in the Canadian High Arctic
- 09.50 – 10:10   *Joel Harper, John Bradford, Neil Humphrey and Tad Pfeffer*: The role of englacial fractures in storing and routing water
- 10:10 – 10:30   *J. Jania, L. Kolondra, G.K.C. Clarke, D. Puczko, T. Budzik and E. Majchrowska*: Subglacial water outflows and related elements of dynamics of Hansbreen – tidewater glacier in south Svalbard

    10:30 – 10:50   Coffee break

- 10:50 – 11:10   *F. Navarro, M. Grabiec, D. Puczko, U. Jonsell, A. Nawrot*: Internal structure of Ariebreen, Spitsbergen, from radio-echo sounding data.
- 11:10 – 11:30   *Bartek Luks, K. Migała, D. Puczko and M. Grabiec*: Local climate and vertical gradients of glaciological processes
- 11:30 – 11:50   *K. Migała, M. Szymanowski and M. Kryza*: Spatial distribution of potential and total radiation on the glaciers in the Hornsund area, SW Spitsbergen
- 11:50 – 12:10   *Jack Kohler*: MODIS albedo and regional mass balance of Svalbard glaciers.

    12:10 – 14:00   LUNCH

Chair: Jason Box

- 14:00 – 14:20   *Christopher Nuth*: On the fast-flowing GLACIODYN target glacier Kronebreen/Holtedahlfonna
- 14:20 – 14:40   *Monica Sund*: Recent surge activity in southern Spitsbergen
- 14:40 – 15:00   *C. Reijmer, M. den Ouden, V. Pohjola, J. Oerlemans*: Mass balance and velocity observations on Nordenskiöldbreen, Svalbard
- 15:00 – 15:20   *Veijo Pohjola*: Altimetry of Nordenskiöldbreen - changes between 1991 and 2007

    15:20 – 15:50   Coffee break

- 15:50 – 16:10   *M. Petlicki, J. Lapazaran, F. Navarro, P. Glowacki, F. Machío*: Ice volume changes of Ariebreen, Spitsbergen, during 1936-1990-2007.
- 16:10 – 16:30   *Gerit Rotschky, J. Kohler, E. Isaksson*: Spatio-temporal variability of snow melt on Svalbard derived from spaceborne scatterometer data (Qscat)
- 16:30 – 16:50   *Matt Nolan*: Polar panoramas: Images worth a thousand megabytes
- 16:50 – 17:10   *Rhian Salmon*: IPY outreach, education, and polar science days

- 17:10 – 18:00   POSTER SESSION

    19:00   DINNER

Wednesday 30

Chair: Regine Hock

- 09:00 – 09:20   *M.A.G. den Ouden, C.H. Reijmer and J. Oerlemans*: Surface mass-balance modeling of Nordenskiöldbreen, Svalbard
- 09:20 – 09:40   *J.O. Hagen*: Mass balance of Austfonna Ice cap
- 09:40 – 10.00   *Thomas Schuler*: The accumulation pattern of Austfonna, Svalbard
- 10.00 – 10:20   *J.A. Dowdeswell, T.J. Benham, T. Strozzi, J.O. Hagen*: Iceberg calving flux and mass balance of the Austfonna ice cap on Nordaustlandet, Svalbard

      10:20 – 10:50   **Coffee break**

- 10:50 – 11:10   *Martin Sharp and Libo Wang*: A five-year record of summer melt on Eurasian Arctic ice caps
- 11:10 – 11:30   *Shuhei Takahashi, Konosuke Sugiura, Takao Kameda, Hiroyuki Enomoto, Yury Kononov and Maria D. Ananicheva*: Glaciological and meteorological observations in Suntar-Khayata Range, Eastern Siberia, in 2004-2007
- 11:30 – 11:50   *Andrey Glazovskiy and Yury Macheret*: RES studies of glaciers on Franz-Josef Land
- 11:50 – 12:10   *Jason Box*: Greenland outlet glacier dynamics from repeat photography

      12:10   **LUNCH**

      19:00   **DINNER**

- 20:30   **Meeting of national delegates of the Working Group on Arctic Glaciology of IASC**

Thursday 31

Chair: Martin Sharp

- 08:30 – 08:50   *Michiel van den Broeke, Paul Smeets, Janneke Ettema, Roderik van de Wal*: Observed and calculated melt in the ablation zone of the West Greenland ice sheet
- 08:50 – 09:10   *Janneke Ettema, Michiel van den Broeke and Erik van Meijgaard*: Greenland surface mass balance using a regional atmospheric climate model
- 09:10 – 09:30   *Jay Zwally*: Mass balance of the Greenland Ice Sheet: A recent increase in rate of ice loss Observed by ICESat and GRACE
- 09.30 – 09:50   *Andrew Sole*: Investigating causes of peripheral thinning of the Greenland Ice Sheet: Constraint on dynamic thinning?
- 09:50 – 10:10   *R.S.W. v.d. Wal, W. Boot, M.R. van den Broeke, P. Smeets, C.H. Reijmer, J.J.A. Donker and J. Oerlemans*: Large and rapid variability in the velocity in the ablation zone of the Greenland ice sheet
- 10:10 – 10:30   *Manfred Stober*: Relations between horizontal strain and elevation change at the Swiss Camp area (West Greenland)

      10:30 – 11:00   **Coffee break**

Chair: Jon Ove Hagen

- 11:00 – 11:20   *Martin Lüthi*: Calving dynamics of Jakobshavn Isbrae
- 11:20 – 11:40   *Tad Pfeffer*: Limits on Greenland dynamic discharge during the next century
- 11:40 – 12:00   *Regine Hock*: Parameterization of longwave incoming radiation on Storglaciaren, Sweden
- 12:00 – 12:20   *Miriam Jackson*: Glaciodyn activities in Svartisen subglacial laboratory
- 12:20 – 12:40   *Antoine Kies, A. Nawrot, H. Surbeck, Z. Tosheva, J. Jania*: Natural Radionuclides in Glacier meltwater as useful tracers
- 12:40 – 13:00   *M. Blaszczyk and J. Jania*: Front types of Svalbard tidewater glaciers

13:00	**LUNCH**
19:00	**DINNER**

POSTERS

- *T. Budzik, M. Grabiec, T. Niedzwiedz, D. Puczko and K. Migala*: Relationships between atmospheric circulation and glaciers´ mass balance elements on Southern Svalbard
- *T. Budzik and D. Ignatiuk*: Short-term variations of the ablation and its sensivity to global radiation recorded on Hans Glacier, SW Spitsberegn, Svalbard
- *Anne Chapuis, Cecilie Rolstad, and Ivar Maalen-Johansen*: Terrerstrial photogrammetry for measurements of the calving rate of Kronebreen, Svalbard
- *Thorben Dunse, Thomas V. Schuler and Jon Ove Hagen*: Application of a numerical ice sheet model on Austfonna, Svalbard - model preparations and input data
- *G. Gajek, M. Grabiec, D. Puczko and J. Jania*: Changes of geometry of Renardbreen (Spitsbergen) and evolution of morphology of its forefield during the last century
- *M. Grabiec, D. Puczko and W. Dobinski*: Some results of radio echo soundings of frontal parts and forefields of selected subpolar glaciers in Svalbard and N Scandinavia
- *M. Grześ, M. Król and I. Sobota*: Glacier geometry chang in the Forlandsundet area using remote sensing data
- *Joel Harper, Neil Humphrey and Tad Pfeffer*: Meltwater runoff and firn densification in the Percolation Facies, Greenland Ice Sheet
- *Antoine Kies, A. Navrot, H. Surbeck, Z. Tosheva, J. Jania*: Natural Radionuclides in Glacier meltwater as useful tracers
- *L. Kolondra, M. Blaszczyk, J. Jania and P. Glowacki*: New satellite map of the Kinnvika Station surroundings, NW Nordaustandet
- *Geir Moholdt and Christopher Nuth*: On the use of ICEsat measurements on Svalbard glaciers.
- *Faezeh Nick*: Modelling the behaviour of Greenland outlet glaciers
- *Christopher Nuth, G. Moholdt, J. Kohler, H.F. Aas and J.O. Hagen*: Rapid surface elevation losses of Spitsbergen glaciers [1936-1990-2005]
- *W. Schöner, A. Richter, A.I. Sharov and Bernhard Hynek*: The Austrian research focus within IPY in Greenland and Franz Josef Land
- *I. Sobota and M. Grześ*: Regional distribution of snow accumulation on north-western Spitsbergen glaciers, Svalbard
- *Dirk van As*: A long-term network of automatic weather and ice monitoring stations in the ablation zone of the Greenland Ice Sheet

LIST OF PARTICIPANTS

1. Andreas Ahlstrøm (apa@geus.dk)
   Geological Survey of Denmark and Greenland, Copenhagen, Denmark
2. Kumiko Azuma (kumiko@pmg.nipr.ac.jp)
   National Institute of Polar Research, Tokyo, Japan
3. Malgorzata Blaszczyk (mbl4@wp.pl)
   Faculty of Earth Sciences, University of Silesia, Poland
4. Jason Box (box.11@osu.edu)
   Byrd Polar Research Center, Ohio State University, Columbus, Ohio, USA
5. Tomek Budzik (tomasz.budzik@us.edu.pl)
   Faculty of Earth Sciences, University of Silesia, Poland
6. David Burgess (David.Burgess@NRCan.gc.ca)
   Natural Resources Canada, Otawa, Canada
7. Anne Chapius (anne.chapuis@umb.no)
   Department of Mathematical Sciences and Technology, Norwegian University of Life Sciences, Norway
8. Marianne den Ouden (M.A.G.denOuden@phys.uu.nl)
   Institute for Marine and Atmospheric Research, Utrecht University, Netherlands
9. Evelyn Dowdeswell (e.k.dowdeswell@bris.ac.uk)
   Bristol Glaciological Centre, Bristol, UK
   Scott Polar Research Institute, University of Cambridge, Cambridge, UK
10. Julian Dowdeswell (jd16@cam.ac.uk)
    Scott Polar Research Institute, University of Cambridge, Cambridge, UK
11. Thorben Dunse (thorben.dunse@geo.uio.no)
    Department of Geosciences, University of Oslo, Oslo, Norway
12. Janneke Ettema (j.ettema@phys.uu.nl)
    Institute for Marine and Atmospheric Research, Utrecht University, Netherlands
13. Grzesiek Gajek (gajcy@o2.pl)
    M. Curie-Sklodowska University, Poland
14. Andrey Glazovsky (icemass@yandex.ru)
    Institute of Geography, Russian Academy of Sciences, Moscow, Russia
15. Piotr Glowacki (glowacki@igf.edu.pl)
    Institute of Geophysics, Polish Academy of Science, Warszawa, Poland
16. Mariusz Grabiec (mariusz.grabiec@us.edu.pl)
    Faculty of Earth Sciences, University of Silesia, Poland
17. Jon Ove Hagen (j.o.m.hagen@geo.uio.no)
    Department of Geosciences, University of Oslo, Oslo, Norway
18. Joel Harper (joel@mso.umt.edu)
    Dept. of Geosciences, Univ. of Montana, Missoula, USA
19. Regine Hock (regine.hock@gi.alaska.edu)
    Geophysical Institute, University of Alaska, Fairbanks, Alaska
20. Bernhard Hynek (bernhard.hynek@zamg.ac.at)
    Dep. of Climatology, Central Institute for Meteorology and Geodynamics, Vienna, Austria
21. Miriam Jackson (mja@nve.no)

Norwegian Water Resources and Energy Directorate, Oslo, Norway

22. Jacek Jania (jjania@us.edu.pl)
    Faculty of Earth Sciences, University of Silesia, Poland
23. Antoine Kies (antoine.kies@uni.lu)
    University of Luxembourg, Luxembourg
24. Jack Kohler (jack.kohler@npolar.no)
    Norwegian Polar Institute, Tromsø, Norway
25. Michael Kuhn (Michael.Kuhn@uibk.ac.at)
    Institute of Meteorology and Geophysics, University of Innsbruck, Austria
26. Martin Lühti (luethi@vaw.baug.ethz.ch)
    Laboratory of Hydraulics, Hydrology and Glaciology, Swiss Federal Institute of
    Technology   (ETH), Zurich, Switzerland
27. Bartek Luks
    Institute of Geophysics, Polish Academy of Science, Warszawa, Poland
28. Yuri Macheret (macheret@gol.ru)
    Institute of Geography, Russian Academy of Sciences, Moscow, Russia
29. Douglas Mair (d.mair@abdn.ac.uk)
    School of Geosciences, University of Aberdeen, Aberdeen, UK
30. Krzystof Migala (migalak@meteo.uni.wroc.pl)
    University of Wroclaw, Institute of Geography & Regional Development,
    Poland
31. Heinz Miller (hmiller@AWI-Bremerhaven.de)
    Alfred Wegener Institute for polar and marine research, Bremerhaven,
    Germany
32. Francisco Navarro (fnv@mat.upm.es)
    Madrid Polytechnical University, Spain
33. Faezeh Nick (Faezeh.Nick@durham.ac.uk)
    Department of Geography, University of Durham, Durham, UK
34. Matt Nolan (fnman@uaf.edu)
    Institute of Northern Engineering, University of Alaska, Fairbanks, Alaska
35. Christopher Nuth (christopher.nuth@geo.uio.no)
    Department of Geosciences, University of Oslo, Oslo, Norway
36. Friedrich Obleitner (Friedrich.Obleitner@uibk.ac.at)
    Institute of Meteorology and Geophysics, University of Innsbruck, Austria
37. Hans Oerlemans (J.Oerlemans@phys.uu.nl)
    Institute for Marine and Atmospheric Research, Utrecht University,
    Netherlands
38. Michal Petlicki (petlicki@igf.edu.pl)
    Institute of Geophysics, Polish Academy of Sciences, Poland
39. Tad Pfeffer (pfeffer@tintin.colorado.edu)
    University of Colorado, Boulder, USA
40. Veijo Pohjola (veijo.pohjola@geo.uu.se)
    Department of Earth Sciences, Uppsala University, Uppsala, Swede
41. Dariusz Puczko (dp@igf.edu.pl)
    Institute of Geophysics, Polish Academy of Science, Warszawa, Poland
42. Gerit Rotschky (Gerit.Rotschky@npolar.no)
    Norwegian Polar Institute, Tromsø, Norway
43. Rhian Salmon (ipy.ras@gmail.com)
    IPY Education and Outreach Coordinator

44. Elisabeth Schlosser (Elisabeth.Schlosser@uibk.ac.at)
Institute of Meteorology and Geophysics, University of Innsbruck, Austria
45. Thomas Schuler (t.v.schuler@geo.uio.no)
Department of Geosciences, University of Oslo, Oslo, Norway
46. Martin Sharp (martin.sharp@ualberta.ca)
Earth and Atmospheric Sciences, University of Alberta, Edmonton, Canada
47. Paul Smeets (c.j.p.p.smeets@phys.uu.nl)
Institute for Marine and Atmospheric Research, Utrecht University, Netherlands
48. Irek Sobota (irso@geo.uni.torun.pl)
Dept. of Cryology and Polar Research, N.Copernicus University, Torun, Poland
49. Andrew Sole (A.J.Sole@bristol.ac.uk)
Bristol Glaciological Centre, Bristol, UK
50. Manfred Stober (manfred.stober@hft-stuttgart.de)
Stuttgart University of Applied Sciences, Stuttgart, Germany
51. Monica Sund (Monica.Sund@unis.no)
University Centre in Svalbard, Longyearbyen, Norway
52. Shuhei Takahashi (shuhei@mail.kitami-it.ac.jp)
Kitami Institute of Technology, Japan
53. Carleen Tijm-Reijmer (C.H.Tijm-Reijmer@phys.uu.nl)
Institute for Marine and Atmospheric Research, Utrecht University, Netherlands
54. Zornitza Tosheva
University of Luxembourg, Luxembourg
55. Dirk van As (dva@geus.dk)
Geological Survey of Denmark and Greenland, Copenhagen, Denmark
56. Roderik van de Wal (R.S.W.vandeWal@phys.uu.nl)
Institute for Marine and Atmospheric Research, Utrecht University, Netherlands
57. Michiel van den Broeke (m.r.vandenbroeke@phys.uu.nl)
Institute for Marine and Atmospheric Research, Utrecht University, Netherlands
58. Jay Zwally Zwally (zwally@icesat2.gsfc.nasa.gov)
NASA Goddard SFC, USA

ABSTRACTS

FRONT TYPES OF SVALBARD TIDEWATER GLACIERS

MAŁGORZATA BŁASZCZYK AND JACEK A. JANIA

Faculty of Earth Sciences, University of Silesia, Poland

We have classified all tidewater glaciers in Svalbard with respect to their dynamics, taking into account patterns of crevasses examined on satellite images and aerial photos. They were used as a proxy for the determination of glacier movement velocity.

Information on glacier velocity close to its terminus is crucial for calculation of the calving flux. The amount of direct data on the Svalbard tidewater glaciers motion velocity is very limited. Moreover, glacier flow velocity varies on different time scales (diurnal, interdiurnal, seasonal and interannual). Therefore, some of the data (e.g. InSAR) were not representative for an annual ice flux. Due to lack of repeated ground survey data close to glaciers' terminus, a feature tracking technique using the sequential high-resolution ASTER imagery from 2000 – 2006 was applied to determine the surface velocities near several glaciers fronts. The annual surface velocity of 10 glaciers was derived by measuring displacements of surface features (crevasses, moraine elements) visible on images acquired in one-year period. An error of feature tracking velocity measurements is estimated as ±30 ma^{-1}. For 16 glaciers very small crevassing areas were noted and no motion of the glaciers' front was observed on ASTER images acquired in one or even two year interval (within the above accuracy).

Table 1. Categories of front types of Svalbard tidewater glaciers

	Types of tidewater glaciers fronts	Length of crevassing zone [m]	Glacier velocity $[ma^{-1}]$
I	very slow or stagnant glaciers	0 - 300	10 ± 5
II	slow glaciers	≥ 300 - 1000	70 ± 30
III	fast flowing glaciers	≥1000	200 ± 50
IV	surging glaciers or fast flowing ice streams	>>1000	700± ?

Evaluation of the dynamic status of tidewater glaciers was based on several characteristics such as: length of glacier, length of crevassed zone, area of glacier, area of crevassed zone and length of cliff acquired from ASTER imagery. All available data (from research and literature) on glaciers' velocity were analyzed in comparison with the above features. The best correlation (r = 0.71) was found between the length of the crevassing zone and the glacier velocity. This parameter was determined as the main criterion for estimation of tidewater glaciers velocity. Four categories of front types of Svalbard tidewater glaciers were distinguished:
I.   very slow or stagnant glaciers (Figure 1a)
II.   slow glaciers (Figure 1b)
III.   fast flowing glaciers (Figure 1c)
IV.   surging glaciers or fast flowing ice streams (Figure 1d).

Length of crevassing zone and an average glacier velocity near the front assumed for each of the group is presented in Table 1.
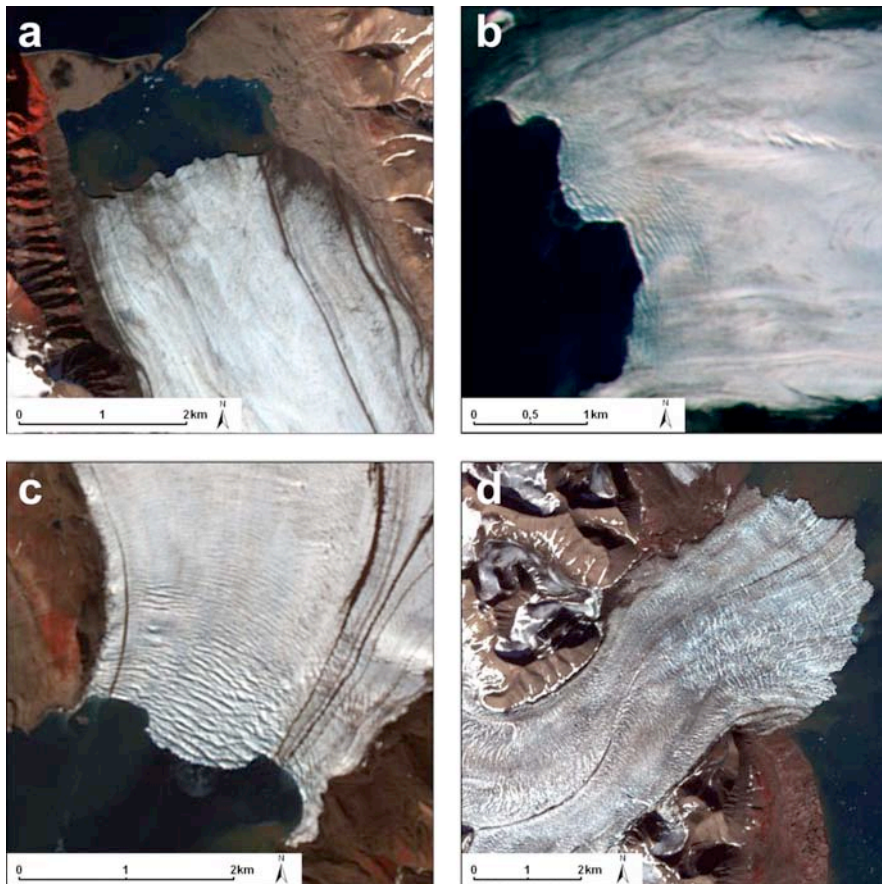
Figure 1. Examples of front types of Svalbard tidewater glaciers: a) Recherchebreen - very slow or stagnant glacier; b) Aavatsmarkbreen - slow glacier; c) Osbornebreen - fast flowing glacier; d) Perseibreen - surging glacier.

Complete length of tidewater glaciers' cliffs was measured using geocoded ASTER images and used as data for the calving intensity assessment. The total length is 859.1 km for the whole Svalbard, while Dowdeswell (1989) reported 1028 km. It shows a reduction of tidewater glacier seaward margin by 16% in c. 40 years. The length of ice cliffs of the main islands of the archipelago is shown in Table 2.

One can calculate calving ice flux from all Svalbard glaciers when having at one's disposal: length of the ice cliffs, average glaciers' velocities and their ice thickness near terminus. Due to very sparse data on sea water depth close to ice cliffs, an average value of 100 m for ice thickness was used in these calculations.

ASTER images also provide a good overview of glacier fronts' fluctuations. Front position changes of about 30 glaciers were measured and, as a result, an average

retreat rate by 20 – 40 ma^{-1} was suggested. After having compiled the available information, the total calving intensity of Svalbard glaciers (without Kvitøya) amounts to 6.7 – 8.2 km^{3}a^{-1} ± 1.5 km^{3}a^{-1}.

Table 2. Length of ice cliffs of the main islands of Svalbard: L1 – from Dowdeswell (1989); L2 – data derived from ASTER satellite images (2000-2006).

Island	Length of ice cliffs	
	L1 [km]	L2 [km]
Spitsbergen	484	388.4
Nordaustlandet	306	272.3
Edgeøya	79	68.7
Prins Karls Forland	17	8.9
Barentsøya	23	8.8
Storøya	13	12
Kvitøya	106	100
Sum	1028 km	859.1 km

Examination of ASTER images from 2000-2006 for the whole Svalbard has shown that 163 glaciers appear as the tidewater type. In comparison to the Hagen et al. (1993) inventory, 14 glaciers have retreated from the sea to land during the period of c. 30-40 years. Basing upon the literature, 54 tidewater glaciers have been considered as surge-type, which makes up 33% of all tidewater glaciers. Taking into account other evidence visible on ASTER images (e.g. badly crevassed glacier surface, distinct lateral shear zones, folded medial moraines, etc.), the number of tidewater glaciers classified as a surge-type may reach even 43%. It is much more than 13% of the whole population of Svalbard glaciers suggested by Jiskoot et al. (1998) and closer to preliminary estimates proposed by Jania (1988).

Acknowledgements.

References:
Dowdeswell J.A., 1989. On the nature of Svalbard icebergs. Journal of Glaciology, 35(120), 224 - 234.

Hagen J.O., Liestøl O., Roland E., Jørgensen T., 1993. Glacier Atlas of Svalbard and Jan Mayen. Norsk Polarinstitutt, Meddelelser, 129, Oslo, 141 pp.

Jania J., 1988. Dynamiczne procesy glacjalne na poludniowym Spitsbergenie w swietle badan fotointerpretacyjnych i fotogrametrycznych [Dynamic glacier processes in southern Spitsbergen in the light of photointerpreration and photogrammetric research - English summary]. Wydawnictwo Uniwersytetu Slaskiego, Katowice 1988, 258 pp.

Jiskoot H., Boyle P., Murray T., 1998. The incidence of glacier surging in Svalbard: Evidence from multivariate statistics. Computers & Geosciences, 24(4), 387 - 399.

Relations between atmospheric circulation and glaciers' mass balance elements on Southern Svalbard (Hansbreen as an example)

T. Budzik[1], M. Grabiec[2], D. Puczko[3] and K. Migała[4]

[1] University of Silesia, Faculty of Earth Sciences, Department of Climatology, Poland
[2] University of Silesia, Faculty of Earth Sciences, Department of Geomorphology, Poland
[3] Institute of Geophysics Polish Academy of Sciences, Department of Polar and Marine Research, Poland
[4] University of Wroclaw, Institute of Geography & Regional Development, Department of Meteorology & Climatology, Poland

Objectives

The atmospheric circulation is one of the most significant elements which shape both the weather and the climate. It plays an important role in the heat and humidity transfer within the Arctic, which is due to geographical location and differentiated light conditions in a yearly course (the polar day and night). As a consequence, circulation conditions shall have a significant influence upon elements of glaciers' mass balance. The aim of this work is to indicate relations between the mass balance of Southern Spitsbergen glaciers and the atmospheric circulation with Hansbreen as the example.
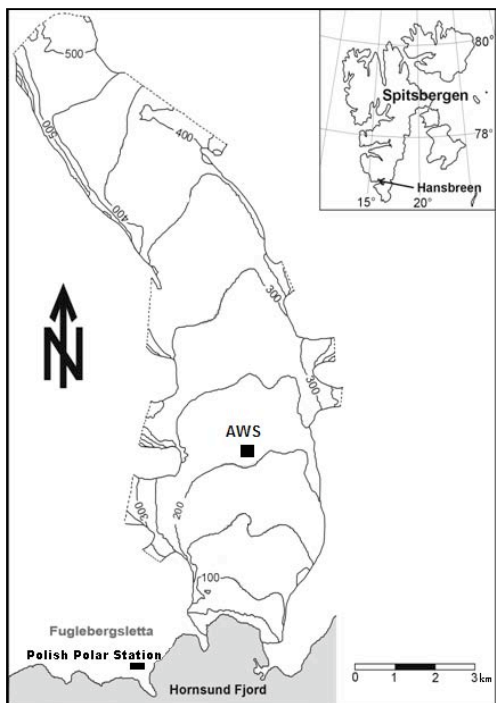
Figure 1. Location of Hansbreen

Methods

Relations between the discussed factors occurring in one summer season as well as in the years 1989-2007 have been analyzed. Types of atmospheric circulation have been drawn up on the basis of the calendar of circulation types for Spitsbergen for the years 1951 - 2007 (Niedzwiedz 1997, 2006). The synoptic conditions have been divided into 2 groups of anticyclonic and cyclonic depending on the direction of inflow of air masses over Svalbard: N, NE, E, SE, S, SW, W, NW. Additionally, two conditions of stagnation have been distinguished: Ca - the centre of high pressure over Svalbard and Ka - a wedge of high pressure, and two situations of variable advection. These situations are: Cc - in case of emergence of the low pressure centre over Svalbard and Bc - the emergence of cyclonic furrow. Also, a type of circulation marked as "x" has been distinguished separately for baric col and situations when the weather situation cannot be defined explicitly.

On the basis of circulation types westerly zonal index (W), southerly meridional index (S) and cyclonicity index (C) have been defined for accumulation and ablation seasons separately. The S index express intensity of latitudinal circulation. Positive values of the index indicate prevailing inflow of the air from the southern sector and diminishing one from the northern sector. The W index defines the intensity of western zonal circulation (positive values) and eastern one (negative values).

The study of mass balance elements relates to Hansbreen (South Spitsbergen). Hansbreen (an area of 56 km^2) is a polythermal glacier terminating in the sea (Figure 1). This glacier's mass balance has been constantly monitored since 1988. Short-term changes in surface elevation in the summer season of 2007 were defined by a SR50 Campbell Sonic Ranging Sensor. The device was located at Hansbreen at the elevation of 210 meters a.s.l. In addition, meteorological data from the Polish Polar Station in Hornsund and automatic weather station (AWS) at Hansbreen were used in the study.
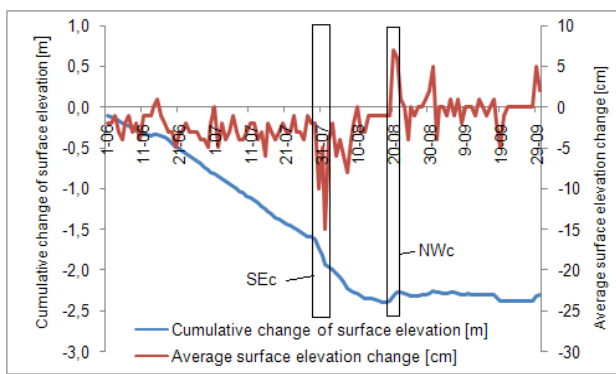
Figure 2. Course of cumulative change of surface elevation [m] and average surface elevation change [cm] on Hansbreen in summer 2007.

Results

The glacier's surface elevation in summer 2007 was decreasing at a considerable rate till the 8th of August (Figure 2). The ablation was stopped in the second part of the season. These stages are connected with types of circulation dominating in

those two periods. In the first half of the season the advection with northern and southern component (Nc, NEc, E and SEc) as well as anticyclonic non-advective types dominated. The circulation conditions after the 8th of August can be characterized with the domination of cyclonic types - chilly and wet ones (Nc and NEc).

The average daily changes in the elevation of glacier's surface can differ in particular types of circulation (Table 1). The most effective melting is accompanied by inflows of the air of Ea and SEa type (3.6 cm per day on average) and Ec, SEc type (3.4 cm per day on average). Humid and chilly air masses of Wc and NWc type, on the other hand, that generate much rainfall can cause an increase in the elevation of glacier's surface even in summer (1.0 cm per day on average).

Table 1. Statistical characteristics of summer 2007 in circulation types

| Circulation type	Na+ NEa	Ea+ SEa	Sa+ SWa	Wa+ NWa	Ca+ Ka	Nc+ NEc	Ec+ SEc	Sc+ SWc	Wc+ NWc	Cc+ Bc	x
Frequency [%]	5.7	6.6	0.8	2.5	13.9	29.5	15.6	4.1	5.7	13.1	2.5
Average teperature [°C]	4.4	4.3	3.0	2.4	3.3	2.5	4.3	3.6	2.9	2.5	2.5
∑PDD [°C]	31.0	34.5	3.0	7.2	55.8	94.3	82.1	18.2	20.4	39.5	7.6
Total precipitation [mm]	0.0	0.6	0.4	3.1	24.1	15.2	17.3	42.4	26.5	25.7	0.0
Average surface elevation change [cm]	-2.9	-3.6	-3.0	-0.3	-2.2	-1.2	-3.4	-1.8	1.0	-1.1	-1.3
Cumulative change of surface elevation [cm]	-20.0	-29.0	-3.0	-1.0	-38.0	-42.0	-64.0	-9.0	7.0	-18.0	-4.0

Extreme ablation event recorded on the 1st of August was caused by advection of SEc type lasting for several days (Figure 2). A shift of advection to NWc provoked a precipitation and positive changes in the glacier's elevation.

Relations between the glacier's balance and atmospheric circulation in a long-term perspective were considered for ablation and accumulation season separately (Table 2). Important statistical relations (p = 0.01) were noted between the summer balance and the frequency of occurrence of circulation of Ca + Ka type (r = -0.61). It reflects the increase in ablation along with the increasing frequency of anticyclonic, cloudless and minimum precipitation weather as well as lessened activity of cyclonic advection from W and NW. The advection of air masses of Wc and NWc type (r = 0.60) cause ablation decrease. Due to the fact that the most of frequency of occurrence of those circulation types fall in summer (14 and 6 % percent respectively), they belong to the key weather shaping factors over southern Spitsbergen.

Table 2. Correlation coefficients (p=0.01) between Hansbreen mass balance elements and frequency of circulation types/indexes occurrence in period 1989-2007.

Balance	Na+ NEa	Ea+ SEa	Sa+ SWa	Wa+ NWa	Ca+ Ka	Nc+ NEc	Ec+ SEc	Sc+ SWc	Wc+ NWc	Cc+ Bc	x	S	W	C
Winter	-0.19	0.04	-0.10	-0.65	-0.20	-0.16	0.26	0.14	0.35	0.15	-0.01	0.45	-0.15	0.33
Summer	-0.35	-0.49	0.05	0.04	-0.61	0.26	0.03	0.40	0.60	0.18	0.28	-0.05	0.50	0.57

The winter balance, in turn, shows the closest relation with the advection of Wa + NWa (r = -0.65). The increase in frequency of such advection results first of all in reduction of winter precipitation. The frequency of occurrence of this advection is low (5% on average). Thus it shall be treated only as an indicative element and not a dominating one.

Within circulation indices, significant statistical relations were observed only among the summer balance and indexes of C and W (Table 2). Seasons with dominating eastern advection and anticyclonic conditions can be characterized with higher surface ablation of glacier.

Conclusions

Relations between elements of Hansbreen mass balance and atmospheric circulation are complex and do not show very strict dependence.

The anticyclonic wedge (Ka 10.4%) is the most frequent synoptic situation on Svalbard (Niedzwiedz 2007). The second one is circulation of Ec (9.9%) type and Ec. The climate of Svalbard is modelled by an intense cyclonic activity during 56% of days in a year.

One can indicate a set of circulation types which influence the mass balance of distinguished summer and winter seasons. Very negative values of the summer balance are generated by circulation types with accompanying radiation weather, i.e. Ca and Ka and advection from the eastern sector. Ablation is limited in a condition of inflow of cyclonic masses from the northern and western sector. The winter balance is conditioned mainly by availability of snow supply. The exemplary type of circulation is the advection of Wa + NWa type, with air mass of continental features: dry, cold and with low precipitation. Frequent emerging of this air mass causes reduced winter accumulation.

Relations between the dynamics of mass balance and circulation types have a complex nature. The preliminary results are indicative only. For example: an increase in C cyclonic indicator with a simultaneous decrease in W indicator value in the ablation season of 2001 can suggest very negative values of the summer balance at that period of time.

Acknowledgements

Bibliography
Niedzwiedz T., 1997, Long-term variability of the atmospheric circulation indices over Spitsbergen and its influence on the air temperature. Problemy Klimatologii Polarnej, 7: 19-40.
Niedzwiedz T., 2006, The main forms of atmospheric circulation above Spitsbergen (December 1950 – september 2006). Problemy Klimatologii Polarnej, 16: 91-105.

Monitoring the Mass Balance of Ice Caps in the Canadian Arctic

David Burgess[1], Roy Koerner[1], Micheal Demuth[1], Laurence Gray[1], Naomi Short[1] and Graham Cogley[2]

[1] Natural Resources Canada, Ottawa
[2] Trent University, Canada

Mass balance monitoring of ice caps and glaciers in the Canadian high Arctic commenced in 1959. Measurements were initially obtained from the Meighen ice cap by Keith Arnold of Energy, Mines, and Resources (now Natural Resources Canada) and from the White Glacier, Axel Heiberg Island, by Dr. Fritz Muller of McGill University, Quebec. Mass balance surveys started on the Devon Island ice cap by Dr. Koerner and S. Ekman of the Arctic Institute of North America in 1961 with a fourth site installed on the South Melville ice cap in 1963. A fifth site on the Agassiz ice cap was added to the network in 1976 (Please refer to: http://pathways.geosemantica.net/WSHome.aspx?ws=NGP_SECG%26locale=en-CA for base-maps of the Arctic monitoring sites and individual site layouts). More recently, mass balance monitoring sites have been established in the lower Arctic regions on the Penny ice cap, Baffin Island (maintained by Christian Zdanowicz [Christian.Zdanowicz@NRCan.gc.ca] – NRCan) and in the Mackenzie Mountains of Nahanni National Park, Northwest Territories (maintained by Mike Demuth [Mike.Demuth@NRCan.gc.ca]–NRCan). With respect to the high Arctic monitoring sites, Dr. Koerner eventually became responsible for maintenance of all sites except for the White Glacier, which has been maintained by researchers from Trent University, Ontario since 1983.

Each of the 4 monitoring sites maintained by NRCan (Devon, Meighen, Melville, and Agassiz) consists of a network of mass balance poles and at least 1 automatic weather station[1]. Winter accumulation is estimated from snow depth and density values taken from each pole location, while summer balance is estimated as the difference between the previous winter balance and the previous annual firn layer. Percolation trays are used in the summit region of the Agassiz ice cap in order to estimate internal accumulation due to refreezing of meltwater within the near surface snowpack or firn. Automatic weather stations (AWS) were installed during the late 1980's and provide records of change in height of the snow pack, and air temperature at hourly intervals between annual site visits. These records highlight the timing of significant temperature (melt onset, intensity, and freeze-up) and snowfall events throughout the year, and provide evidence from which the magnitude and timing of internal accumulation events are inferred.

In-situ observations reveal a significantly negative mass balance of all high Arctic monitoring sites since observations began, becoming increasingly negative since the late 1980's (Figure 1). The South Melville ice cap exhibits the most negative cumulative balance of all sites monitored, having thinned by ~18 cm a^{-1} and losing approximately 0.45 km^3 of ice over the past >40 years. The Meighen ice cap has

experienced a significantly lower thinning rate of ~10 cm a^{-1}, equating to a total volume loss of ~0.3 km^3 since 1960. The White Glacier and the Northwest Devon sector have been thinning by 13 and 8 cm a^{-1} respectively. While preliminary results indicate that the in-situ data can be used to accurately quantify volume changes of small stagnant ice caps (Koerner and Burgess, in preparation), the spatially limited nature of these data, and their lack of accounting for mass loss due to ice-berg calving, make them less representative of mass changes across the much larger dynamic ice caps.
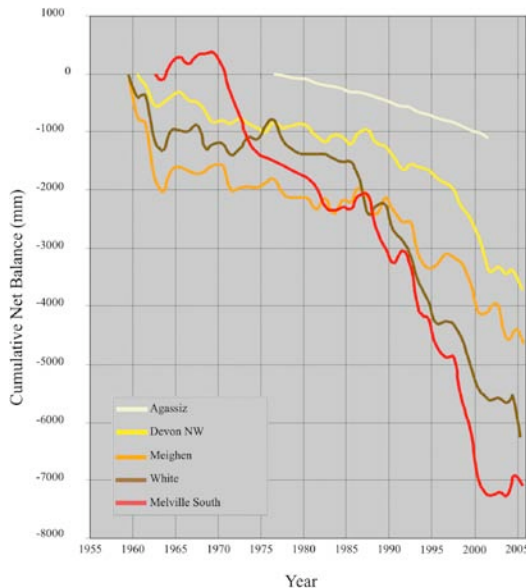
Figure 1. Cumulative net mass balance for 5 ice caps/glaciers in the Canadian high Arctic. Mass balance values are spatially averaged across 100m elevational bands at the basin-wide scale for the Devon ice cap and White Glacier measurements, and at the ice-cap wide scale for the Meighen and Melville observations. Cumulative mass balance measurements along the Agassiz transect represent 2-dimensional values only.

As part of NRCan's Glacier-Climate Observing System (GCOS), efforts are currently underway to augment in-situ observations with remote sensing data in order to provide a more complete estimate of mass balance across all land ice in the Queen Elizabeth Islands. One component of mass balance that will be included in GCOS is annual calving flux from tidewater glaciers that drain the main ice caps in the QEI. Surface velocities of 12 tidewater glaciers draining the Prince of Wales, North Ellesmere, and Axel Heiberg ice caps have been mapped on an annual basis since 2000, and on the Devon ice cap since 2005, using radar speckle tracking techniques as described in Short and Gray (2005). Annual velocity measurements coincide with ice thickness profiles flown by NASA in 2005 across the terminus of 5 major outlet glaciers that drain the Prince of Wales ice field and the Devon Island ice cap. Both datasets (ice thickness and surface velocity) are required to quantify flux through a glacier cross-section thus, future campaigns aimed at acquiring ice thickness profiles across the remaining flux gates are a high priority for this program. The second component of mass balance that we plan to monitor with remote sensing technology is the spatial distribution of water equivalent snow mass and near surface firn across land ice in the QEI. Preliminary results from the CryoSat-2 Cal/Val experiments over the Devon Island ice cap reveal that these layers can be tracked continuously over large distances from ASIRAS (Figure 2), which is an airborne version of the Ku band radar altimeter that

will be onboard CryoSat-2. Over regions where the average density of the near-surface firn is relatively low (ie < ~500 kg m^{-3}), annual firn layers up to ~4 m below the ice cap surface can be identified. These measurements provide important insight into the topographic, elevational, and distance-from-moisture-source controls on snow distribution, and provide spatial continuity to point measurements collected in the field. Incorporating remote sensing techniques with traditional in-situ observations will thus provide a more complete estimate of mass balance of land ice in the Arctic regions.
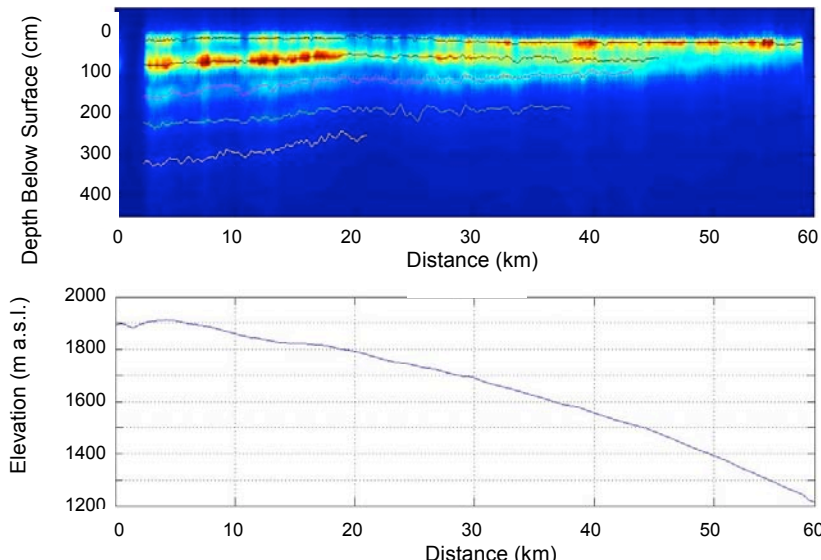
Figure 2. Upper frame displays a section of radar backscatter from the ASIRAS airborne radar altimeter (13 Ghz) acquired across the Devon ice cap in May, 2006. Above ~1800 m a.s.l., subsurface firn layers were tracked continuously over horizontal distances of >20 km to depths of ~300 cm below the surface. Below ~1400 m a.s.l., boundaries between annual layers were obscured by the effects of wind and downward percolation of meltwater within the snowpack.

In-situ mass balance measurements acquired from high Arctic ice caps and glaciers to date provide an invaluable climate record from a region that is predicted to experience significant warming over the next century (IPCC, 2007). The development of an operational mass balance monitoring system through GCOS, based on integration of in-situ and remote sensing observations, will provide knowledge critical for quantifying freshwater flux to the ocean, and for understanding the future impact of climate change on the state of health of land ice across the Canadian high Arctic.

References

IPCC. 2007. Climate Change 2007: The Physical Science Basis: Contribution of Working Group 1 to the Fourth Assessment Report of the Intergovernmental Panel on Climate Change, S. Solomon et al., Eds., Cambridge University Press, New York, 2007.

Short, N.H. and A.L. Gray, 2005. Glacier dynamics in the Canadian High Arctic from RADARSAT-1 Speckle Tracking. Can. J. Remote Sensing, Vol. 31, No. 3, pp. 225–239.

TERRERSTRIAL PHOTOGRAMMETRY FOR MEASUREMENTS OF THE CALVING RATE OF KRONEBREEN, SVALBARD

ANNE CHAPUIS, CECILIE ROLSTAD, AND IVAR MAALEN-JOHANSEN

Department of Mathematical Sciences and Technology, Norwegian University of Life Sciences (UMB).

Abstract

Calving is a large component in the mass budgets of tide water glaciers. Measurements of calving rates are essential for the determination of a calving law that can be used in a mass balance model of the glacier. Changes in climate may alter the ice dynamics and the melt water production, thus the calving rates may change rapidly. Despite their importance, calving processes are not well represented in numerical ice dynamic models, partially due to the difficulties and dangers of field data collection. Measurements of calving must be conducted in a safe distance to the calving front, and in this project we have applied terrestrial photogrammetry to the front of Kronebreen, Svalbard, in August-September 2007. Seven repeated stereo pairs were photographed from Nielsen-fjellet mountain side over a four-days period. Markers were placed on the strand and measured with GPS to georeference the images. The digital images are processed photogrammetrically for velocity measurements and volume estimates of the calving ice loss. The velocity data are compared to ground based interferometric radar measurements conducted in the same period, showing a velocity of 2.7 md^{-1}.

Surface mass-balance modeling of Nordenskiöldbreen, Svalbard

Marianne den Ouden, C.H. Reijmer and J. Oerlemans

Institute for Marine and Atmospheric Research, Utrecht University, the Netherlands

Introduction

Evidence shows that increased meltwater production on a glacier or ice sheet may result in higher ice-flow velocities (e.g. Iken and Bindschadler (1986), Zwally and others (2002)). This mechanism is an especially interesting feature on Arctic glaciers, as this area experiences large climatic changes (ACIA, 2005). To investigate this relation on seasonal and inter-annual time scales, on the one hand detailed temporal information on the flow velocity is needed, while on the other hand the amount of meltwater on a glacier has to be estimated. Finally, the route from the surface to the bed is of interest.

On the Arctic glacier Nordenskiöldbreen (Svalbard) the flow velocities are measured by means of a stand-alone GPS technique. Furthermore, the net mass balance is measured using stakes, and one Sonic Ranger (SR) providing a continuous record of the change in surface height. However, measurements offer a poor spatial resolution. Thus, to gain more insight in the spatial variations of melt distribution, we present a mass-balance model, based on the equations described in Klok and Oerlemans (2002), and (preliminary) results for the year 2006-2007.
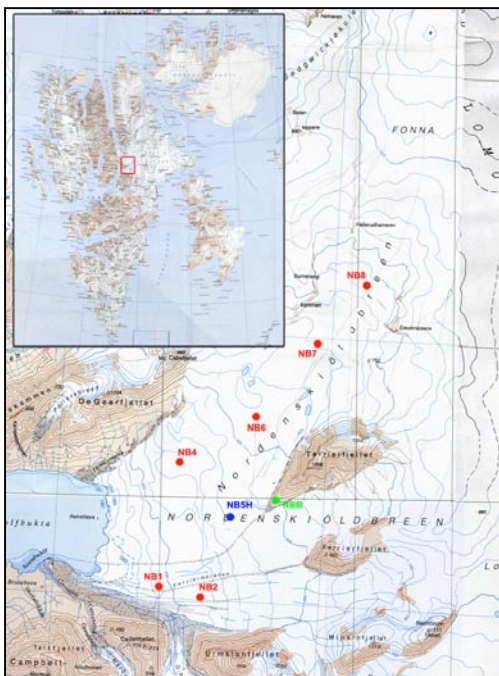

Figure 1. Map of the outlet glacier Nordenskiöldbreen. The red dots represent the mass-balance stakes, the blue dot gives the location of the SR and the green dot marks the location of the GPS reference station.

Location

Nordenskiöldbreen is located on central Spitsbergen (Figure 1). It has an area of 242 km^2, and the length of its main streamline is ±26 km (Hagen and others, 1993). Its depth varies from ±600 m at 7 km from the terminus to ±100 m at the top, 1200 m a.s.l. (V. Pohjola, personal comm.). The glacier flows with an average velocity of ±50m/a (GPS). Currently, Nordenskiöldbreen is changing from a tidewater glacier into a glacier ending on land.

MB model

Following Klok and Oerlemans (2002), the mass-balance model is based on the following equation for the specific mass balance:

$$M = \int \left\{ \frac{Q_m}{L_m} + P + \frac{Q_L}{L_S} \right\} dt, \tag{1}$$

where Q_m/L_m is the mass lost through melt, P is the mass gained from precipitation and Q_L/L_S is the mass lost through sublimation. To obtain the energy available for melt, the model calculates the six components of the total surface energy flux, namely incoming and reflected solar radiation (S_{in} and S_{out}), incoming and outgoing longwave radiation (L_{in} and L_{out}), sensible turbulent heat (Q_H) and latent turbulent heat (Q_L). In case the surface temperature is not at the melting point, or the flux is directed away from the surface, the energy (G) is used to heat or cool the surface layer, otherwise the energy is available for melting (Q_m):

$$S_{in} - S_{out} + L_{in} - L_{out} + Q_H + Q_L = Q_M + G \tag{2}$$

The model runs for the period March 30th 2006 until March 21st 2007, which corresponds to the period of continuous MB observations.

Input

As input to the model we use synoptic weather data from two stations located in the vicinity of Longyearbyen (see Table 1).

The air temperature at different heights is obtained by using a constant lapse rate of 6.5 K/km, based on measured temperatures. The cloud fraction is assumed constant with height. Lastly, the precipitation is determined so that its annual sum at a specific elevation corresponds with the observed snow pack at the beginning of the melt season.

The record of the SR and stake mass-balance measurements serve as comparison for the model output. The SR is located at an altitude of ±430 m a.s.l., while the 7 stakes are placed at 100m altitude intervals, ranging from ±150 m a.s.l. to ±700 m a.s.l. (Figure 1).

Table 1. Details input data

Parameter	Station	Distance	Altitude	Time interval
Air temperature, Ta	Adventdalen	±60 km	75 m a.s.l	10 min
Relative humidity, RH	Adventdalen	±60 km	75 m a.s.l	10 min
Air pressure, p	Adventdalen	±60 km	75 m a.s.l	10 min
Cloud fraction, n	LYB Airport	±60 km	28 m a.s.l	6 hour
Precipitation, P	LYB Airport	±60 km	28 m a.s.l	12 hour

Results and comparison to observations

In a general sense the model performs reasonably well. At the altitude of the SR for example, the snow pack disappears at approximately the right moment (±10 days too early in the model).

To validate the model, its output is compared to observations (Figure 2). In the first graph the model places the onset of melt too early. Another noticeable feature is the discrepancy between observed and modelled precipitation. In the beginning the model misses a snow event altogether, while in the second half of the year there is a mismatch in timing. A likely reason is the large distance between the source of the precipitation input and the target glacier.

In Figure 2b the model captures the net annual mass balance below the ELA (located at ±600 m a.s.l.) well. Nevertheless, it underestimates the mass balance in higher parts. Note that the observations in Hagen and others (2005) span the period 1986-1996. In recent years the mass balance has probably increased (V. Pohjola, pers. comm.), enlarging the difference even more. This discrepancy is either caused by an overestimation of melt, an underestimation of precipitation and/or the absence of refreezing.
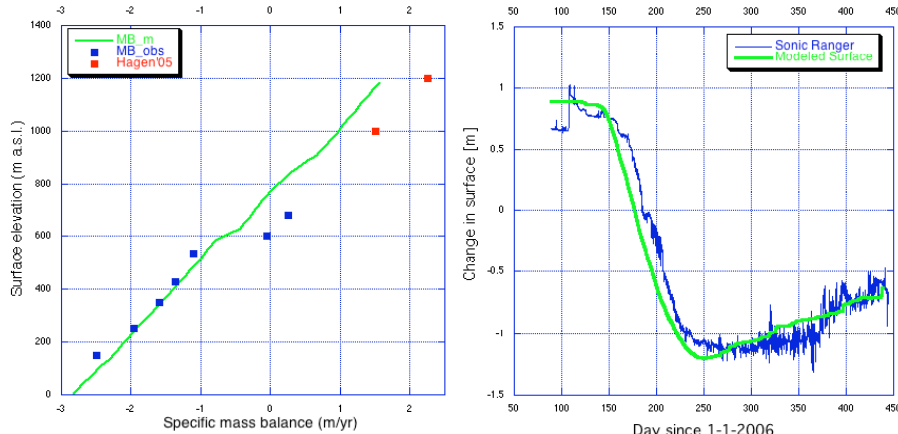
Figure 2. a) Modelled change in surface height (green line) compared to observations with a SR(blue line). Please note that the instrument detached from its housing around day 165. b) Modelled mass balance (green line) compared to mass-balance observations for 2006-2007 (blue dots) and from Hagen and others, 2005 (red dots).

Outlook

- Fine tune the model, including an extensive sensitivity analysis
- Run the model with different input data (Temperature series from GPS, RACMO)
- Extend the model to a 2D topography
- Include a refreezing routine

Acknowledgements

References

ACIA, 2005. Arctic Climate Impact Assessment Report. C. Symon, L. Arris and B. Heal, eds. Cambridge University Press, Cambridge, UK, pp 146.

Hagen, J.O., O. Liestøl, E. Roland, and T. Jørgensen. 1993. Glacier atlas of Svalbard and Jan Mayen. Norsk Polarinst., Oslo.

Hagen, J.O., T. Eiken, J. Kohler and K. Melvold. 2005. Geometry changes on Svalbard glaciers: mass-balance or dynamic response?. Ann. Glaciol., 42: 255-261.

Iken, A. and R.A. Bindschadler. 1986. Combined measurements of subglacial water pressure and surface velocity of findelengletscher, Switzerland: conclusions about drainage system and sliding mechansim. J. Glaciol., 32(110):101–119.

Klok, E.J. and J. Oerlemans. 2002. Model study of the spatial distribution of the energy and mass balance of Morteratschgletscher, Switzerland. J. Glaciol., 48(163), 505–518.

Zwally H.J., W. Abdalati, T. Herring, K. Larson, J. Saba, and K. Steffen. 2002. Surface melt-induced acceleration of greenland ice-sheet flow. Science, 297:218–222.

ICEBERG CALVING FLUX AND MASS BALANCE OF THE AUSTFONNA ICE CAP ON NORDAUSTLANDET, SVALBARD

J.A. DOWDESWELL[1], T.J. BENHAM[1], T. STROZZI[2] AND J.O. HAGEN[3]

[1] Scott Polar Research Institute, University of Cambridge, Cambridge, UK
[2] Gamma Remote Sensing, Gümligen, Switzerland
[3] Department of Geosciences, University of Oslo, Oslo, Norway

Abstract

Satellite radar interferometry, 60 MHz airborne ice-penetrating radar data, and visible-band satellite imagery were used to calculate the velocity structure, ice thickness, and changing ice-marginal extent of Austfonna (8,120 km2 and 2,500 km^3), the largest ice cap in the Eurasian Arctic. Ice-cap motion is less than about 10 m yr^{-1}, except where faster-flowing curvilinear features with velocities of several tens to over 200 m yr^{-1}. Most drainage basins of Austfonna have undergone ice-marginal retreat over the past few decades at an average of a few tens of metres per year. Integrating margin change around the whole ice cap gives a total area loss of about 10 km^2 yr^{-1}. Iceberg flux from the marine margins of Austfonna is about 2.5 ± 05 km^3 yr^{-1} (w.e.), about 45% of the total calving flux from the whole Svalbard archipelago. When mass loss by iceberg production is taken into account, the total mass balance of Austfonna is negative, by between about 2.5 and 4.5 km^3 yr^{-1}. This iceberg flux represents about 33 ± 5% of total annual mass loss from Austfonna, with the remainder through surface ablation. Iceberg flux should be included in calculations of the total mass balance of the many large Arctic ice caps, including those located in the Russian and Canadian Arctic that end in tidewater. The neglect of this term has led to underestimates of mass loss from these ice caps and, thus, to underestimates of the contribution of Arctic ice caps to global sea-level rise.

APPLICATION OF A NUMERICAL ICE SHEET MODEL ON AUSTFONNA, SVALBARD - MODEL PREPARATIONS AND INPUT DATA

THORBEN DUNSE[1], THOMAS V. SCHULER[1,2] AND JON OVE HAGEN[1]

[1] Department of Geosciences, University of Oslo, Norway
[2] Norwegian Water Recourses and Energy Directorate, Oslo, Norway

Covering an area of 8120 km[2], Austfonna on Nordaustlandet, Svalbard is among the largest arctic ice caps outside Greenland (Figure 1). It has a polythermal regime with a simple dome-shaped topography and well defined drainage basins, several of them known to be of surge-type.

Surface elevation measurements since the mid 1990s suggest thickening in the interior and thinning at the margins[1]. There is still considerable uncertainty about to what degree this changes are driven by surface processes (accumulation and ablation) or ice dynamics (possible build-up towards surge activity)[2,3,4]. To better understand both surface processes and glacier dynamics, we complement ongoing glacier observations with numerical modelling.

We use the Simulation Code for Polythermal Ice Sheets (SICOPOLIS), developed by Ralf Greve[5]. The code accounts for different mechanical behaviour of cold and temperate ice regions, separated by a phase-transition surface, called the cold-temperate transition surface, and for which jump conditions of mass, momentum and energy must be fulfilled[6]. It is based on the shallow-ice approximation and uses finite-difference discretization.

Figure 1. Map of Svalbard with the red frame indicating the position of the model domain Austfonna on Nordaustlandet.

Figure 2. Colour-coded bedrock topography of the model domain overlain by a mesh of the
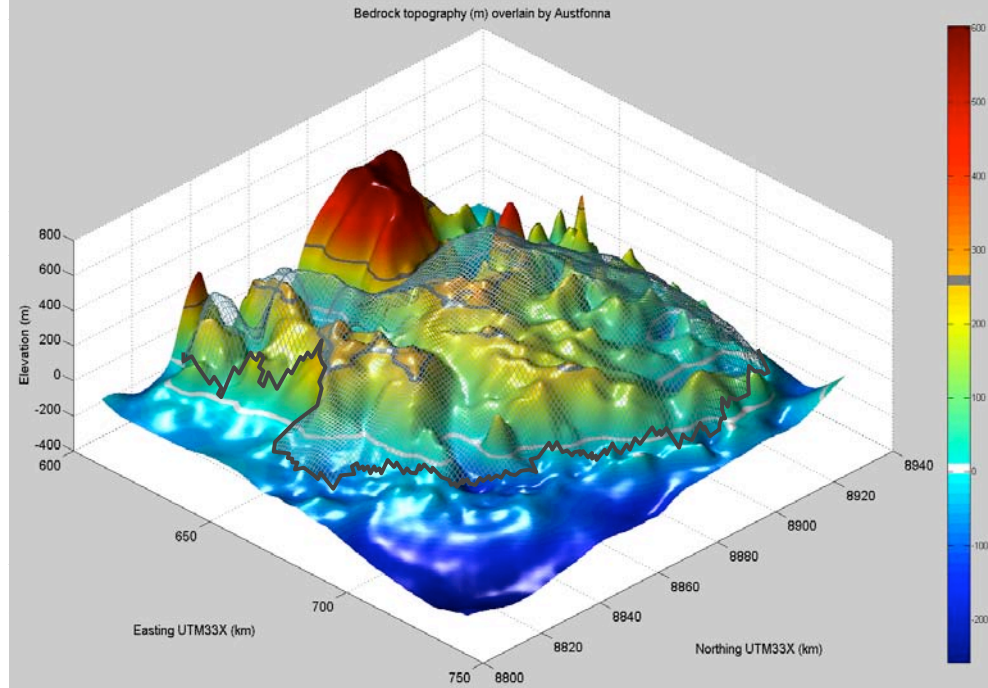
1983-RES survey over Austfonna available.
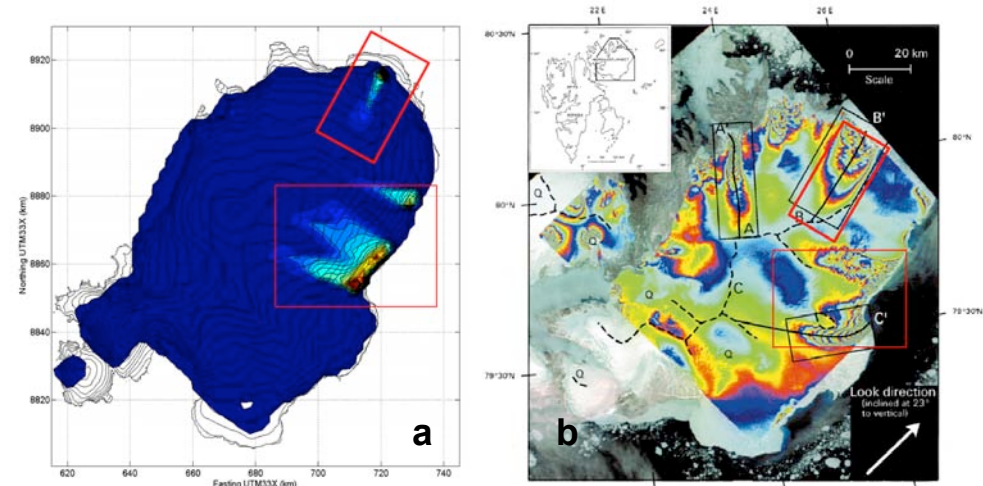
Figure 3. Preliminary model results of the surface velocity field overlying contours of the initial surface topography (a). ERS-1 SAR interferogram superimposed on Landsat image (b), modified from Dowdeswell[4].

References

[1] Bamber, J., W. Krabill, V. Raper, and J. Dowdeswell. 2004. Anomalous recent growth of a part of a large Arctic ice cap: Austfonna, Svalbard. Geophysical Research Letters, 31, L12402-1 – L12402-4.

[2] Bevan, S., A. Luckman, and T. Murray. 2007. Positive mass balance during the late 20th century on Austfonna, Svalbard revealed using satellite interferometry. Annals of Glaciology, 46, 117-122.

[3] Hagen, J.O., T. Eiken, J. Kohler, K. Melvold. 2005. Geometry changes on Svalbard glaciers: mass-balance or dynamic response? Annals of Glaciology, 42, 255 - 261.

[4] Dowdeswell, J. A., B. Unwin, A.-M. Nuttall and D. J. Wingham. 1999. Velocity structure, flow instability and mass flux on a large Arctic ice cap from satellite radar interferometry. Earth and Planetary Science Letters 167, 131-140.

[5] Greve, R. 1995. Thermomechanisches Verhalten polythermer Eisschilde - Theorie, Analytik, Numerik. Doctoral dissertation, Department of Mechanics, Darmstadt University of Technology, Germany, 226 pp. Shaker Verlag, Aachen, Germany.

[6] Greve, R. 1997. A continuum-mechanical formulation for shallow polythermal ice sheets. Philosophical Transactions of the Royal Society London A 355 (1726), 921-974.

[7] Dowdeswell, J. A., D. J. Drewry, A. P. R. Cooper and M. R. Gorman. 1986. Digital mapping of the Nordaustlandet ice caps from airborne geophysical investigations. Annals of Glaciology 8, 51-58.

[8] Schuler, T.V., E. Loe, A. Taurisano, T. Eiken T., J.O. Hagen and J. Kohler. 2007. Calibrating a surface mass balance model for the Austfonna ice cap, Svalbard. Annals of Glaciology, 46, 241-248.

[9] Taurisano, A., T.V. Schuler, J.O. Hagen, T. Eiken T., E. Loe, K. Melvold and J. Kohler. 2007. The distribution of snow accumulation across Austfonna (Svalbard): direct measurements and modelling. Polar Research 26 (1), 7-13.

Greenland surface mass balance using a regional atmospheric climate model

Janneke Ettema[1], Michiel van den Broeke[1], Erik van Meijgaard[2] Jonathan Bamber[3] and Rupert Gladstone[3]

[1] Utrecht University, Institute for Marine and Atmospheric Research, The Netherlands
[2] Royal Netherlands Meteorological Institute (KNMI)
[3] Bristol University, School for Geographical Sciences, UK

Introduction

As part of the RAPID Climate Change program we investigate the effects of rapid climate changes on the surface mass balance and freshwater contributions of the Greenland ice sheet. For this purpose we use the Regional Atmospheric Climate Model (RACMO2.1/GRN). The period September 1989 to December 2005 is simulated to validate the model output with other regional climate model studies and direct mass balance measurements along the K-transect in West-Greenland. This leads to an assessment of the spatial and temporal variability in the surface mass balance (SMB) and its subcomponents.
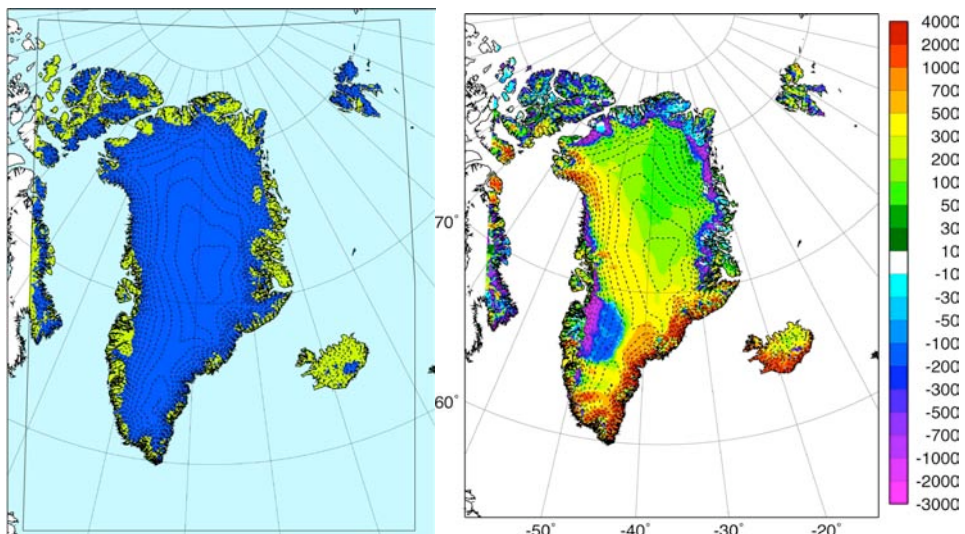
Figure 1. Left: RACMO2.1/GRN model domain for Greenland with dashed height contours every 250 m. Dark blue area is land ice, green tundra and light blue sea or sea ice. Right: annual surface mass balance for 2004 in mm w.e.; values have no meaning over land points.

Model setup

RACMO2.1/GRN is adapted from the second version of the Regional Atmospheric Climate Model (RACMO). It consists of the atmospheric dynamics of the High-Resolution Limited Area Model (HIRLAM) and the physical processes package from the European Centre for Medium-Range Weather Forecasts (ECMWF). To

better represent the conditions on Greenland the multi-layer snow parameterization of Bougamont et al (2005) is implemented. This scheme computes subsurface and snow metamorphism processes like ice and snow melt, percolation and refreezing of meltwater, snow densification and ageing within the upper 25 meter of firn. Feedback between the snow surface and the overlying atmosphere is based on a skin temperature formulation and the surface albedo as function of the snow density of the first firn layer (Greuell and Konzelman, 1994).

The horizontal resolution of RACMO2.1/GRN is about 11 km. The model has 40 hybrid levels in the vertical, of which the lowest is about 10 m above the surface. ERA-40 fields force the model at lateral boundaries complemented with operational analyses until December 2005. Height data of the digital elevation model of Bamber et al. (2001) is used for an accurate topographic representation as shown in Figure 1a.

Model evaluation
The surface mass balance in the model is defined as the total precipitation (solid plus liquid) minus meltwater production and sublimation. The runoff component in the model is incorrectly parameterized, which makes this data unusable for explicit SMB calculation. Therefore, we assume that the meltwater production is an acceptable first order estimate of the runoff. This may lead to an overestimation of the mass loss since part of the meltwater will refreeze in the firn layer.

The pattern of the annual SMB of 2004 shown in Figure 1b agrees with other estimates based on observations (Zwally and Giovinetto, 2001) and models (Fettweis, 2007; Box et al., 2006). The simulated minimum and maximum values are more extreme than in previous estimates. Most mass is gained northeast of Baffin bay and the southeastern coastal area. These areas are associated with steep slopes that enhance solid precipitation rates. The regions with the most negative mass balance occur along the western margin south of Jacobshavn glacier and the northern ice margin where most melt occurs. Due to the low temperatures in the latter area, most of the meltwater will refreeze and actually not contribute to mass loss.
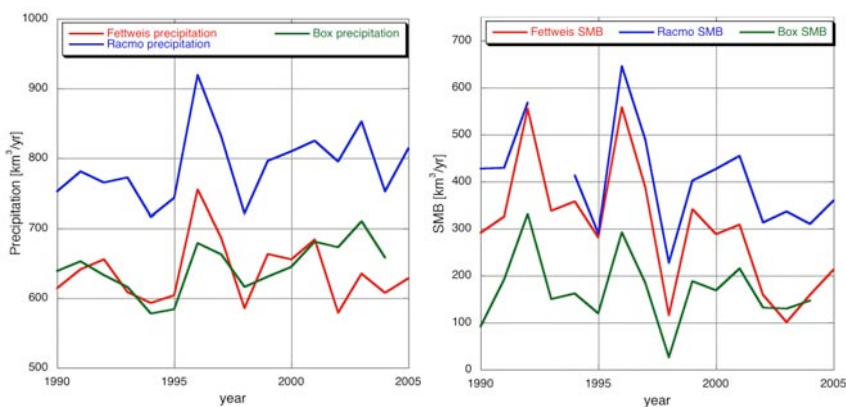
Figure 2. Left: Time series of the annual total precipitation for period 1990-2005. Right: the same plot as a for the annual surface mass balance

The RACMO2.1/GRN annual precipitation rates for the period 1990-2005 are plotted in Figure 2a, together with estimates based on the MAR (Fettweis, 2007) and the polar MM5 model (Box et al., 2006). RACMO2.1/GRN shows an enhanced precipitation rate mainly due to its horizontal resolution of 11 km, where the MAR model is running at 25 km and MM5 at 24 km resolution. The higher precipitation rates in RACMO2.1/GRN lead to a more positive SMB than the other models as seen in Figure 2b. The simulated interannual variability of the different SMB components is consistent with the other models.

In-situ data helps us to determine if the larger precipitation rates simulated are realistic or not. Figure 3 displays the simulated and observed (Van de Wal et al., 2005; complemented by pers. comm. Van de Wal) surface mass balance along the K-transect located at 67°N on the western margin in the ablation zone. For the year 2004, the simulated ablation is slightly weaker close to the ice margin due to an overestimation of winter snowfall, which prevents the darker glacier ice to surface early in the melt season. Overestimation further from the margin may be the result of the assumption that all meltwater produced runs off, while at these locations about half of the meltwater refreezes in the firn. Overall, the modeled values stay within the range of the measurements, which is promising for further validation of the model with other observational datasets.
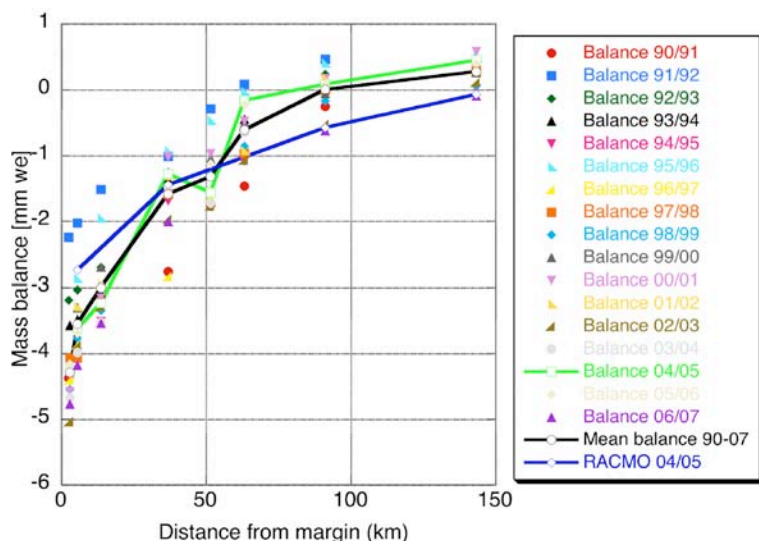
Figure 3. Surface mass balance as function of the distance to the ice margin. Dots are the measurements are for the period 1990-2007; black line is the mean over the entire period; the green line for the year 2004. The blue line is RACMO2.1/GRN for 2004.

Conclusions and outlook
RACMO2.1/GRN is able to simulate a realistic spatial and temporal SMB for the Greenland ice sheet. Compared to other model studies it simulates enhanced precipitation rates, mainly on the steep southeastern slopes. Even with the assumption made that all meltwater produces runs off, the total SMB is more positive than in other estimates.

The stake measurements show a steep gradient in SMB with distance from the margin, which is reasonably represented in RACMO2.1/GRN. Resolving the runoff problem by removing more efficiently the water from the ice surface and refreezing the meltwater in the firn pack will further improve the model agreement.

More validation of the model results is planned for the near future using available automatic weather stations data, ice core accumulation datasets and coastal precipitation gauge data.

References

Andreas, E.L. A theory for the scalar roughness and the scalar transfer coefficients over snow and sea ice. Boundary-Layer Meteorol., 38(1-2):159–184, 1987.

Bamber, J.L., S. Ekholm, and W.B. Krabill. A new, high resolution digital elevation model of Greenland fully validated with airborne laser data. J. Geophys. Res., 106:33773–33780, 2001.

Bougamont, M., J. L. Bamber, and W. Greuell. Development and test of a surface mass balance model for the greenland ice sheet. J. Geophys. Res., 110(F04018), 2005. doi:10.1029/2005JF000348.

Box, J.E., D.H. Bromwich, B.A. Veenhuis, L-S. Bai, J.C. Stroeve, J.C. Rogers, K. Steffen, T. Haran, and S-H. Wang. Greenland ice sheet surface mass balance variability (1988-2004) from calibrated polar MM5 output. J. Climate, 19(12):2783–2800, 2006.

Fettweis, X. Reconstruction of the 1979-2006 Greenland ice sheet surface mass balance using the regional climate model MAR. The Cryosphere Discuss, 1:123–168, 2007.

Greuell, W. and T. Konzelman. Numerical modelling of the energy balance and the englacial temperature of the Greenland ice sheet. Calculations for the ETH-camp location (West Greenland, 1155 m a.s.l.). Global and Planetary Change, 9(1-2):91–114, 1994. doi:10.1016/0921-8181(94)90010-8.

Van de Wal, R.S.W., W. Greuell, M.R. van den Broeke, C.H. Reijmer, and J. Oerlemans. Surface mass-balance observations and automatic weather statiuon data along a transect near kangerlussuaq, west greenland. Ann. Glaciol., 42:311–316, 2005.

Zwally, H.J. and M.B. Giovinetto. Balance mass flux and ice velocity across the equilibrium line in drainage systems of greenland. J. Geophys. Res., 106, 2001.

Changes of geometry of Renardbreen (Spitsbergen) and evolution of morphology of its forefield during the last century

G. Gajek[1], M. Grabiec[2], D. Puczko[3] and J. Jania[2] " \L 3 \N

[1] M. Curie-Sklodowska University, Poland
[2] University of Silesia, Poland
[3] Institute of Geophysics, Polish Academy of Sciences

Introduction

Warming of the climate during the last century caused changes in geometry (volume and extent) of the Arctic glaciers. The process has gained in speed in the recent decades (ACIA, 2005). Such intensive changes can also be observed on Svalbard, in tidewater glaciers. Special cases are the glaciers that – due to geometry changes – have retreated from the sea to land. The presented project covers transformation of tidewater glaciers into land-based ones, on the example of Renardbreen (northwestern Wedel Jarlsberg Land, southern Spitsbergen). The main purpose of the project is to create a model of glaciological and geomorphological processes during such a transformation. This poster presents the geometry changes of the glacier throughout the 20th century, as well as the geomorphological consequences of the recession on its forefield.
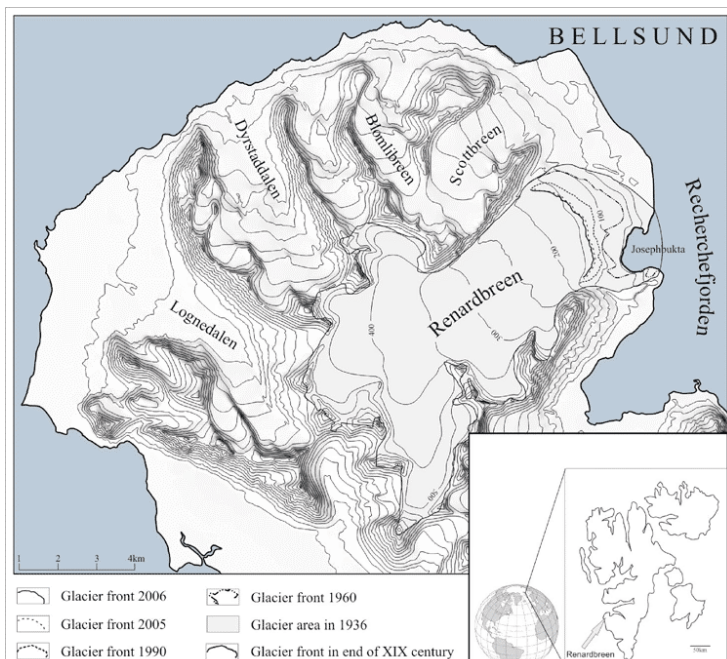

Figure 1. Changes of the Renardbreen glacier area and terminus position during last century.

The glacier and its environmental setting

Renardbreen is located in the central area of the northwestern Wedel Jarlsberg Land (Figure 1). It is surrounded from the west, north and south by the mountains reaching 831 m a.s.l. It is the largest glacier in the area. Its drainage basin covers the area of 39 km^2, while the area of the glacier is 28 km^2 (in 2006). The glacier is 8 km long and its width ranges from 2.5 to 6 km. The glacier surface is exposed towards north-east. The highest parts of the glacier reach 720 m a.s.l. and its front descends almost to the sea level. The tongue of Renardbreen is supplied by six firn fields, amphitheatrically located at 450-550 m a.s.l. The glacier is relatively poorly crevassed. Minor crevasses can be seen in the southern part of the terminus; major crevasses are located in the break of the glacier on 200-250 m a.s.l. In the early decades of the 20th century, the glacier tongue descended towards Recherche Fjord. It is on average 3.5 km wide and it gets slightly wider towards mountain range forefield. In its northern part the ice wall currently lies on transformed, rocky raised marine terraces on the level of several to 40 m a.s.l. and in its southern part it descends almost to the sea level, while it used to reach Josephbukta bay. The glacier snout is flat-protuberant. At present the glacier does not reach the shoreline, although in late 1980s calving of the tongue was observed in the narrow part of the active cliff.

Renardbreen glacier is sub- and supraglacially drained. Subglacial channels function predominantly in the southern and central part of the glacier tongue. The main outflow is located in the central part of the tongue and has a form of a glacier mouth that is 8 m wide and 3-5 m high. The mouth usually activates as late as the second decade of July. The glacier is also hydrologically active during winter, the evidence of which are naled ice covers in its forefield. In the middle of the summer season the total outflow from the glacier reaches approximately 5 m^3/s (Bartoszewski et al., 2006).

Up till 2005, the glacier was not systematically observed from the glaciological point of view. Located nearby is a building, formerly a part of the Calypsobyen mining camp – currently it serves as a base for seasonal expeditions of scientists from Maria Curie-Skłodowska University.

Geometry changes

Evaluation of the geometry changes of Renardbreen was possible thanks to using archival maps, aerial photos, ASTER satellite imagery and GPS measurements. The materials used are as follows:

- Topographic map in 1:100 000 scale, issued by Norwegian Polar Institute, based on oblique aerial photos taken in 1936;
- Photogeological map of Renardbreen, Scottbreen and Blomlibreen forefield in 1:10 000 scale, based on aerial photos from 1960 (Szczęsny et al. 1989);
- Orthophoto map of the northwestern part of Wedel Jarlsberg Land in 1:25 000 scale, based on aerial photos from 1990 (Zagórski 2005);
- GPS measurements carried out using the kinetic method in 2005-2007.

Furthermore, publications on geomorphological research of the region (Reder 1993, 1996) were referred to.

At the end of the 19th century, the glacier wall was reaching the frontal moraine rampart, formed during the Little Ice Age. In 1896, the glacier ended with an ice cliff

in the Recherche fjord, in the area now occupied by Josephbukta bay (Figure 1). Between 1896 and 1936, the cliff recessed by 400 m to the west, which averages to a recession speed of 10 m per year. In 1936, Josephbukta was a small bay, surrounded by an ice cliff from the south, west and north. Between 1936 and 1960 the bay quickly expanded, mainly towards west and north. The northern part of the glacier tongue, neighbouring the moraine ramparts and separated from the waters of the bay, was undergoing a relatively slow frontal recession. At that time, recession of the glacier reached 250-300 m on land and up to 400-500 m by the bay, averaging 16 m per year. The northern part of the tongue recessed at an average speed of 12.5 m per year, while the southern part – at 20.8 m per year, the latter was mainly due to glacier calving.

In 1960, the shape of the ice cliff was irregular, featuring small embayments and tips. It is most probably the result of the influence of the bedrock on the calving frequency and its low speed on shallow waters. At that time, bay expansion into the glacier was hardly noticeable, the ice cliff moved slightly towards the west. Recession of the glacier between 1960 and 1990 totalled to only 292 m, with its pace dropping to 9.7 m per year. However, the northern part, rather little dynamic before, started retreating much faster. During those thirty years, the glacier wall recessed by 684 meters, averaging to 22.8 m per year. Field observations carried out in the early 1990s led – among other things – to the discovery of preserved dry marginal river channels, parallel to the northwestern edge of the glacier wall, and indicated that the recession pace of the on-land part of the glacier wall was about 20 m per year (Reder 1993, 1996).

Table 1. Changes of the Renardbreen glacier area and terminus position during last century

	1936	1960		1990		2005	
		on-land part	bay	on-land part	bay	on-land part	bay
Changes of the Renardbreen terminus position (metres)	0	300	500	984	792	1245	898
changes of the Renardbreen area (km^2)	0		-2,1		-3,4		-4,7
Renardbreen area (km^2)	33		30,9		29,6		28,3

In the spring of 2005, the glacier front extent was measured using differential GPS method. In comparison to 1990, the glacier extent in the northern land based part has decreased by 261 m, and in the southern part (by the bay) – by 106 m. It averages to 17.4 m per year and 7.0 m per year respectively. GPS differential measurements carried out in the spring of 2006 proved that the glacier terminus recessed on average by 12 m when compared to 2005. The recession speed decrease at that time may be connected with the change in the position of the glacier tongue, which retreated to a higher hypsometric level (Table 1).

The glacier front recession is accompanied by the changes in ice thickness. Elevation measurements have been taken in 2005 along two longitudinal profiles in the northern and southern part of the glacier. In the frontal part, glacier height

reduction reached 25-30 m when compared to 1990, which averages to 1.6-2.0 m per year.

Geomorphology of the glacier forefield and its changes

At the time when the glacier descended to the sea, the marginal zone consited of ice-core frontal and lateral moraines and areas of sub-marine glacigenic deposits. The geomorphology of the marginal zone was registered as the photogeological map in 1960 (Szczęsny at al., 1960). Routes of sandur outflow, a few esker ridges and – next to the frontal moraine – kame terrace developed in the central zone. The characteristic form of the forefield is a vast naled ice, upon which fluvioglacial forms are developing. The sediments were deposited by the northern subglacial lateral torrent. They constituted almost 20% of the whole marginal zone at that time. The southern part of the glacier snout had a form of an ice cliff. Sub-marine deposition was related to the ground moraine and the material transported by two subglacial rivers – the central river and the lateral southern river (bedload and suspended matter of turbid subglacial waters).
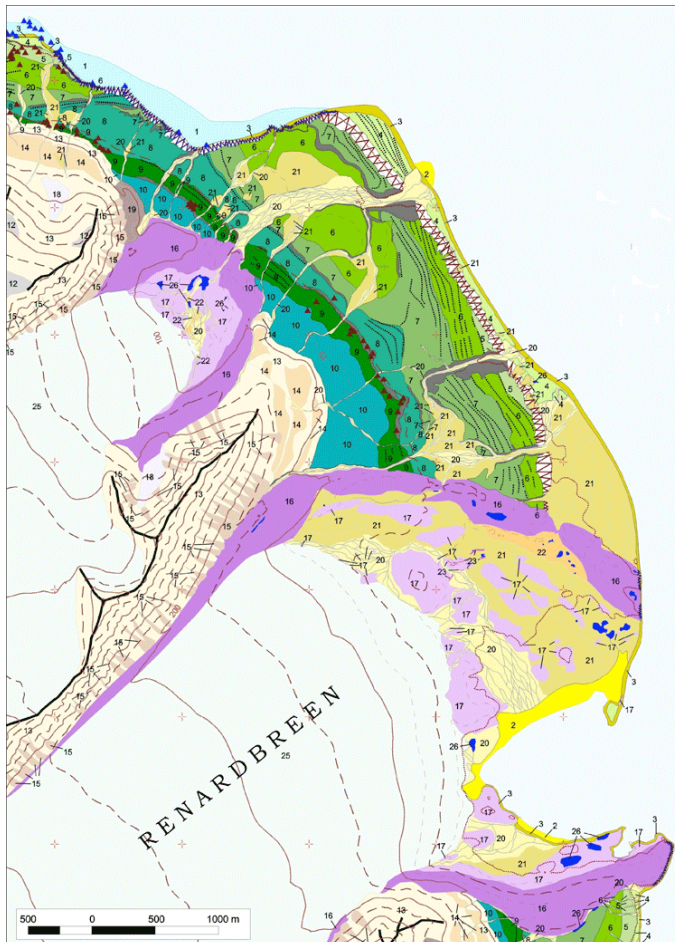

Figure 2. Northwestern part of Wedel Jarlsberg Land (Spitsbergen, Svalbard, Norway). Orthophoto 1:25 000, Zagórski 2005, [ed.] K. Pękala and H. F. Aas.

As a result of the recession of the glacier, its marginal zone expanded significantly by 1990 (Figure 2. Zagórski 2005). Distribution of forms and sediments depends on the topography of the bedrock, i.e. the raised marine terraces, remodelled by glacial processes. Apart from the rock-knobs covered with a thin layer of ground and fluted moraine, large areas are occupied by fluvioglacial sediments, formed by the central outflow among others. The statistics of the area of the marginal zone occupied by particular landforms are as follows: moraines (ablation moraine, terminal and lateral moraine, ground and fluted moraine) occupied 56% of the Renardbreen forefield in 1990, while the fluvioglacial forms (young outwash plains, old outwash plains, kame terraces, delta and others) – 44%.

Conclusions

Recession of the cliff part of the ice wall in the period of intensive calving was faster in comparison to the extent change of the on-land part of the ice wall. When the ice cliff retracted into a shallow bay and the calving slowly died away, the recession rate slowed down from 20 m per year to 10 m per year recently. Transportation of mineral deposits by the subglacial rivers resulted in forming a delta and shallowing of the bay.

Phase 1. The glacier terminates with an ice cliff in the sea. All of the fluvioglacial and ground moraine sediments are deposited in the bay. The bay is being shallowed directly in front of the terminus. The delta emerges and is built up.
Phase 2. Intensive frontal recession takes place. Glacier terminus gets separated from the sea water by the sediments. The ice cliff withers. Ground moraine material is no longer deposited in the bay. The material is transported by subglacial rivers (from the central outflow and minor marginal outflows). Fluvioglacial forms start to dominate on the forefield.
Phase 3. As a result of intensive ablation and predominance of negative mass balance, the recessing glacier uncovers larger area of internal marginal zone, between the ice-moraine ridges and the contemporary edge of the ice wall, in the area of which fluvioglacial accumulation forms start to prevail. The marginal river gains length, and thus the volume of material accumulated in the bay is decreasing. The delta is built up at a much slower rate.

Renardbreen seems to be a good example of the evolution of frontal and marginal zone of Spitsbergen glaciers retreating to the shallow seas. Quantitative analysis of mineral mass transfer from the glacier to its forefield and to the seathe is planned in the next stage of the project.

Acknowledgements

References

ACIA 2005: Arctic Climate Impact Assessment - Scientific Report, Cambridge University Press, 1042 pp.

Bartoszeksi, S., A. Gluza and K. Siwek, 2006. Selected problems of shaping of meteorological and hydrological conditions in the northwestern part of Wedel Jarlsberg Land (Spitsbergen) – The state and changes of natural environment of the northwestern part of Wedel Jarlsberg Land (Spitsbergen) in the conditions of climate change and anthropopressure. 20 Years of Polar Research of the Institute of Earth Sciences UMCS on Spitsbergen, UMCS, Lublin, 53-60.

Reder J. 1993. Contemporary deglaciation of the Recherche and Renard Glaciers in the Bellsund region (Western Spitsbergen). – XX Polar Symposium, Lublin: 421-427.

Reder J. 1996. Evolution of marginal zones during a continued glacial retreat in northwestern Wedel Jarlsberg Land, Spitsbergen. – Polish Polar Res. 17(1-2): 61-84.

Szczesny, R., J. Dzierzek, M. Harasimiuk, J. Nitychoruk, K. Pekala and J. Repelewska-Pekalowa, 1989. Photogeological map of the Renardbreen, Scottbreen and Blomlibreen forefield (Wedel Jarlsberg Land, Spitsbergen, 1:10 000). – UMCS Geographical Expeditions to Spitsbergen. Wyd. Geol., Warszawa.

Some results of radio-echo soundings of frontal parts and forefields of selected glaciers in Svalbard and N Scandinavia

Mariusz Grabiec[1], Wojciech Dobiński[1], Dariusz Puczko[2], Piotr Dolnicki[1]

[1] Faculty of Earth Sciences, University of Silesia, Sosnowiec, Poland,
[2] Institute of Geophysics, Polish Academy of Sciences, Warsaw, Poland

Objectives
This work presents results of GPR surveys performed in a transition zone between glaciers and their forefields on selected locations in Svalbard and Northern Scandinavia. The purpose of the study is to identify relations between glacial and periglacial/paraglacial processes which occur at the glacier termini and in the nearest proglacial area, affected by permafrost (Dobinski 2006).
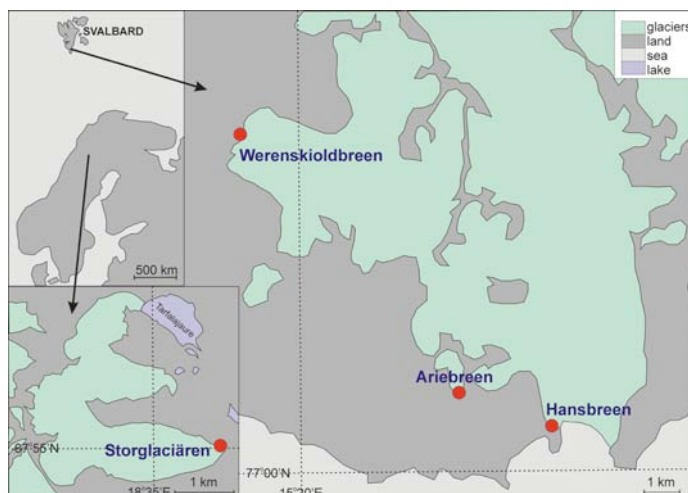
Figure 1. Location of GPR surveys.

Study area
Research was performed in Northern Sweden and the High-Arctic (Svalbard) in August and September 2007 (Figure 1).
- Storglaciären in Northern Sweden is a polythermal valley-glacier partly frozen to the bed with area of about 3.1 km^2 (Pettersson et al 2003).
- Werenskioldbreen (S Svalbard) is a valley-type, polythermal glacier terminating on the land. The surface area of the glacier is about 28 km^2 and the length ca. 7 km. Folding of medial moraine shows that glacier surge took place in the past.
- Ariebreen in Hornsund area is a small (0.4 km^2), entirely cold valley-glacier (Machio et al. 2007).
- Hansbreen (56 km^2) is an outlet glacier calving to Hornsund, with forefield only partly developed on land. It is a typical subpolar glacier with cold ice layer.

Methods

Ground penetrating radar (GPR) was used for data collection for the study. GPR is an effective tool for identifying the sedimetological structure of subsurfaces of the lithosphere (Neal 2004). Particularly good survey depth has been found in glaciological research (Jansson et al 2000). At periglacial areas affected by ice-reach permafrost this method has been also applied (Moorman at al 2003). In our work the research was performed in glacial as well as in periglacial environments.

Surveys were performed with using ground-penetrating radar Ramac/GPR CUII, equipped with unshielded 200 Mhz antennas. GPR surveys were conducted along profiles, which started on frontal part of the glacier and finished on its forefield. GPS receiver was used for recording position and distance of survey profile.

Radexplorer software and filters: DC removal, time-zero adjustment, background removal, amplitude correction, trace edit, topography and radio-wave velocity models were used for data processing and analysis.

Radio-wave velocity in the glacier ice and in the forefield sediments was calculated based on common mid-point (CMP) surveys. In the ice radio-wave velocity of 16 cm/ns has been calculated as a typical value. On the forefield affected by permafrost the recorded velocity value was of about 10 cm/ns, whereas published values of velocity for permafrost are slightly higher: 11-15 cm/ns (RAMAC/GPR Operating Manual).

Temperature measurements made with Pt100 thermistors gave indirect information about buried ice existence.

Results

Analyzed GPR profiles show some common features as well as some differences. In all cases contact between the glacier and its bed was detected and it is visible very clearly (Figure 2). The permafrost table is also clear-cut noticeable. The depth of permafrost active layer is going to be thinner in the direction towards the glacier front. Thickness of this layer is variable and reaches its maximum of about 2.8 m at Storglaciären forefield (Figure 2.IV). On the forefield of Svalbard glaciers the active layer is no more than 2 meters deep (Figure 2.I-III).

On the presented graphs ice cores and other types of buried ice have been also found. In the frontal/lateral moraine of Hansbreen an ice-core is very likely (Figure 2.I). Its thickness might be more than 5 meters. Ice-cored moraines are common in vicinity of the measurement site. Summer ground temperature courses on the moraine are also typical, as for places where massive ice was detected. Ground temperature increase is remarkably slower than in tundra with no ice body beneath. Similar features in Ariebreen frontal moraine can be observed (Figure 2.III).

On Werenskioldbreen forefield, in general, the permafrost table is equal to the depth of the buried ice (Figure 2.II). Thickness of this layer varies between 1.5 and 2.5 m. Existence of massive ice covered by fluvioglacial sediments can be directly verified in profiles cut out by the proglacial river. The thickness of the ice core/ice layer is up to 6 m and sharply decreases in the direction towards glacier terminus,

which is covered by the debris cover. It seems to be possible that the glacier front has connection with not active ice on the forefield, as it is shown in Etzelmüller and Hagen (2005). Close to the front of Werenskioldbreen, in places where the ice is sufficiently thin, big outburst of subglacial water might occur. Massive ice-bodies were not detected on the forefield of Storgläciaren (Figure 2.IV). In this location on the radargram also several englacial debris bands are visible. These bands are parallel to the foliation in the ice and hence have an arcuate shape.
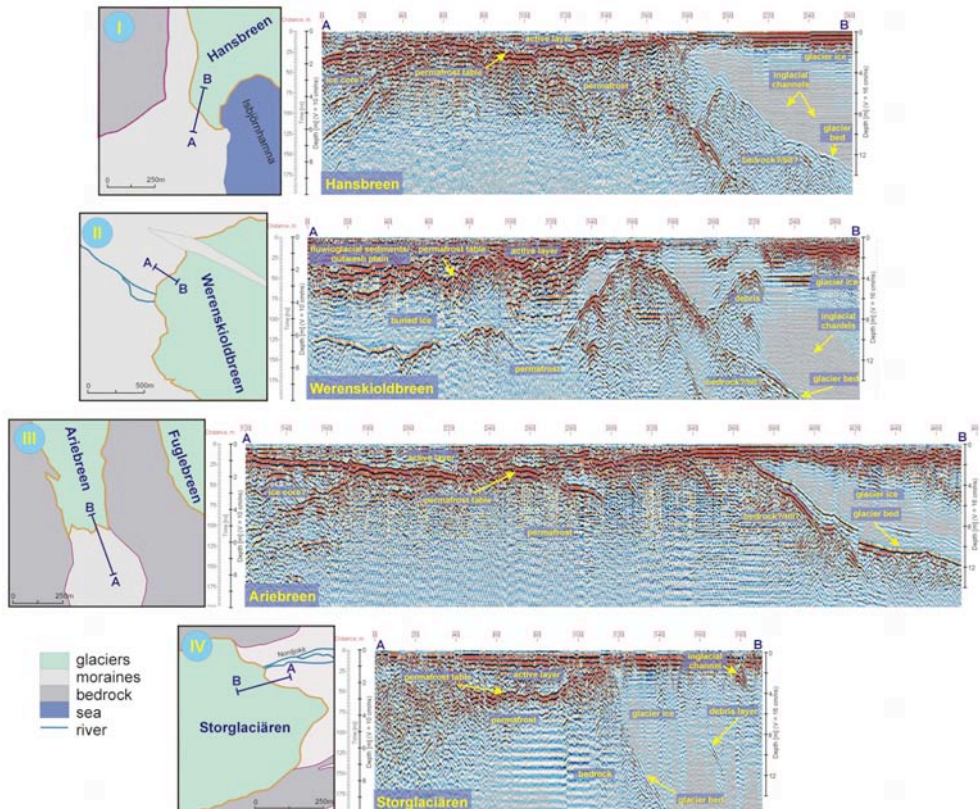
Figure 2. Examples of GPR sections and interpretation on selected glaciers and their forefields (uncorrected for topography): I – Hansbreen, II – Werenskioldbreen, III – Ariebreen, IV - Storgläciaren.

Conclusions

- Ground penetrating radar with 200 Mhz antennas is the effective tool for research in glacial and periglacial environments especially for active layer, buried ice and glacier ice detection.
- The general scheme of overlapping glacial and periglacial environments occurs in different parts of Arctic with some varieties.
- The occurrence of buried ice and ice-cored moraines on glacier forefields is more likely in High Arctic than in lower latitudes. The thickness of buried ice bodies detected on Svalbard may reach 6 m or even more.

- The active layer is thinning towards glaciers' fronts and the depth of permafrost table varies from 2.8 m in Low Arctic to 1.5 m on Svalbard.
- The transition of ice from the glacial into the periglacial zone is gradual and the glacier ice becomes an element of the periglacial environment by losing its movement steadily.
- In permafrost affected areas application of other geophysical methods i.e. electroresistivity tomography can give more complete insight in the distribution of permafrost.

Acknowledgements

References

Dobinski W 2006: Ice and environment: A terminological discussion. Earth Science Reviews 79: 229-240

Etzelmüller and Hagen 2005. Glacier – permafrost interaction in Arctic and alpine mountain environments with examples from southern Norway and Svalbard. In: Harris C., & Murton J.B., (eds.) 2005. Cryospheric systems: Glaciers and Permafrost. Geological Society, London, Special Publications, 242, 11-27

Jansson P., Näslund J-O., Pettersson R., Richardson- Näslund C., Holmlund P., 2000. Debris entrainment and polythermal structure in the terminus of Storglaciären. In: Debris-Covered Glaciers (Proceedings of a workshop held at Seattle, Washington, USA, September 2000).IAHS Publ. no. 264, 2000. 143-151

Machio F., Lapazaran J., Dolnicki P., Petlicki M., Głowacki P., Nawarro F., 2004. Preliminary results of radio-echo sounding at Ariebreen, Hornsund Spitsbergen. In: The Dynamics and Mass Budget of Arctic Glaciers. Extended abstracts. Workshop and GLACIODYN (IPY) Planning Meeting, 15 - 18 January 2007, Pontresina (Switzerland), 64 – 66

Moorman B.J., Robinson S.D., Brugess M.M. 2003. Imaging periglacial conditions with ground-penetrating radar. Permafrost and Periglacial Process. 14. 319-329.

Neal A., 2004. Ground-penetrating radar and its use in sedimentology: principles, problems and progress. Earth-Science Reviews 66: 261–330

Pettersson, R., P. Jansson and P. Holmlund. 2003. Cold surface layer thinning on Storglaciären, Sweden, observed by repeated ground penetrating radar surveys. J. Geophys. Res., 108(F1), 6004. (10.1029/2003JF000024.)

RAMAC/GPR Operating Manual 1997. Version 2.28. Malå Geoscience. Appendix 1.

Glacier geometry change in the Forlandsundet area (NW Spitsbergen) using remote sensing data

Marek Grześ, Michał Król and Ireneusz Sobota

Department of Cryology and Polar Research, Institute of Geography, N. Copernicus University, Poland

Fluctuations of glacier ranges are one of the basic elements in the study of their geometry changes. The studies of the fluctuation of the glaciers in the Forlandsundet area (NW Spitsbergen) were made in three main regions: Kaffiøyra, St. Jonsfjorden and Prins Karls Forland. The investigations refer to mountain and calving type glaciers.

The main investigative aim of this article is to estimate and interpret changes of glacier ranges in the Forlandsundet area in the XX and XXI centuries by remote sensing data and field measurements.

We used ASTER ortho-images and a digital elevation model derived from 3N and 3B bands to determine the fluctuations of the glaciers. The data analysis confirmed that most of the glaciers in this area are in a recession phase (Figure 1). In the 21th century the rate of recession increased. The most quickly retreating are the calving type glaciers - Aavatsmarkbreen, Konowbreen, Osbornebreen and Dahlbreen. The front of the Aavatsmarkbreen retreated from 2000 to 2006 max. about 700 m (100 m/y). Between 2000 and 2006, the glacier area reduced by over 1.6 (km^2/y). The glaciers terminating in the sea were characterized by a distinct retreat at the beginning of 21th century. The six small valley glaciers in Kaffiøyra in this period retreated several m/year. Maximum glacier front recession in the period 2000-2006 we noted on the Osbornebreen (700-800 m/y). The retreat and mass loss noted on almost all these glaciers have been observed on entire Spitsbergen. The recession (retreat and mass loss) is triggered by changes in climatic conditions. Due to various factors of the topoclimatic - geomorphologic nature, the recession has taken a diverse course with respect to particular glaciers.

Moreover in this article we present the results of soundings profiles made during the summer seasons 2004, 2005 and 2006 on chosen calving type glaciers. Based on submarine relief evidence and marginal zones we made an attempt to determine old zones of glaciers (at glacial episode 3.0-2.5 ka BP and Late Vistulian 13-10 ka BP).

One of the key issues while modelling subaqual glacial relief is the dynamics of the ice cliffs. The research carried out by Brown et al. (1982), Boulton (1986) and Jania (1986) showed that ice cliffs can undergo considerable fluctuations in short periods of time (such as a hydrological year or a balance year), irrespective of the general recessive tendency characteristic for most Spitsbergen glaciers. Moreover, these oscillations are much larger than the rate of the multi-year recession. This means that during a balance year, mainly in May and June, a glacier advances as a result

of 'using' the masses of snow delivered in winter; it also has minimal rate of ice cliff calving. Winter advance may result in pushing glacial and fluvioglacial deposits up, thus forming annual small push moraines. It often happens that the distance between these moraines equals the mean annual recession. Accumulation of larger push moraines, both subareal and subaqual ones, is predominantly connected with intensive dynamics of movement and surge (Jania 1988).
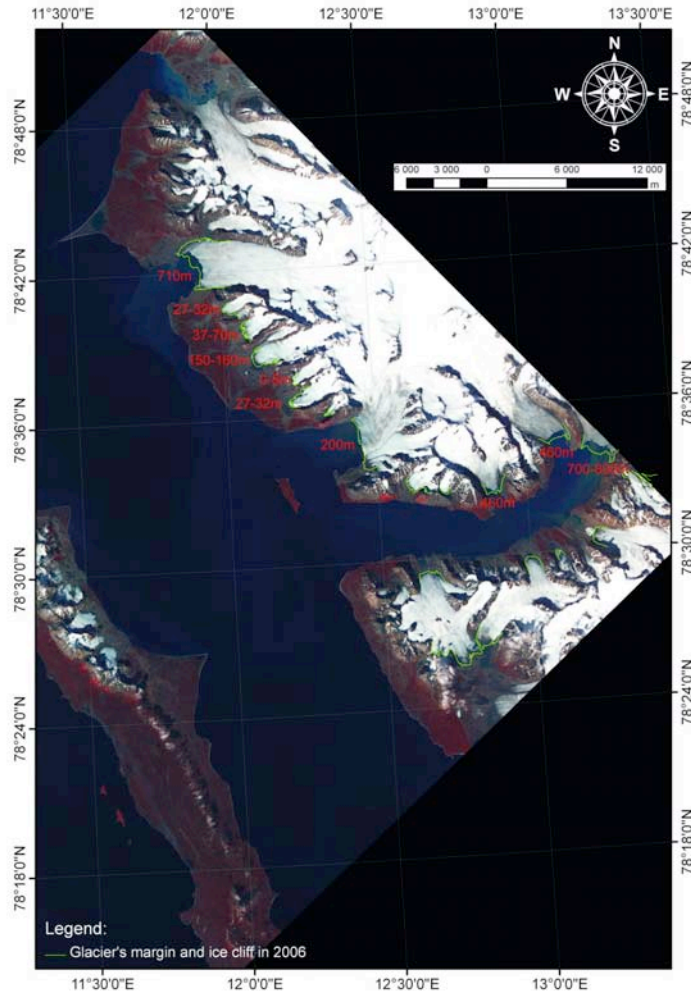
Figure 1. The retreat of glaciers in Forlandsundet region (Spitsbergen). Numbers means the maximum recession of a front of glaciers in the period 2000-2006.

Using the forms of the sea bottom and of the land marginal zones the author tried to delimit the old ranges of the Aavatsmarkbreen and Dahlbreen. As the first results show, the subaqual relief of the sea forefield of the selected glaciers was created by pushing both glacial and marine material up by the anchored zone of a glacier which ends in the sea. In the presented profiles perpendicular to the ice cliffs forms both seasonal and multi-annual oscillations are visible. Seasonal forms (Fig. 2) are from 3 to 10 m high; their genesis is probably connected with the winter re-advance

of the ice front. Such a mechanism has already been described in the literature by Boulton (1986) and Jania (1988). Marsz (1987) states a longer stagnation of an ice cliff with an underwater bottom leads to the formation of a subaqual frontal moraine at the foot of the cliff.
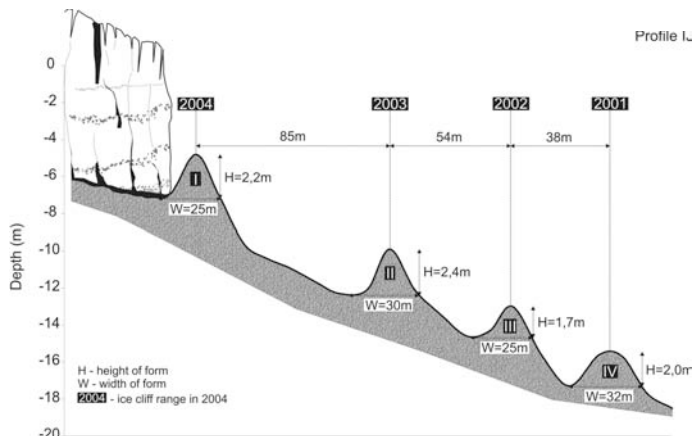
Figure 2. Annually push moraines in the forefield of Aavatsmarkbreen formed between 2004 and 2001 H- height of form, W- width of form, 2004- ice cliff range in 2004.

The oldest range of Dahlbreen, recorded in the sea bottom relief, is probably connected with the glacial episode of 3.0-2.5 ka BP. It is, however, smaller than the one delimited by Szupryczyński (1983). A trace of the Little Ice Age is clearly visible in the bottom relief. It corresponds with the deposits of that age left on the land (Grześ et al. 2007, Lankauf 2002). Morphogenetic analysis of the subaqual forms of the sea bottoms where the studied glaciers end needs further research. However, their sequence as well as the fact that they correspond with the old ranges of glaciers proves their glacial genesis. Echo sounders' results of the surging Aavatsmarkbreen are also interesting.

References
Boulton G.S., 1986. Push-moraines and glacier-contact fans in marine and terrestrial environments, Sedimentology, 33, 677-698.
Brown C.S., Meier M.F., Post A. 1982. Calving speed of Alaska tidewater glaciers, with application to Columbia Glacier. U.S. Geological Survey Professional Paper 1044-9612, C1-C13.
Grześ M., Król M., Sobota I. 2007. Subaqual recordings of the changes in the range of glaciers in the Forlandsundet region (NW Spitsbergen). Landform Analysis, 5, 148-150.
Jania J. 1986. Dynamika czół spitsbergeńskich lodowców uchodzących do morza (Dynamics of the Spitsbergen tidewater glaciers fronts - Engl. summary), Geographia, Studia et dissertationes, vol. 9, Uniwersytet Śląski, Katowice.
Jania J. 1988. Dynamiczne procesy glacjalne na południowym Spitsbergenie (w świetle badań fotointerpretacyjnych i fotogrametrycznych), Prace Naukowe Uniwersytetu Śląskiego w Katowicach Nr 955, Katowice. pp. 257.
Lankauf K.R. 2002. Recesja lodowców rejonu Kaffiøyry (Ziemia Oskara II-Spitsbergen) w XX wieku, IG i PZ PAN, Warszawa, pp. 221.
Marsz A. 1987. Brzegi lodowe, Wydawnictwo Polskiej Akademii Nauk, Wrocław, pp. 117.
Szupryczyński J. 1983. Some problems of the Quaternary on Spitsbergen, [in:] Studies in Quaternary Geomorphology, Geo Books, Cambridge, pp. 149-156.

Recent changes in surface mass balance of the Austfonna ice cap, Svalbard

Jon Ove Hagen[1], Trond Eiken[1], Thomas V. Schuler[1], Thorben Dunse[1], Kjetil Melvold[1], Geir Moholdt[1], Andrea Taurisano[2], Ola Brandt[2] and Jack Kohler[2]

[1] Department of Geosciences, University of Oslo, Norway
[2] Norwegian Polar Institute, Tromsø, Norway

Austfonna (79.5°N, 25°E) at 8120 km^2 is by far the largest ice cap in Svalbard and one of the largest in the Arctic. The ice cap has a maximum elevation of about 800 m a.s.l., a thickness up to about 560 m (Dowdeswell and others, 1986) and a relatively simple geometry, characterized by one main dome feeding a number of drainage basins. Austfonna is polythermal, and probably much of the bed is at the pressure melting point. Most of its boundary is calving and several of the outlet glaciers are of surge-type (Dowdeswell, 1986; Hagen and others, 1993) (Figure 1). For example, when an outlet from Austfonna, Bråsvellbreen, surged in 1936, the front advanced c. 10 km out into the sea over a width of about 10 km.
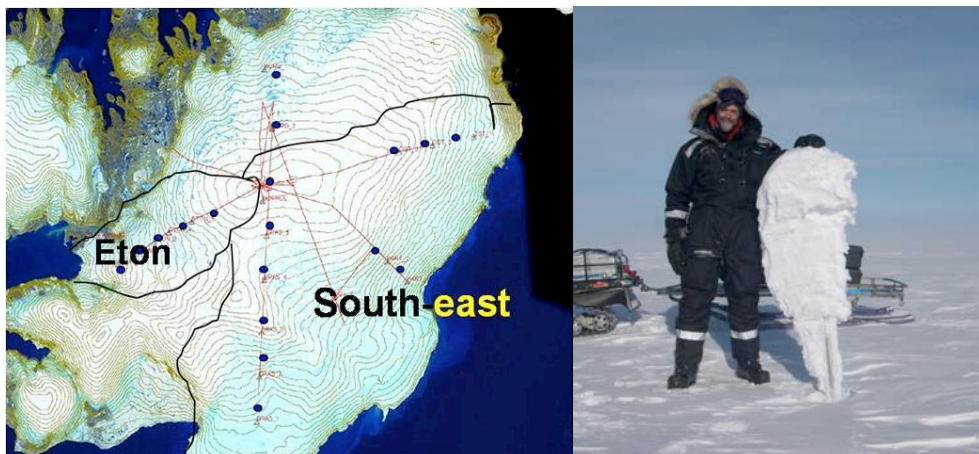
Figure 1. Austfonna and the stake net marked with dots. To the right typical riming on the stakes is shown.

Austfonna is a target glacier for the IPY Glaciodyn project and also selected by ESA as a CalVal site for CryoSat II. A number of investigations have been carried out since 2004, these include GPS-elevation profiles, GPR measurements of the snow thickness and snow distribution, operation of two Automatic Weather Stations, shallow cores, snow pits and mass balance stakes. In spring 2004, 20 mass balance stakes were deployed across the ice cap (Figure 1). This network of stakes has been maintained since then. The stakes have been remeasured once a year, during the annual visits in springs 2005, 2006 and 2007. During the spring

measurements the snow thickness at each stake is measured and thus we get the height of the stakes above the previous summer surface. From these measurements we derive the annual net surface mass balance at each stake location. Riming is a serious problem for all installations on Austfonna, so every year some of the stakes disappear probably because they break down due to heavy riming (Figure 1).

The dominant precipitation direction for Austfonna is from the east. This explains the general pattern of snow accumulation across the ice cap, which shows a pronounced gradient from high values in the SE to lower ones in the NW (Pinglot and others, 2001; Taurisano and others, 2007). The distribution of snow thickness is measured using extensive GPR-profiling together with manual snow thickness probing, and the snow water equivalent is obtained from density measurements in snow pits. The winter snow accumulation varies from year to year by 100 %, but the pattern of the snow distribution is fairly stable, often with about three times more snow in the south-east than in the north-west (Taurisano and others, 2007). The snow thickness is usually between 0.5 m up to 3 m (Figure 2).
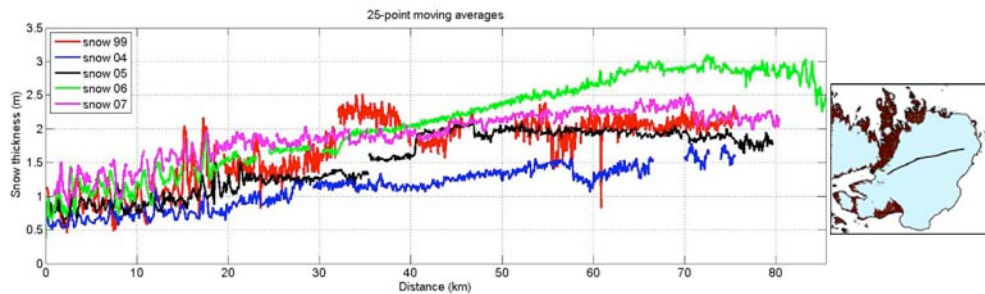
Figure 2. Snow distribution and yearly variations across Austfonna.

The net mass balance of Austfonna has been calculated for the period 1986 to 1999 based on shallow core data (Pinglot and others 2001). They drilled altogether 29 shallow cores across the ice cap in 1998 and 1999. The depth down to the Chernobyl fallout in 1986 was found in 19 cores in different elevations in the accumulation area. Thus they could estimate the net mass balance gradients and calculate the mean overall net surface mass balance to be very close to zero:
$B_n = \sum b_{ni} (z) \cdot A_i [10^9 \text{ m}^3]$, $B_n \sim 0 \text{ km}^3$,

Surface elevation measurements both by airborne laser profiling in 1996 and 2002 (Bamber and others 2004) and using our own ground-based GPS profiles show a clear thickening in the interior and a thinning along the lower parts of the ice cap. Bamber and others (2004) suggest a recent increase in precipitation being responsible for this. Bevan and others (2007) have suggested that the mass balance over this period was positive, based on the laser data, the shallow core data and satellite radar interferometry for flux calculations.. Bevan and others (2007) stressed that the result emphasizes the importance of considering the dynamics of glaciers when attempting to draw any conclusions on climate change based on snapshot observations of the cryosphere.

We calculated the average net mass balance in two large parts of the ice cap, Etonbreen and South-East area as shown in Figure 1. In each of these areas the net balance gradient was plotted and assuming that the stakes are representative for each elevation band, the basin net balances and the overall total net balance were calculated (Figure 3). The two areas cover ca. 4670 km^2 (of 8120 km^2). The mean total surface net balance for the whole of Austfonna is then given by:

$B_n = \sum b_{ni} (z) \cdot A_i [10^9 \ m^3]$ yielding $B_n \sim$ - 2 km^3,

and the mean specific net balance:

$b_n = B_n / A [m] = - 0,25 \ m \pm 0,1 \ m.$
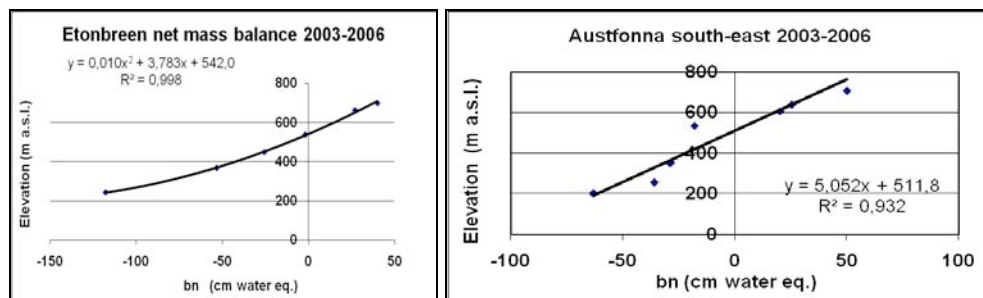
Figure 3. Average mass balance gradients for the period 2003 – 2006 plotted as a polynomial curve at Etonbreen basin and as a linear curve on the South-East area.

Schuler and others (2007) used a degree-day approach to model mass balance for the same period as the measured surface balance and for the year 2004 they came up with a negative balance: b_n 2004 = - 0,32 m w.eq. The model agrees well to a number of observations including specific balance at stakes, snow accumulation from GPR, snow distribution at the end of summer as derived from satellite imagery and sonic ranger records of ice melt.

New shallow cores drilled in 2004 and 2006 at three of the former locations in the upper accumulation area of the ice cap indicated no recent increase in the precipitation since 1999. So we stress again the importance of understanding the dynamics of an ice mass when interpreting observed geometry changes (Hagen and others 2005, Bevan and others 2007).

Compared to the previous results by Pinglot and others (2001), the surface net mass balance is clearly negative after 2003, while it was close to zero for the period 1986 – 1999. However, we have only three years of data and these also include the very warm summer of 2004 were melting was observed high up on the ice cap.

References
Bamber, J.L., Krabill, W.B., Raper, V. and Dowdeswell, J.A., 2004. Anomalous growth of part of a large Arctic ice cap: Austfonna, Svalbard. Geophysical Research Letters, 31, L12402, doi.10.1029/2004Gl019667.

Bevan, S., Luckman, A., Murray, T., Sykes, H. and Kohler, J., 2007. Positive mass balance during the late 20th century on Austfonna, Svalbard, revealed using satellite radar interferometry. Annals of Glaciology, 46, 117-122.

Dowdeswell, J.A., 1986. Drainage-basin characteristics of Nordaustlandet ice caps, Svalbard. Journal of Glaciology, 32, 31-38.

Dowdeswell, J.A., Drewry, D.J., Cooper, A.P.R, Gorman, M.R., Liestøl, O. and Orheim, O., 1986. Digital mapping of the Nordaustlandet ice caps from airborne geophysical investigations. Annals of Glaciology, 8, 51-58.

Hagen, J.O., Liestøl, O., Roland, E., Jørgensen, T., 1993. Glacier Atlas of Svalbard and Jan Mayen. Norsk Polarinstitutt, 141 pp.

Hagen, J.O., T. Eiken, J. Kohler and K. Melvold, 2005. Geometry changes on Svalbard glaciers: mass-balance or dynamic response? Annals of Glaciology 42, 255-261.

Pinglot, J.F., Hagen, J.O. Melvold, K. Eiken, T. and Vincent, C., 2001. A mean net accumulation pattern derived from radioactive layers and radar soundings on Austfonna, Nordaustlandet, Svalbard. Journal of Glaciology, 47, 555-566.

Schuler, Thomas; Loe, Even; Taurisano, Andrea; Eiken, Trond; Hagen, Jon Ove; Kohler, Jack. 2007. Calibrating a surface mass balance model for the Austfonna ice cap, Svalbard. Annals of Glaciology, 46, 241-248.

Taurisano, A., Schuler, T.V., Hagen, J.O., Eiken, T., Loe, E., Melvold, K. and Kohler, J., 2007. The distribution of snow accumulation across the Austfonna ice cap, Svalbard: direct measurements and modelling. Polar Research, 26, 7-13.

THE ROLE OF BASAL FRACTURES IN STORING AND ROUTING WATER

JOEL HARPER[1], JOHN BRADFORD[2], NEIL HUMPHREY[3], TAD PFEFFER[4] AND TOBY MEIERBACHTOL[1]

[1] Department of Geosciences, University of Montana
[2] Center for the Geophysical Investigation of the Shallow Subsurface, Boise State University
[3] Department of Geology and Geophysics, University of Wyoming
[4] Institute of Arctic and Alpine Research, University of Colorado

Introduction

Interest has grown in the role of the glacier hydrologic system in ice sliding due to recent observations of increased surface melt of Arctic Glaciers and the margins of the Greenland Ice Sheet (e.g., Mote, 2007). Fractures in glaciers have received growing attention as an important mechanism for routing water from the surface to the bed of glaciers. For example, Boon and Sharp (2003) documented the drainage of a supraglacial lake to the bed via a newly opened fracture, and observations at Storglaciären were used to postulate that englacial fractures are the primary pathway for routing surface water to the bed (Fountain et al., 2005). Here we investigate the role of englacial fractures in storing basal water.

Methods

Field experiments were conducted at Bench Glacier, Chugach Mountains, Alaska. Bench Glacier is a temperate valley glacier ~8km long with a straight and simple geometry. The ice is 180-200 m thick along most of the ablation zone. We conducted experiments in more than 50 boreholes drilled to the bed of the glacier with a hot water drill. Borehole video observations were used to quantify the orientation and distribution of englacial fractures. Dye tracing experiments using a pair of down-hole fluorometers were used to document pathways and rates of water flow through the fractures. Radar surveys using 3D and multi-offset data acquisition schemes imaged the spatial extent and orientation of cracks within the ice mass. Lastly, water level monitoring in a network of boreholes during the drilling of new boreholes quantified englacial water connections and head gradients.

Results and Conclusions

Our multi-faceted observations can be used to draw three main conclusions about fractures at Bench Glacier.

First, fractures are common and are concentrated in lower two thirds of the ice mass. Borehole video observations documented open fractures in every borehole with an average of 2 per hole (Figure 1). The fractures are always steeply dipping, and range in size from a few centimeters up to about 1 m across (Figure 2). Measurements of fracture orientation show their orientation rotates at depth following the stress field. Radar profiling shows that scattering events (from water filled macro scale voids) are concentrated in the lowest two thirds of the ice mass, and distinctly lacking in the 20-50 m of ice below the surface.
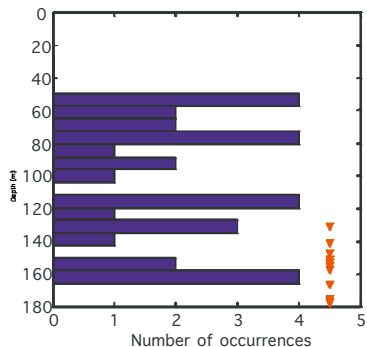
Figure 1. Histogram showing open fractures logged with a borehole video camera lowered through 16 boreholes drilled in 2003. Logging was terminated above the bed due to turbid water; red triangles show depth where logging was terminated for various holes. The histogram is biased toward shallow depths since the lowest 10-20% of the boreholes were not logged.

Second, many fractures are connected to bed. Drilling experiments showed that boreholes frequently drain or fill during the drilling process, suggesting water drains to the bed via englacial connections (Figure 3). Video observations show open fractures coincident with the location of the drill tip at the time of a draining event. Also, dye tracing experiments revealed water in boreholes was preferentially routed down fractures intersecting the borehole, rather than past the fracture and down the borehole.

Figure 2. Photograph from borehole video camera showing typical open fracture. Fracture depth is 116 m below the ice surface. Vertical bright line is a signal cable which can be seen entering the borehole at the base of the fracture.

Third, some fractures open upward from the bed. We collected two separate time lapse video sequences that show fractures opening with turbid water and upward water flow. In 2002, for example, filming of a borehole just after drilling revealed no open fractures in the lower half of the glacier. Eleven days later we filmed the hole and observed vigorously upwelling turbid water and frazzle ice formation at a depth of 139 m (35 m above the bed). Over a period of several days the turbidity settled and a new ~15 cm diameter fracture was visible. In fact, the fracture had displaced the borehole with respect to gravity and the camera could no longer be lowered into the borehole and would only follow the open fracture when lowered. Water was clearly flowing up the borehole from a lower depth and then back down the fracture. A similar observation of fracture opening was also made in 2006.

Fracture volume and basal water storage.
We estimated fracture volume from geophysical inversion of radar data (Bradford and Harper, 2005) and from direct observation of fractures via borehole video. Based on our sampling of fracture volume, we estimate that the fractures maintaining an open connection to the bed occupy 0.5% to 3% of the ice mass by

58

volume in the lowest 60 m of ice. The storage capabilities of this fracture space equates to a layer of water between 3 cm and 18 cm thick covering the bed. Fractures may therefore be an important element of subglacial drainage system development due to their ability to store and release water. Further, they likely play an important role in the interplay between water and sliding dynamics.
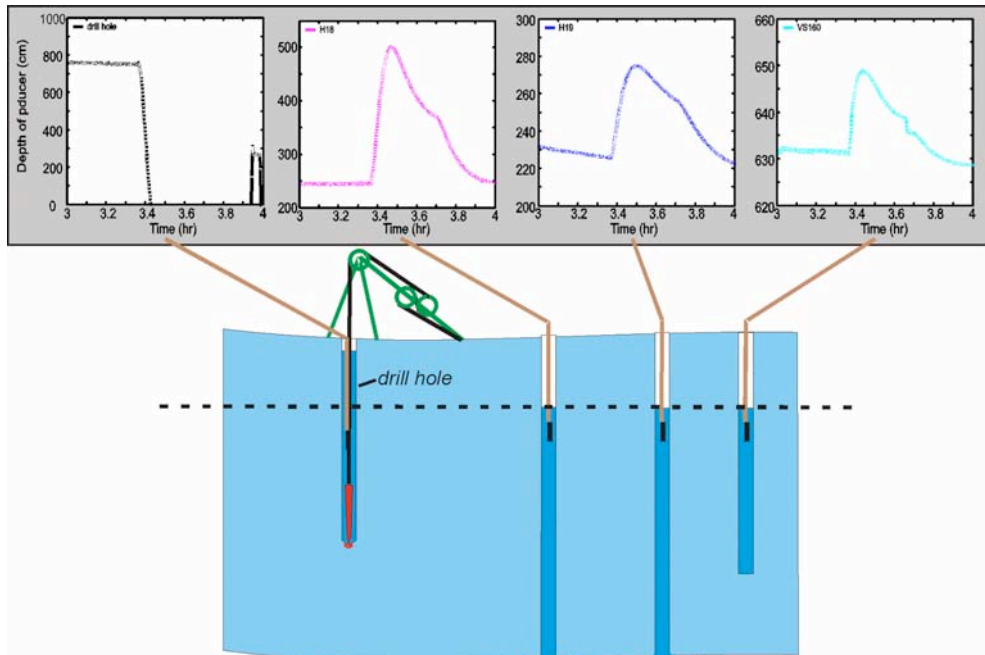
Figure 3. Schematic showing setup of borehole drilling experiments (lower graphic) and response curves during a draining event (upper plots). Water levels were monitored in up to six boreholes while a new borehole was being drilled. Dashed line shows approximate piezometric surface defined by borehole intersections with the bed. Top left plot shows draining of high head in the drill hole (which is artificially high due to the addition of drilling water) at 100 m below the surface and 60 m above the bed. Upper right three plots show simultaneous rise in water levels in boreholes when the drill hole drained. A rise even occurred in a borehole which terminated 20 m above bed (far upper right plot).

References

Boon, S., and M. Sharp (2003), The role of hydrologically-driven ice fracture in drainage system evolution on an Arctic glacier, Geophysical Research Letters, 30(18).

Bradford, J. H., and J. T. Harper (2005), Wavefield Migration as a Tool for Estimating Spatially Continuous Radar Velocity and Water Content in Glaciers, Geophysical Research Letters, 32(L08502), doi:10.1029/2004GL021770.

Fountain, A. G., et al. (2005), Fractures as the main pathways of water flow in temperate glaciers, Nature, 433(7026), 618-621.

Mote, T. L. (2007), Greenland surface melt trends 1973-2007: Evidence of a large increase in 2007, Geophysical Research Letters, 34.

Meltwater runoff and firn densification in the percolation facies, Greenland Ice Sheet

Joel Harper[1], Neil Humphrey[2], Tad Pfeffer[3], Joel Brown[4], David Schuler[1] and Dan Sturgis[2]

[1] Department of Geosciences, University of Montana
[2] Department of Geology and Geophysics, University of Wyoming
[3] Institute of Arctic and Alpine Research, University of Colorado
[4] Center for the Geophysical Investigation of the Shallow Subsurface, Boise State University

We present results from a field campaign focused on meltwater infiltration and horizontal water transport processes in the percolation zone of the Greenland Ice Sheet. Field data were collected during a period of heavy melt in June/July 2007 along a ~50 km transect (from ~2000 m to ~1600 m elevation) of the EGIG line of west Greenland (Figure 1).

Figure 1. Image showing location of 2007 study transect (Crawford Point to T1) and planned activities during April/May of 2008 (T1 to Swiss Camp). Study reach follows the EGIG line.

Snow and firn stratigraphies of the upper 10 m were documented with snowpit measurements, analysis of 21 firn cores drilled to 10+ m, and with over 60 km of constant offset radar profiles collected at a variety of frequencies. We also acquired 15 constant midpoint radar profiles to characterize depth-density relationships in the upper 80 meters of the firn column. Dye tracing experiments were used to identify meltwater migration pathways and to quantify the relative rates of horizontal and vertical water movement. Five thermister strings with 33 channels and a 30 min time base were installed for long term monitoring of the thermal signature of meltwater migration and ice layer formation in the upper 10 m of firn (Figure 2). Two meteorological stations were installed to provide information on surface boundary conditions.
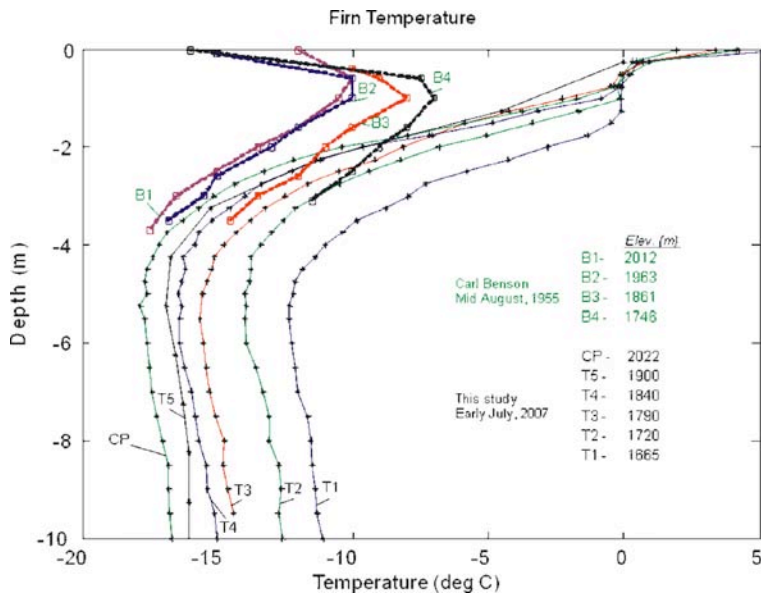
Figure 2. Temperature profiles from six 10 meter holes between CP and T1 (see Figure 1). Also shown are four temperature profiles collected in 1955 by C. Benson.

Our work shows massive ice layers (up to 0.4 m thick) form at depth under conditions of heavy surface melt. The ice layers, however, lack spatial coherence over meter length scales and therefore allow vertical meltwater infiltration. Hence, we found no evidence of significant horizontal water transport along internal ice layers within this elevation band of the GIS percolation zone. We also found that densification rates to 80 m depth show significant elevation dependency, and a recent increase in surface densification rate at lower elevations.

61

GLACIODYN ACTIVITIES ON AND UNDER ENGABREEN

MIRIAM JACKSON[1] AND TORBORG HAUG[2]

[1] Norwegian Water Resources and Energy Directorate, Oslo, Norway.
[2] Institute of Mathematical Sciences and Technology, University of Life Sciences, Ãs, Norway

Engabreen in northern Norway is an outlet glacier of the Svartisen icecap (Figure 1). There is a set of mass balance observations for Engabreen going back nearly four decades. These are performed in connection with a hydropower station in the area that uses water from the glacier that is collected as run-off as well as being collected directly through subglacial intakes. The mass balance was strongly positive in the 1990s and this was reflected in a strong advance of the glacier front. However, mass balance has been mainly negative since 2000, and the glacier front has retreated 200 m in the last eight years.

Engabreen is a unique glacier in the existence of a subglacial laboratory underneath the glacier. This laboratory was excavated for the purpose of glaciological research and has access from the tunnels created as part of the hydropower network.
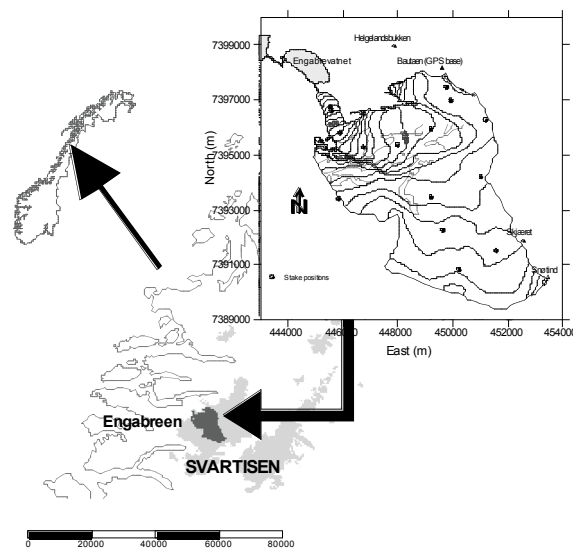
Figure 1. Location map for Engabreen, an outlet glacier of Svartisen.

Several load cells are installed at the glacier bed and measure the total hydrostatic pressure normal to the load cell. The pressure is measured at 15 minute intervals and shows variations in pressure at the bed due to variations in surface meltwater or changes in the subglacial discharge. Lappegard et al (2006) presented a summary of pressure variations and related them to the hydrological regime at the base of the glacier.

The dynamics of Engabreen have also been studied, including variations in surface velocity both seasonally (Jackson et al, 2005) and over shorter time scales. As part of the Glaciodyn IPY project, several parameters will be studied simultaneously, in order to see how different parameters are related to one another, and to better understand glacier dynamics. In May 2007 a preliminary investigation was made studying the relation between surface motion and subglacial pressure. Nine stakes were placed on the glacier tongue in an approximately square pattern at a few hundred metres spacing (Figure 2). It was not possible to place the stakes in a longer profile across the glacier due to severe crevassin on both sides; the central part is relatively flat and crevasse-free. Stake positions were measured over a 21-day period from 8th May to 29th May 2007, with measurements on days 1 to 4, and days 16 to 21. Some stakes were not measured on days 1 and 2. Velocities were an average of 40 cm per day over the whole period.
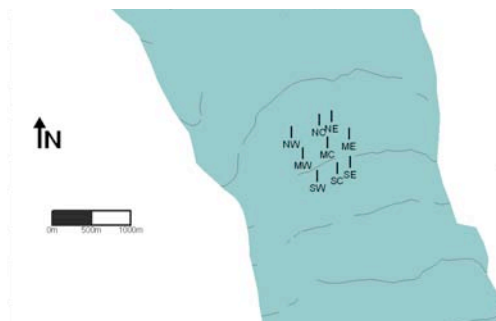
Figure 2. Movement stakes on Engabreen tongue. Glacier motion is towards the top of the page, and elevation on the glacier decreases towards the top of the page.

Stake elevations were also measured and it is interesting to look at changes in these. The general trend is to lower elevations as the glacier flows downhill. However, there appears to have been an uplift event that is seen on the western side of the glacier. It is recorded first in the uppermost stake (SW) on the west side on 25th May, next in the middle stake (MW) on 26th May and finally in the lowermost stake (NW) on 27th May (Figure 3). It may also be detected in the stake SC on 27th May.
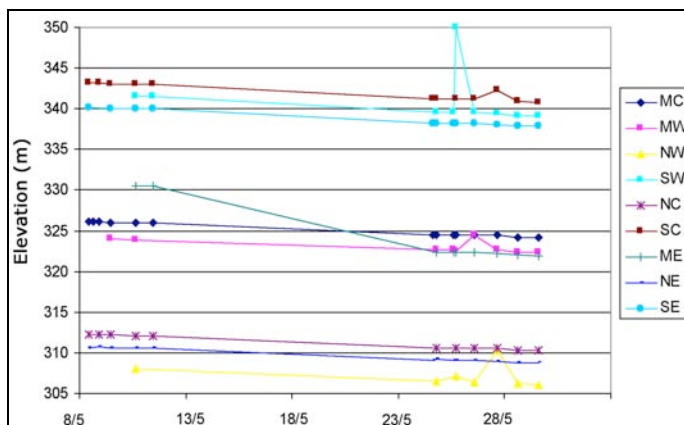
Figure 3. Elevation of stakes over the 21-day period.

Uplift events have been detected on several glaciers (e.g. Iken et al, 1983), especially in connection with the onset of spring melting. Records at the subglacial pressure cells, that lie about 1.5 km upstream of the measurements stakes, show that there was a pressure event on about 23rd May (Figure 4). There were also several stronger events in the preceding week, but the stakes were not measured in this period. These suggest an increase in the available meltwater at the bed that was registered on all the pressure sensors (number 4, 6, 2a, 1e, 97-2 and 97-1 and situated within 20 m of each other). This then travelled downstream and was registered predominantly on the side of the glacier that is thickest (due to an asymmetrical basal topography) and where meltwater presumably drains predominantly before coming out at the pro-glacial river that is also on the western side of the glacier (see Figure 1).
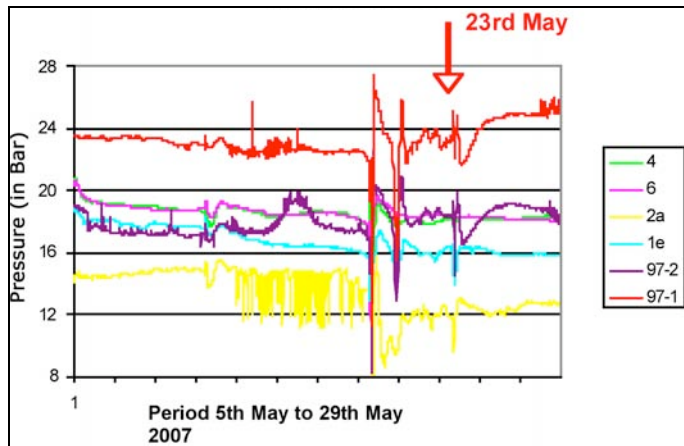
Figure 4. Pressure variations over the measurement period.

References

Iken A., H. Röthlisberger, A. Flotron and W. Haeberli. 1983. The uplift of Unteraargletscher at the beginning of the melt season – a consequence of water storage at the bed? Journal of Glaciology, 29 (101): 28-47.

Jackson, M., I. Brown and H.Elvehøy, 2005. Velocity measurements on Engabreen. Annals of Glaciology, 42, 29-34.

Lappegard, G., J. Kohler, M. Jackson and J.O. Hagen. 2006. Characteristics of subglacial drainage systems deduced from load-cell measurements. Journal of Glaciology 52 (176), pp. 137-148.

NATURAL RADIONUCLIDES IN GLACIER MELTWATER AS USEFUL TRACERS

A. KIES[1], A. NAWROT[2], H. SURBECK[3] AND Z. TOSHEVA[1]

[1] Laboratoire Physique des Radiations, University of Luxembourg
[2] Institute of Paleogeography and Geoecology, Adam Mickiewicz University
[3] Centre of Hydrogeology, University of Neuchâtel

We present an alternative method to investigate the character of the meltwater supplied by glacierized basins in introducing radioactive ionic measurements together with classical parameters like electrical conductivity, pH, dissolved gases. Among the natural radioactive ions the most promising is the nobel gas radon with a short half life of 3.8 days and the possibility of an automated continuous measurement using sensors that can be controlled by data loggers. Radon (^{222}Rn) is a radioactive noble gas (T=3.8 d), it originates from the decay of radium (^{226}Ra), member of the natural ^{238}U series. In solids, only the radon produced very close to the grain surface, within less than a fraction of a micrometer, will be able to reach the pore space and get dissolved in water.

Glaciers are active erosional agents, continuously crushing and abrading the substrate over which they flow resulting in an effective high exchange surface between substrate and water. Different ionic species are acquired from contact during water flow through the glacier drainage system and contribute to the increased electrical conductivity and, in the case of radon, to an uptake of radon escaping from bed rock and sediments. Such contact is achieved most effectively at the glacier bed. In meltwater, temporal variations of radon and ionic concentration may be interpreted in terms of the water flow pathways. High conductivity, high ionic stable and radioactive element concentrations indicate contact with reactive sediments and rocks, possibly for extended periods of time. On the other hand high radon concentrations simply indicate contact with radium located close to the surface of sediments/rocks, this contact happening less than 20 days before sampling. In both cases the period of contact is important. In the case of radon a steady equilibrium concentration can be expected whenever uptake of radon is counterbalanced by decay. The obtained ionic signatures are generally interpreted in terms of flow through the subglacial drainage system, via hydraulically inefficient pathways with slow transit speeds and involving much contact with large amounts of freshly eroded debris. In contrast, low ionic/radon concentrations are consistent with no, or only a short period of, flow at the glacier bed, via a hydraulically effective drainage pathway characterized by large water fluxes and rapid transit speeds.

Radon concentrations depend on the radium concentrations of the rocks, the rock/sediment- water contact surface and the contact duration. Meltwater containing radon is a secure information that part of this water has been recently in contact with the bedrock, the more radon the higher is the fraction of meltwater in contact with bedrock, the fraction without contact being nearly radon free.

For our investigation we chose the well studied Werenskioldbreen situated in the south-western part of Wedel-Jarlsberg Land, Spitsbergen. Its closeness to the Polish Polar Station in Hornsund has made the glaciated catchment well studied in terms of climatology, geomorphology and geology (Bukowska, 2007). Werenskioldbreen is a polythermal glacier with terminus on land, a 27 km^2 area and a 100-140 m maximum thickness. The terminus is divided into two parts by a central moraine, one third to the north and two third southern part. Four areas were sampled between September 2006 and end of July 2007: 2 areas in the northern part called N-a and N-b, N-a being close to the lateral moraine, W is an important summer outflow to the south of the central moraine; N is an area close to the southern end of the moraine.

Werenskioldbreen provides evidence for considerable basal routing of water. High radon concentrations and conductivity of the subglacial upwelling provides evidence of the passage of icemelt through a subglacial weathering environment characterized by high rock-sediment:water ratios, prolonged residence times and restricted access to the atmosphere, preventing radon to degas. At higher discharges, basal bulk runoff becomes dominated by icemelt from the lower parts of the glacier that is conveyed through a weathering environment, characterized by low rock: water ratios, short residence times and free contact with atmospheric gases, to the glacier margins. In Werenskioldbreen icemelt is routed via a hydrological system composed of englacial and supraglacial components to the glacier margins by the ice surface slope. Before upwelling, water flows relatively independently of icemelt to the terminus via a subglacial drainage system, possibly constituting flow through a sediment layer. Cold basal ice at the terminus forces it to take a subterranean routing in the latter stages. The existence of spatially discrete flow paths conveying icemelt and subglacial snowmelt to the terminus is the norm for polythermal-based glaciers on Svalbard (Wadham, 1998).
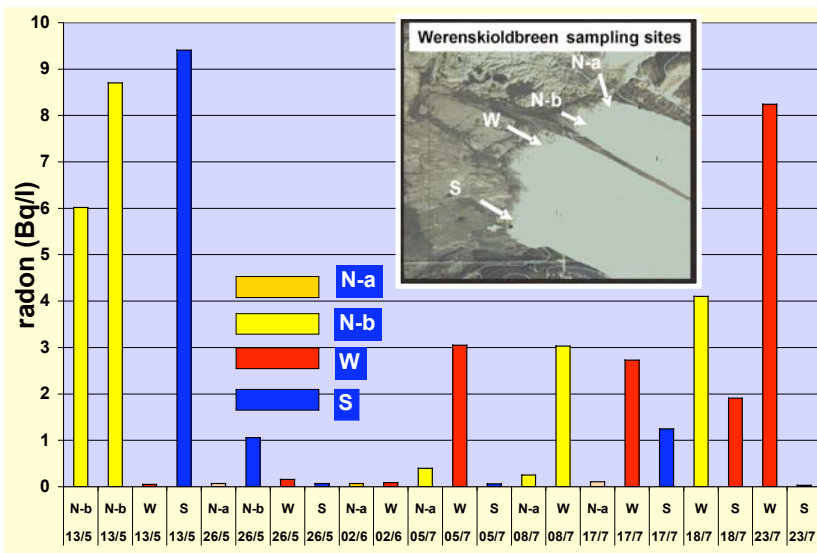

Figure 1. Meltwater radon concentrations measured at 4 different sites in May-July 2007.

In September and April air temperatures were below zero, very high radon concentrations were measured. Due to the lack of surface melting during these periods one may assume that steady state radon concentrations are approached. Effectively highest radon concentrations were measured in September (one sample, 22 Bq/l, el. conductivity) at location W, 16 to 28 Bq/L at varying water outflows in April in N-a, N-b and S (50 samples collected over 3 weeks), (Figure 1).

The sampling dates at Werenskiold glacier covered the different periods of the glacial cycle: end of September 2006; in 2007 April, the start of ablation period, in May-June and part of the ablation period until end of July. Pulina (1990) refers that, based on the glacial river of the Werenskioldbreen, ablation water in summer is as much as 80–95% of the total meltwater flow, but, beginning in September, the share of subglacial sources increases, possibly representing the entire flow by the end of that month.

In September radon and conductivity measurements show highest values in spring upwelling waters at location W (radon concentration 22 Bq/L) reflecting the subglacial origin.

Table 1. Natural radioactive isotopic content in meltwater sampled at the Werenskiold glacier front in April 2007.

Date 2007	Location	U-238 mBq/l	+/-	U-234 mBq/l	+/-	Ra-226 mBq/l	+/-	Po-210 mBq/l	+/-	Rn Bq/l	+/-
9.04	**N-b**, 'old' hole, opened	6.7	0.2	5.1	0.3	9.9	1.1	90	10.0	27.4	2.4
9.04	**N-b**, new dome outflow	28.4	1.2	22.9	0.3	50.8	8.1	466	66.5	11.0	1.2
10.04	**N-b**, outflow small dome	3.6	0.1	2.8	0.3	5.2	0.8	17.8	2.5	16.2	1.6
10.04	**N** lat. moraine	0.4	0.1	0.7	0.1	0.3	0.05	15.0	2.5	0.10	0.02
10.04	**N-a** flowing	4.2	0.1	5.5	0.2	7.2	0.6	8.1	1.0	12.0	1.2
13.04	**S** outflow small dome	1.4	0.1	1.8	0.1	1.1	0.2	27.6	3.4	10.4	1.0
21.04	**S** outflow small dome	4.1	0.1	4.2	0.1	1.9	0.3	7.1	3.2	12.0	1.2
21.04	**N-a** small dome running	5.0	0.1	4.2	0.1	2.1	0.3	2.6	0.8	0.86	0.14
21.04	**N-b** outflow big dome	7.2	0.2	7.4	6.0	1.3	0.2	37.6	6.7	16.2	1.6

From 5th to 21st of April 2007, on six different days, 50 flowing water samples were collected. Over the 2.5 km glacier front 5 naled ice fields of varying area with ice domes could be observed, in three of them, N-a, N-b and S, running water outflow close to the glacier could be accessed and sampled. Flowing water was normally on or close to ice domes, some of them 2 m high but generally there heights were below one meter. Often ice had to be broken to access running water, sometimes under pressure. A particular outflow never lasted more than 3 days before refreezing. It was not possible to take samples at area W sampled in September. Table 1 gives an overview of the natural isotopic content of some samples taken to

the home laboratory for radiochemical analyses; radon was measured by liquid scintillation at the Polish Base; electrical conductivity, temperature and sometimes pH in situ.

In area N-b highest April radon (12-16 Bq/L) and conductivity values (specific el. conductivity 400-500 µS/cm) were measured. One outflow, lasting for 3 days, showed a very high electrical conductivity (2700 µS/cm) and the highest radon concentrations so far measured at Werenskioldbreen (27 Bq/L). In N-a, radon concentrations were lower (maximum 11 Bq/L) and very variable, sometimes down to 0.1 Bq/L, specific electrical conductivities varied around 400 µS/cm. In area S electrical conductivity was 2.5 times lower than in N-b, whereas with 12 Bq/L radon concentrations were high.

A general trend was that high radon concentrations are often linked to high electrical conductivity.

In irregular intervals sampling was done from May to July. Figure 1 resumes the measured radon concentrations. At location W, at the maximum of upwelling water outflow, highest radon concentrations (8.2 Bq/L) were measured at the end of July. If one assumes a simple mixture model of subglacial and radon depleted endo-supraglacier water, 37% could be allocated to subglacial water.

Conclusion
At Werenskioldbreen unexpected high radon concentrations were measured. Combined with traditional investigation tools, radon proves to be a valuable tracer for the study of artesian glacier meltwater.

Highest radon concentrations were measured in September and April, in periods of no supraglacier melting, lowest in period of the beginning of thawing, intermediate concentrations in the periods of maximum thawing with high combined sub-, endo- and supra- glacier circulation.

We report here of preliminary investigations with radon and other natural radionuclides as natural tracers. We have to learn more how to use and read the obtained information

Acknowledgements

References
Bukowska-Jania E., 2007. The role of glacier system in migration of calcium carbonate on Svalbard, Polish Polar Research, vol. 28, no. 2, pp. 137–155.
Pulina M., 1990. Geomorphological effects of the cryochemical processes. Questiones Geographicae 13/14 (1987/1988), Poznań: 99–112.
Wadham J. L., Tranter M., Dowdeswell J. A., 1998, The hydrochemistry of meltwaters draining a polythermal-based, high Arctic glacier, south Svalbard: I. The ablation season, Hydrological Processes, vol.12, no.12, pp 1825-1849.

MODIS ALBEDO AND REGIONAL MASS BALANCE OF SVALBARD GLACIERS

JACK KOHLER

Norwegian Polar Institute, Tromsø, Norway

Abstract

MODIS albedo products are compared to glacier mass balance measured on several glaciers in the high Arctic, in northwestern Svalbard. The glaciers range in size from ca. 5-500 km^2. We use MODIS L3 albedo products (MOD43B3), which have a nominal resolution of 1 km, and for which data cover the spring to autumn months of 2000-2006. We compare the albedo data to four glaciers for which there are mass balance measurements in each of the years in the study period (Austre Brøggerbreen, Midtre Lovénbreen, Kongsvegen, and Waldemarbreen), as well as two glaciers with some years of mass balance measurements (Holtedahlfonna, Etonbreen). There is still good overall correlation between parameters derived from annual albedo minima and the equilibrium line altitude (ELA) of the study glaciers. Simple threshold methods can potentially be used to directly extract an ELA proxy from the albedo data.

CALVING DYNAMICS OF JAKOBSHAVN ISBRAE

MARTIN LÜHTI

Laboratory of Hydraulics, Hydrology and Glaciology, Swiss Federal Institute of Technology (ETH), Zurich, Switzerland

Abstract

Jakobshavn Isbrae, a large outlet glacier of the Greenland ice sheet, has changed dramatically in the last ten years. Fast surface lowering, calving front retreat and doubled flow velocity are hallmark changes, similar to those observed at other Greenland ice streams. To understand the interaction between processes that lead to the fast changes in geometry and dynamics, and to answer the question whether ice streams react to changes in ocean temperatures or to increased ablation and melt water production on the ice sheet, we measured flow velocity at high time resolution along a central flow line from 50 km inland to the terminus. Geodetic GPS were installed where landing a helicopter was possible, and conventional survey reflectors tracked by an automatic total station were deployed in the difficult to access region near the terminus. Tidal forcing has no significant effect on flow velocities in the terminus area, as was observed twenty years ago. The glacier terminus reacts with a spatially and temporally consistent acceleration to the 1 km retreat of the terminus during each big calving event, when tens of ice bergs of typically 500m width, 500 m length and 900 depth break off. The bergs are accelerated to more than 10 m/s by the energy released by rotation, inducing seismic events that could be detected at a nearby seismometer.

MASS BALANCE OF THE PRINCE OF WALES ICE-FIELD, ELLESMERE ISLAND, NUNAVUT, CANADA

DOUGLAS MAIR[1], DAVID BURGESS[2], MARTIN SHARP[3], SHAWN MARSHALL[4], FIONA CAWKWELL[5], JULIAN DOWDESWELL[6] AND TOBY BENHAM[6]

[1] Department of Geography and Environment, School of Geosciences, University of Aberdeen, UK
[2] Canadian Centre for Remote Sensing, Natural Resources Canada, Ottawa, Canada
[3] Department of Earth and Atmospheric Sciences, University of Alberta, Edmonton, Canada
[4] Department of Geography, University of Calgary, Calgary, Canada
[5] Department of Geography, University College Cork, Republic of Ireland
[6] Scott Polar Research Institute, University of Cambridge, Cambridge, UK

Extended abstract

The mass balance of the Prince of Wales Icefield (POW), Ellesmere Island, Canada is determined from measurements of surface mass balance and iceberg calving. Despite being the second largest ice mass of the Canadian High Arctic there have until recently been only sporadic glaciological measurements carried out across POW (Koerner, 1977 and 1979) as is not one of the ice caps regularly measured as part of the Geological Survey of Canada's long-running mass balance monitoring program (Koerner, 2005). This paper presents the first mass balance measurements from POW in over 25 years.
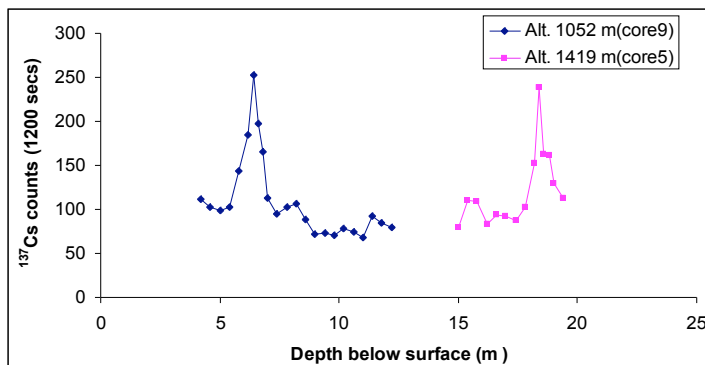
Figure 1. ^{137}Cs against depth for two sites showing clear bomb layer peak at depth.

In April-May 2001 and 2002, thirteen shallow cores were drilled across the accumulation areas of POW, ranging in elevation from 941 m to 1730 m above sea level. Using a down-borehole gamma spectrometer, gamma activity profiles of boreholes created by removal of each shallow core was measured. The count profiles for ^{137}Cs showed a secondary peak at depth (e.g. Figure 1) that is associated with peak fall-out from atmospheric testing of thermonuclear weapons in 1962-63. Using the depths of the 1963 radioactive fallout layers and measurements of the densities of firn and snow above this layer, the average mass balance, b_n, over the period 1963-2001/2002 was calculated at each core site in the field.

From May 2002 to May 2003, measurements were made of changes in the heights of winter snow and previous summer firn or ice surfaces against a network of mass balance stakes deployed across two transects of the ice-field. In conjunction with measurements of snow-pit densities, near-surface firn core densities, and assuming a glacier ice density of 900 kg m-3 across ablation areas, these stake measurements were used to calculate b_n for the year 2002-2003 at 24 locations across the ice-field.

Shallow ice core net accumulation measurements and annual mass balance stake measurements are used in conjunction with a digital elevation model and knowledge of the location of the dominant moisture source to interpolate and extrapolate the spatial pattern of surface mass balance (SMB) across the Prince of Wales icefield. Ten different approaches yield different estimates of the contribution of SMB to the overall mass balance of the icefield, thereby highlighting and quantifying the methodological uncertainty of such estimates.

The contribution of iceberg calving to the mass balance is calculated from estimates of (a) the volume of ice flux discharged at the major tidewater glacier termini per annum and (b) the volume loss or gain due to the observed change of termini position per annum. The former is calculated from airborne radio echo sounding (RES) measurements of ice thickness at the glacier termini and RADARSAT-1 speckle tracking surface velocity measurements. The latter is based on comparison of 1959/1960 aerial photography with 1999/2000 satellite imagery of marginal advance or retreat of major glacier basins. The results of this are summarized in Table 1.

Table 1. Iceberg calving totals, Q_{Total}, and components Q_{flux} and Q_{v-loss} by glacier basin, where Q_{flux} is the annual volume of ice flux discharged at the tidewater termini and Q_{v-loss} is the volume loss due to the observed change of terminus position

Glacier basin	Q_{flux} (km^3 w.e. a^{-1})	Q_{v-loss} (km^3 w.e. a^{-1})	Q_{Total} Calving total (km^3 w.e. a^{-1})
Leffert	-	0.01 ± 0.002	0.01 ± 0.002
Cadogan	0.08 ± 0.013	0.02 ± 0.003	0.10 ± 0.016
Eckblaw	0.17 ± 0.043	-0.02 ± 0.003 (terminal advance)	0.15 ± 0.046
Trinity & Wykeham	1.36 ± 0.221	0.21 ± 0.032	1.57 ± 0.253
SE Margin	-	0.04 ± 0.006	0.04 ± 0.006
Totals	1.61 ± 0.28	0.26 ± 0.05	1.87 ± 0.32

We conclude that the surface mass balance of the icefield is positive (+1.4 ± 0.7 km^3 w.e. a^{-1}) largely due to high accumulation in south-east catchments facing the main year round moisture source of the Smith Sound portion of the North Open Water Polynya. Iceberg calving is a major component of mass loss (1.9 ± 0.3 km^3 w.e. a^{-1}) and is sufficient to cause the overall mass balance of the icefield to be most probably negative (-0.5 ± 0.8 km^3 w.e. a^{-1}). The Prince of Wales Icefield therefore has a lower contribution to global eustatic sea level rise than neighbouring ice masses in the Canadian High Arctic which is consistent with previous observations showing just a slight reduction in surface area of the icefield over the period 1959-2000 (-0.7%).

ABLATION AND VERTICAL GRADIENTS OF AIR TEMPERATURE – A STUDY FROM HANS GLACIER, SW SPITSBERGEN

K. MIGAŁA[1], B. LUKS[2], D. PUCZKO[2], S. SIKORA[1], A. DRZENIECKA–OSIADACZ[1], M. GRABIEC[3] AND P. GŁOWACKI[2]

[1] University of Wrocław, Institute of Geography and Regional Development
[2] Institute of Geophysics Polish Academy of Sciences,
[3] University of Silesia, Faculty of Earth Sciences

Introduction

Glaciers are a derivative of climate and dynamics of glaciological processes depending on unremitting atmospheric processes in the 3D space. Gradients of: air temperature, moisture, solar incoming energy, precipitation and chemical composition are the important attributes in the vertical structure of the atmosphere.

Vertical differentiation of atmospheric processes has an impact on stratification of glacial phenomena. The atmospheric boundary layer (ABL) should be considered in this case. The depth of the ABL and changes of air temperature in the vertical profile mark the border in dynamics of the processes concerned with the development of stratus/stratocumulus clouds and the surface radiation budget (Curry 1985, Bing Lin and Minnis 2003). In consequence, the structure of the ABL modifies the chemistry of precipitation and dynamics of other processes e.g. freeze/thaw cycles. Numerous investigations confirm that the ABL in the Arctic is very shallow, often not exceeding 200 m (Tjernström et al. 2004, Drzeniecka et al. 2007). Knowledge of local climate, orography and glaciers morphology lead to the conclusion that one can expect hypsometric gradients in glaciological processes, shaped by the Arctic ABL.
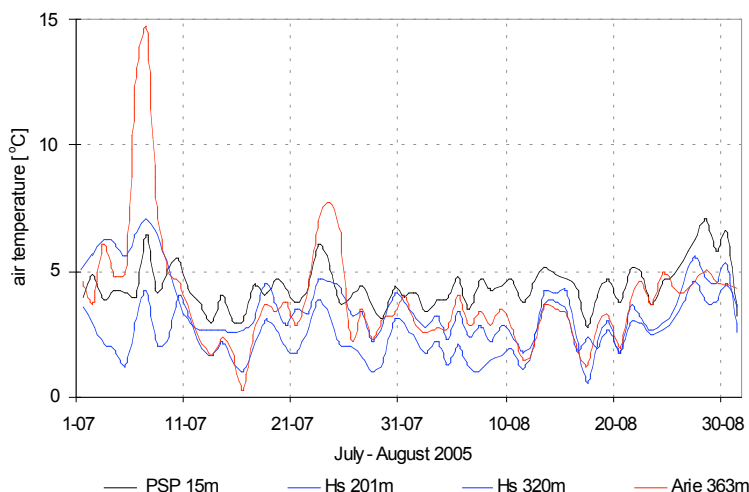

Figure 1. Plot of daily mean air temperature at the Polish Polar Station (PPS), Hans Glacier (Hs) and mountain ridge (Arie), July – August 2005.

Table 1. Mean monthly air temperature (MMAT) and sums of positive daily air temperature (PDD) in the period July (VII) - August (VIII) 2005 at the Polish Polar Station (PPS), Hans Glacier (Hs) and mountain ridge (Arie).

	Unglaciated	Glacier		Unglaciated
	PPS 15 m	Hs 200 m	Hs 320 m	Arie 363 m
MMAT (VII)	4,3	2,4	4,2	4,6
MMAT (VIII)	4,6	2,8	3,0	3,4
PDD (VII-VIII)	275,9	162,2	221,4	247,1

Case study 2005

Experimental measurements were carried out in July–August 2005 at the Polish Polar Station in Hornsund Fjord, Spitsbergen. Variability of the ABL was described based on air temperature measurements, monostatic Doppler sodar and tethered balloon soundings. The main features of that season were two short-period episodes of strong temperature inversion evident on the Ariekammen ridge, 363 m a.s.l. (July 6-8 and 23-25) and, long-lasting inversion on Hans Glacier on the elevation of 200 – 320m a.s.l. (Figure 1, Table1). The thickness of the ABL was mostly around 250-300 m. and the lowest clouds commonly appeared within the ABL (Table 2). In consequence, the glacier zone of 320 m a.s.l. was warmer then that at the height of 200 m a.s.l. It should be stressed that air temperature recorded at the Polish Polar Station (15 m a.s.l.) did not deflected from the long-term mean conditions.

Table 2. Frequency of the sodar echo types in the classes of height - Hornsund July – August 2005).

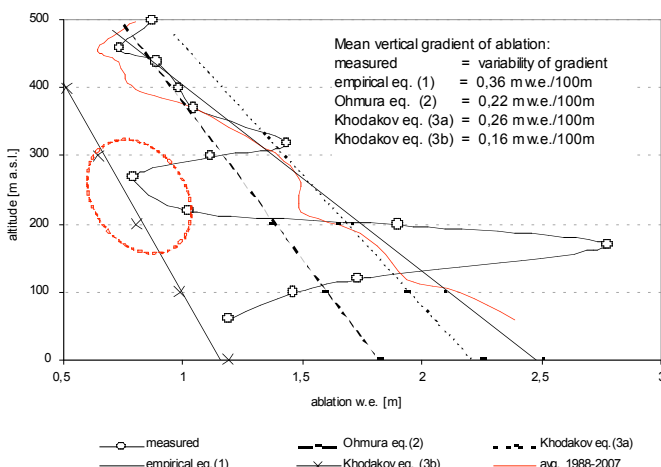| Types of sodar echo	Classes of height [m a.g.l.]				
	≤50	100	150	200	>200
	Frequency [%]				
Ground based layer	16,28	22,21	18,17	14,66	5,22
Elevated layer		5,94	31,96	34,25	27,85
Turbulence			23,47		

Figure 2. Measured and computed vertical gradient of ablation of the Hans Glacier in the summer of 2005.

Long-lasting inversion of air temperature resulted in higher sum of PDD on the height of 320 m a.s.l (221,4 PDD) then that recorded at the zone of 200 m a.s.l (162,2 PDD). In consequence, values of ablation reversed in the hypsometric profile. Application of the Khodakov (1965) and Ohmura (1992) formulas to calculate ablation did not expressed the changes in vertical profile (Figure 2).

Long-term data from Hans Glacier (1988-2007) indicate that the mean ablation has a vertical gradient of 0,43m w.e./100m and vary in hypsometric profile between 1,91 m and 2,38 m w.e. in the frontal zone (60-120 m a.s.l.) and to 0,80 m w.e. in the accumulation area, in the altitude of 400-500 m a.s.l.
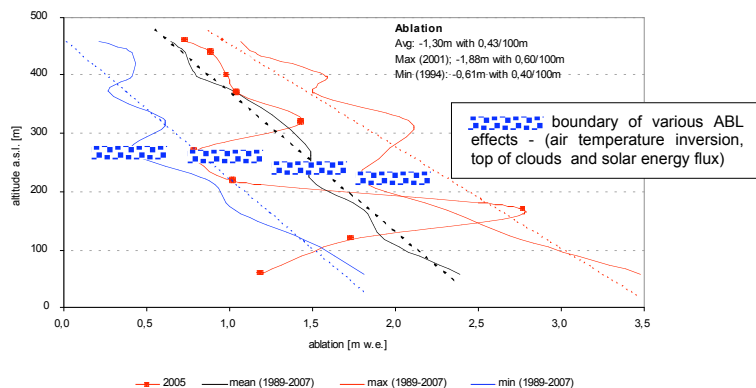
Figure 3. Vertical gradient of ablation effected by ABL structure – case study in 2005, mean and extremes in the period of 1988 – 2007.

Figure 4. Frontal area of Hans Glacier with marked line at the height of 300 m a.s.l.,(left) and the sea of clouds with top height of 300m a.s.l., Hornsund Fjord. (Photos Marek Kowalczyk

Plots of the mean gradient as well as the gradients in the seasons with maximum and minimum ablation indicate a boundary at the height of 200-300m a.s.l. A zone with decreased rate of ablation is evident in the lower part of the glacier (Figure 3). It can be concluded that the effect of the arctic ABL and frequent air temperature

inversions with low level clouds reduce the solar energy income at the surface (Figure 4).

However, the other phenomena, which modify dynamics of ablation, should be considered e.g. poorly recognized foehn winds with warming effect and katabatic winds cooling the lower parts of a glacier.

References

Bing Lin B., Minnis, P., 2003: Cloud liquid water path variations with temperature observed during the Surface Heat Budget of the Arctic Ocean (SHEBA) experiment, Journal of Geophysical Research, 108, D4

Curry J.A., 1985: Interactions among Turbulence, Radiation and Microphysics in Arctic Stratus Clouds, Journal of Atmospheric Sciences, 43,1 :90-106

Khodakov V.G., 1965, O zavisimosti summarnoj abljacii poverchnosti lednikov ot temperatury vozducha. Meteor. i Gidrol., 7: 48-51.

Drzeniecka-Osiadacz A., Migała K., Sikora S., 2007, Cechy warstwy granicznej atmosfery w rejonie Hornsundu w lipcu i sierpniu 2005 roku. [w]: Abiotyczne Środowisko Spitsbergenu w latach 2005-2006 w warunkach globalnego ocieplenia, Wyd. Uniwersytetu Mikołaja Kopernika: 131-146.

Ohmura A., Kasser P. and Funk M., 1992, Climate at the equilibrium line of glaciers. Journal of Glaciology, 38: 397-411.

Tjernström M, Leck C., Persson P.O.G., Jensen M.L., Oncley S.P., Targino A., 2004, The Summertime Arctic Atmosphere Meteorological Measurements During The Arctic Ocean Experiment 2001, Bull. Amer. Meteor. Soc., 85: 1304-1321.

Internal Structure of Ariebreen, Spitsbergen, from Radio-Echo Sounding Data

F. Navarro[1], M. Grabiec[2], D. Puczko[3], U. Jonsell[4] and A. Nawrot[5]

[1] Dept. Matemática Aplicada, ETSI de Telecomunicación, Universidad Politécnica de Madrid, Spain.
[2] Dept. of Geomorphology, Faculty of Earth Sciences, University of Silesia, Poland
[3] Institute of Geophysics, Polish Academy of Sciences, Poland
[4] Dept. of Earth Sciences, Uppsala University, Sweden
[5] Institute of Paleogeography and Geoecology, Adam Mickiewicz University, Poland

Introduction

Ariebreen (77º 01' N, 15º 29' E) is a small valley glacier (ca. 0.36 km^2 in August 2007) located at Hornsund, Spitsbergen, Svalbard, ca. 2.5 km to the west of Hornsund Polish Polar Station. Ariebreen, like many other Svalbard glaciers, has experienced a significant recession at least since the 1930s, and most likely since the end of Little Ice Age (LIA) in the early part of the 20th century. Moreover, the thinning rate of western Svalbard glaciers has shown an acceleration during the most recent decades. Ariebreen follows this general retreat pattern, as is shown in another contribution to this workshop (Petlicki et al., 2008). Most investigated glaciers in Hornsund area, in the neighbourhood of Ariebreen, are known to be polythermal (e.g. Hansbreen and Werenskioldbreen, Pälli et al., 2003). It has been suggested (Macheret et al., 1992) that the thinning of polythermal glaciers may result in a switch to cold thermal structure under appropriate conditions. The strong thinning experienced by Ariebreen during the recent decades makes it an ideal candidate to undergo such change.

The main aims of this contribution are to understand the internal structure of Ariebreen, in particular, its hydrothermal regime, and to determine whether the glacier is undergoing or has already experienced a transition from polythermal to cold structure. The main tool to accomplish this will be the analysis of radio-echo sounding data.

Ground-penetrating radar measurements and data analysis

During summer 2006 and spring 2007 radar profiles were done providing a full coverage of Ariebreen (Figure 1). The total length of useful radar profiles was 2200 m in the summer campaign and 4000 m in the spring campaign, resulting a total length of profiles of 6200 m. The radar data were acquired using an ice-penetrating radar Ramac/GPR with unshielded antennae, of 200 MHz in summer 2006 and 25 MHz in spring 2007. The choice of the 200 MHz antennae was dictated by the interest in accurately determining the presence and extent, or the absence, of a firn layer. For this reason, the sampling frequency within each radar trace was set quite high, 2012 MHz, resulting a total time window of 509 ns and thus limiting the maximum depth sampled to about 42 m. Consequently, the bedrock was not reached in the areas of thickest ice. Using the 25 MHz antennae, sampling frequency was set to 250 MHz, resulting a time window of 2044 ns, so that bedrock

was reached in all cases. In addition to the radar data, navigation information from a stand-alone GPS receiver was also recorded; in the summer campaign, the profile endpoints were also measured by differential GPS.

No common midpoint measurements were done on this glacier in order to determine the radio-wave velocity (RWV). However, they are available, both for spring and summer periods, for the neighbouring Hansbreen glacier (Jania et al. 2005). On the basis of such measurements, we took a value of 168 m/μs (typical of cold ice) for the RWV at Ariebreen. This gives us a vertical resolution of the radar data of ±1.68 m for the 25 MHz antennae, and ±0.42 m for the 200 MHz antennae, considering the vertical resolution as one quarter of the wavelength in ice.

The processing of radar data included DC correction, amplitude scaling, band-pass filtering, deconvolution, migration where required and conversion to depth.
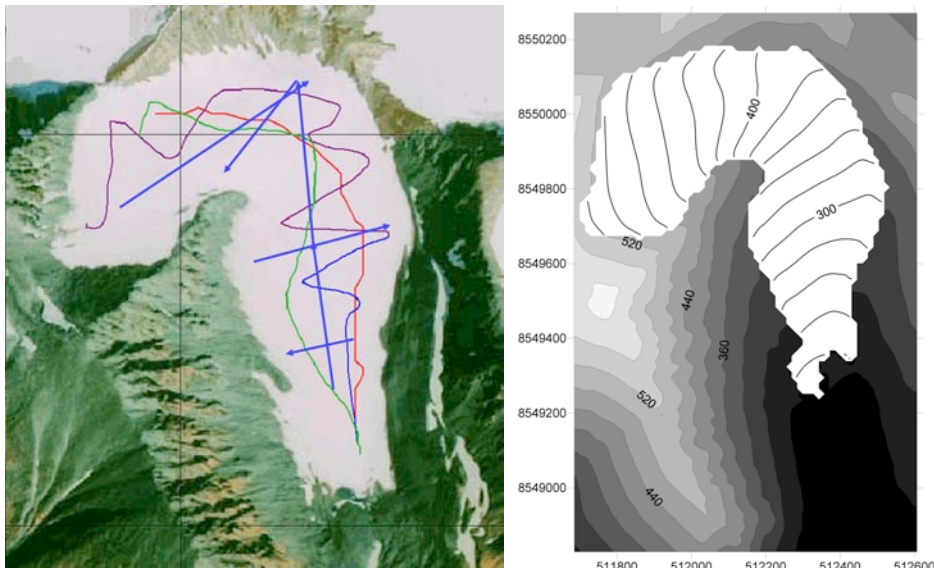

Figure 1. Left: Schematics of the radar profiles done in Ariebreen, drawn on an image showing the glacier extent in 1990. The straight blue lines correspond to profiles surveyed in summer 2006, and the remaining ones correspond to those surveyed in spring 2007. Right: Ariebreen surface topography based on geodetic measurements done by the authors in 2007.

Results, discussion and conclusions

The ice thickness map for 2006-2007, constructed from radar data, and the subglacial relief map, constructed by subtracting the ice thickness from the surface topography map, are shown in Figure 2. The average ice thickness in 2007 was only 22.29 ± 1.66 m. The thickest ice, with a maximum value of 81.24 ± 1.68 m, is found in the west-east orientated upper part of the glacier; thickness for the north-south orientated mid-lower part of the glacier only exceeds 50 m in its uppermost part. The lower part shows very thin ice. The subglacial relief map shows gentle slopes in the lower part of the glacier, steadily increasing as we approach the upper part.

The analysis of the radar sections shows three main features concerning the internal structure of Ariebreen:

1. Nearly absence of endoglacial diffractions. This is true for both high (200 MHz) and low (25 MHz) frequency radar data.
2. Absence of any internal reflector, which could be interpreted as an interface between cold and temperate ice layers. Again true for both high and low frequencies.
3. Absence of a firn layer or, if any, a very thin one (2-3 m). The vertical resolution of the radar data is 1.7 m for the 25 MHz radar and 0.4 m for the 200 MHz. Though the uppermost 2-3 m are obscured in the radar records, neither layering nor near-surface interface is visible below some 3 m depth.
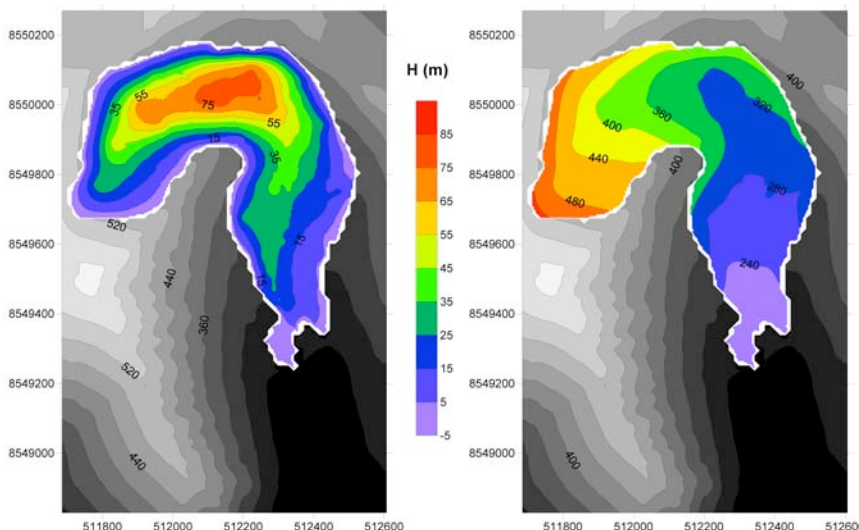

Figure 2. Left: Ice thickness map of Ariebreen in 2006-2007. Right: Subglacial relief map.

On the basis of the above assertions, we preliminarily conclude that Ariebreen is a cold glacier, in contrast with the polythermal structure of the neighbouring Hansbreen and Werenskioldbreen. This is, however, not surprising, because of the low ice thickness of Ariebreen, which allows for a relatively fast transmission through the ice column, and release through the glacier surface, of the geothermal heat flow warming the glacier bed. In the accumulation area, the extremely small thickness of the firn layer also implies that any possible heat generated by refreezing of percolating meltwater rapidly reaches the glacier surface and therefore does not substantially contribute to heating the glacier body. In the ablation area, if a polythermal structure were assumed the small ice thickness would also contribute to a fast transmission to the glacier surface of the latent heat generated by the freezing of liquid water in temperate ice at the cold-temperate interface, and therefore to the downward migration of the freezing front. This, combined with strong thinning, could justify a slow transition from polythermal to cold structure.

References

Jania J., Macheret Yu.Ya., Navarro F.J., Glazovskiy A.F., Vasilenko E.V., Lapazaran J., Glowacki P., Migala K., Balut A., Piwowar B.A. 2005. Temporal changes in the radiophysical properties of a polythermal glacier in Spitsbergen. Annals of Glaciology 42, 125-134.

Macheret Yu.Ya., Krass M.S., Glazovsky A.F. 1992: Structure, hydrothermal state and regime of subpolar glaciers. In V.M. Kotlyakov (ed.): Regime and evolution of polar ice sheets. Pp. 48-115. Saint-Petersburg: Gidrometizdat. (In Russian).

Pälli A., Moore J.C., Jania J., Kolondra L., Glowacki P. 2003. The drainage pattern of Hansbreen and Werenskioldbreen, two polythermal glaciers in Svalbard, Polar Research 22, 355-371.

Petlicki M., Lapazaran J., Navarro F., Glowacki P., Machío F. 2008. Ice volume changes of Ariebreen, Spitsbergen, during 1936-1990-2007. Workshop on the dynamics and mass budget of Arctic glaciers/ Glaciodyn (IPY) meeting, Obergurgl, Austria, January 2008.

POLAR PANORAMAS: IMAGES WORTH A THOUSAND MEGABYTES

MATT NOLAN

University of Alaska Fairbanks

Recent developments in digital camera and photo editing software offer earth scientists new ways to document and explore the landscapes they work in through use of spherical and gigapixel panoramas. For polar scientists working in remote areas with landscapes that are affected on human time-scales by climate change, panoramic photography offers many new possibilities for long-term change assessment, après-field landscape analysis, and public outreach. This paper provides an overview of the basic concepts in photo acquisition, post-processing, and scientific uses.

Panoramic photography has existed since the early days of photography itself, but the advent of digital cameras and processing have made panoramic photography easier, better, and much higher resolution than previously possible. Panoramic photography takes three basic forms: 1) a single acquisition using a specialized camera that achieves a wide field of view by sweeping the lens or film, 2) cropping an elongated image (typically with aspect ratio of 3:1 or higher) from a single image, or 3) creating a single, seamless mosaic using a series of individual images taken with a standard camera. This paper describes the latter, called the 'stitching technique', and focuses on pure digital techniques. The digital mosaic can consist of any field of view, from a traditional 90° x 30°, to a single-row cylindrical stripe covering 360°, to a full spherical view of 360° x 180°. Gigapixel panoramas can cover any field of view, with the distinguishing feature being a total pixel count of at least 5×10^6. The final resolution of the digital mosaic is a function of the focal length of the lens used and the resolution of the digital sensor in the camera. For example, one can created a spherical panorama using a 10.5mm fisheye lens or a 50 mm prime lens – with a 12 megapixel (MP) camera, the fisheye lens will require 7 photos for a final resolution of about 11,000 x 5500 pixel (60 MP) and the 50 mm lens will require 486 photos for a final resolution of over 4 gigapixels (GP). Obviously there is a trade-off between time spent taking/stitching the photos and the final resolution desired.

Creating a digital mosaic has several basic steps:
1. acquiring the images
2. performing any pre-stitching photo adjustments (such as conversion from RAW format, pre-sharpening, exposure adjustments, etc)
3. stitching the images
4. blending the images to obscure the seams, exposure differences, or parallax errors
5. using a photo editing software such as Photoshop to make any final adjustments
6. converting to VR format to view at full resolution using pan, tilt and zoom features

There are a few principles to keep in mind when acquiring the photos to create high-quality panoramas. There are many websites, forums, and a few books that offer tutorials on digital stitching of panoramas (of note are http://wiki.panotools.org/ and the Panotools NG forum on Yahoo.com). Here I simply list a few of the principles to be aware of:

- Panoramic photography is at heart still photography – the better you understand your camera, its optical physics, the nature of light and its dynamic range, and the essentials of composition, focus, and exposure, the better your panoramas will be. The best books I have found on photography are the series by Ansel Adams: The Camera, The Negative, and The Print.
- Panoramic photography requires you to think and expose in 360 degrees, meaning that there will always be back-lighting and front-lighting on a sunny day. Your camera exposure (aperture, shutter speed and white balance) must remain constant (or nearly so) for all of your photos if you want them to blend to look like a single photo, and so you need to plan your exposure carefully and use a camera that has manual settings.
- The camera must be spun about its no parallax point (NPP) which varies with the lens used, otherwise the photos will not stitch together perfectly, especially if you have subjects in both near- and far-grounds. The NPP is almost always **not** located at the tripod mounting screw in the camera body, and so a special panoramic rig is required (I use the one from www.reallyrightstuff.com).
- The photos must have enough overlap between them to ensure enough points in common to stitch them together. Typically 30% is enough. The main difficulties are with pure blue skies, and here it helps to use a fixed rotational increment between photos and input this value into the stitching software directly.
- As with traditional photography, shooting in RAW format is best, as it allows for the most control of the exposure, white balance, sharpening, and saturation after the image is taken.

In terms of equipment, there is a lot to choose from, and here I will only describe the basics along with the equipment that I use and have found reliable. For spherical panoramas, the easiest method for field scientists is to use a fisheye lens and a monopod (or trekking pole with camera mount) with a tilting head. The Nikkor 10.5 mm fisheye is commonly considered the sharpest lens in the sub-$1000USD category, though ones from Sigma and Tokina are also used widely. Depending on the size of the camera sensor and the lens used, you will need between 3 and 7 photos to get full spherical coverage. The issue is that most lens/body combinations will not result in a true 180° coverage, so there will be a gap at either the top (zenith) or bottom (nadir) in the photo, and the camera must be tilted up or down (or both) to fill those holes. My preferred method is to shoot 6 shots around with camera tilted down to eliminate the nadir hole, then tilt the camera up to fill the zenith hole; the monopod must remain vertical during this process (use a bubble level), otherwise parallax errors will result. For gigapixel panoramas (or any panoramas using other than the fisheye lens) a tripod is required due to the larger number of shots. For scenes requiring hundreds of photos, a motordrive is helpful to help move the camera at a fixed increment and automatically release the shutter. I have used the motordrive from Seitz and can recommend it for its reliability and lightweight in remote field work. Nearly any modern D-SLR camera

can be used for acquiring images; I use the Nikon D2xs and found it rugged, reliable in any temperature, and with long battery life and recommend its use.

Once the photos are acquired, they must be stitched and blended. There are numerous applications available for this. Arguably the best software is open-source code called PanoTools, developed by Dr. Helmut Dirsch, and many commercial packages use this engine. The most popular and among the cheapest commercial packages is PTgui, which I use exclusively, and it has an active and friendly on-line user community. Though the packages differ in implementation, the fundamentals remain the same: find points in common between photos ('control points'), use those control points to determine how to shift (or warp) the photos, and then blend the photos together to obscure any remaining errors. The best approach is to calibrate your lens (something you can do on your own with test photos) and enter those calibration coefficients into the stitching software, as this reduces the number of control points required and prevents the software from warping the photos in ways not intended by the user. Stitching and blending a spherical fisheye panorama at 16 bit and 11,000 x 5,500 resolution can take a fast modern computer between 5 minutes to 5 hours, depending on the software algorithms used. The blending algorithms have the most variations, and recently released algorithms appear to be 2 orders of magnitude faster than those of last year.

The final steps in production are preparing it for distribution and use, typically either print or on-line viewing. Tools like Photoshop are useful here, especially with cleaning up any visible seams or with overall contrast and exposure adjustments. Once the flat image is finalized, there are a number of tools that can be used to create the on-line display. I use "Pano2VR", as it is easy to use and inexpensive. Tools like these will take your flat image (typically a JPG) and convert them to QuickTime VR or Flash (or any number of other similar formats). The issue here is that only about 90° field of view can be shown without introducing substantial distortion, so that user's field of view must be restricted to this amount. The Quicktime and Flash applications allow the creator to limit the field of view as desired, and allow the user to pan, tilt and zoom to see the remaining image. For gigapixel panoramas, the best software currently available is Microsoft's HDview, but Zoomify is also a popular and useful tool. These applications take the enormous gigapixel panorama and split into thousands of smaller images with the 'pyramid resolution layers', such that the software can carefully manage the available bandwidth by only sending the user as much resolution as required given the zoom level and location of the user's browser. This is the same way that Google Earth and many other mapping software works.

To explore the scientific utility of spherical and panoramic photography, I took approximately 375 panoramas during an expedition to McCall Glacier Alaska in July/August of 2007. I have stitched approximately 60 of these at this time, and have found that it takes me about 2 hours for the complete workflow for each. I have uploaded all of these to http://arctic.360cities.net and they can also be viewed in Google Earth from http://arctic.360cities.net/ge.kml.

It remains to be seen what the long-term value of these panoramas will be, but I can offer several possibilities. I have found that my gigapixel panoramas allow me

to explore the landscape from the office nearly as well as or better than standing in the field does, as the photo resolution is better than my eyes can see alone and there I can spend hours or days looking at the photo, but typically only a few minutes in the field. The spherical panoramas, which can be taken in a minute or so in the field, cover a broad spatial area and so provide nice documentation of the complete landscape of our primary glacier field site. I have used these photos on numerous occasions now to help collaborators who have not been to our study areas better understand the area, and all have commented on the power of the technique. In terms of being a long-term record, based on my own experiences using old photos, the panoramic technique is far superior, as it not only gives the would-be repeat photography a 360 degree view against which to assess change but also shows exactly the location of the photographer through the nadir image.
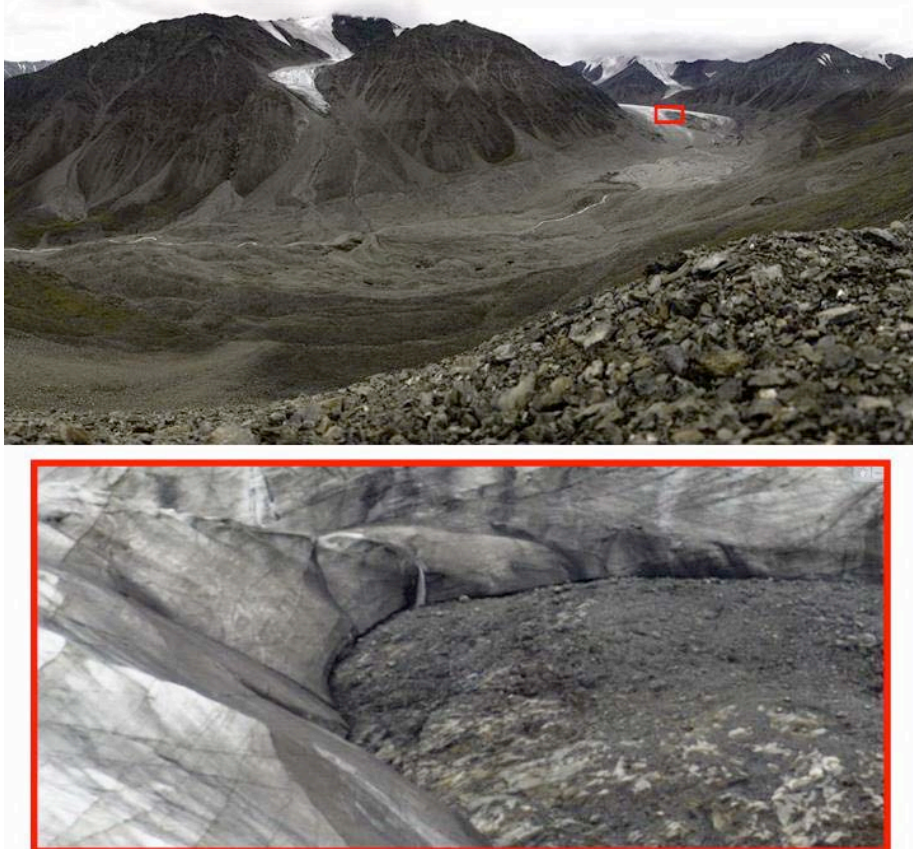

Figure 1. Gigapixel panorama of Okpilak Glacier, AK. The upper image is a mosaic composed of 504 images acquired with a 200 mm lens. The lower image is a cut-out of the mosaic demonstrating the detail captured by this technique. This photo-location was first used 100 years ago by Ernest Leffingwell, when the glacier almost completely filled the fresh moraine seen here. Gigapixel panoramas like this offer polar scientists new ways to document climate-sensitive landscapes, detect temporal change, and potentially develop better insights into the processes involved.

RAPID SURFACE ELEVATION LOSSES OF SPITSBERGEN GLACIERS (1936-1990-2005)

CHRISTOPHER NUTH[1], GEIR MOHOLDT[1], JACK KOHLER[2], JON OVE HAGEN[1] AND HARALD FASTE-AAS[2]

Dept. of Geosciences, Section of Physical Geography, Faculty of Mathematics and Natural Sciences, University of Oslo, Norway
Norwegian Polar Institute, Norway

Introduction

Elevation changes are a common approach towards extracting glacier changes of the largest ice caps Greenland and Antarctica (Krabill et.al., 2000; Wingham et.al., 1998), as well as regions comprising of smaller glaciers like Alaska (Arendt et.al., 2002). ICESat contains a satellite laser altimeter that acquires elevation data with remarkable precision and accuracy (Zwally et.al., 2002; Brenner et.al.,2007). In this study, previous long term elevation changes from 1936 to 1990 (Nuth et.al., 2007) are compared to modern changes derived from comparing the 1990 DEM (Norwegian Polar Institute) to ICESat profiles from 2003 to 2007.

Methodology and Accuracy

Elevations from the 1990 DEM are compared at each ICESat point disregarding the date of aquisition. Elevation change curves are then averaged altitudinally and by region. These change curves therefore represent annual averages of different time intervals ranging from 13 years (1990-2003) to 17 years (1990-2007). The affect of seasonal snow cover, though minimal, results in underestimated thinning and over estimated thickening. The accuracy is derived by comparing non-glacierized stable terrain. The histogram of these changes (Fig. 1) show that 95% of all the datapoints lie within ±5 meters with a standard deviation of 2.3 meters.
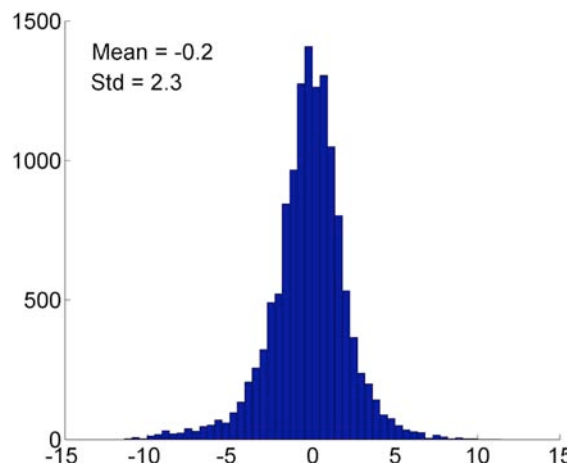

Figure 1. Histogram of elevation differences between ICESat and the 1990 DEM (NP) over non-glacierized terrain.

Results and Perspectives

Figure 2 shows the elevation change curves for the older time series, 1936-1990 (Nuth et.al., 2007) as compared to the newest time interval (1990-2003/07) for six geographic regions. In all regions, the elevation change curves have become more negative. Averaged thinning rates at the glacier fronts have doubled between the two periods with recent losses of up to -2.5 m/yr. Seasonal snow cover is not accounted for, though removal only increases thinning rates. The upper altitudes have generally decreased in elevation. These decreases may not be an indication of water loss, but rather the result of internal accumulation and firn densification. Future work should focus on determing how much internal accumulation is occuring, and how this affects firn densification and thus elevation changes. If this process is occuring and not accounted for, water equivalent volume losses would be overestimateed. In summary, the glaciers of southern Spitsbergen are recently thinning more rapidly, even at upper altitudes which are prone to firn densification. The assumption of constant density for water equivalent conversion therefore needs to be addressed.
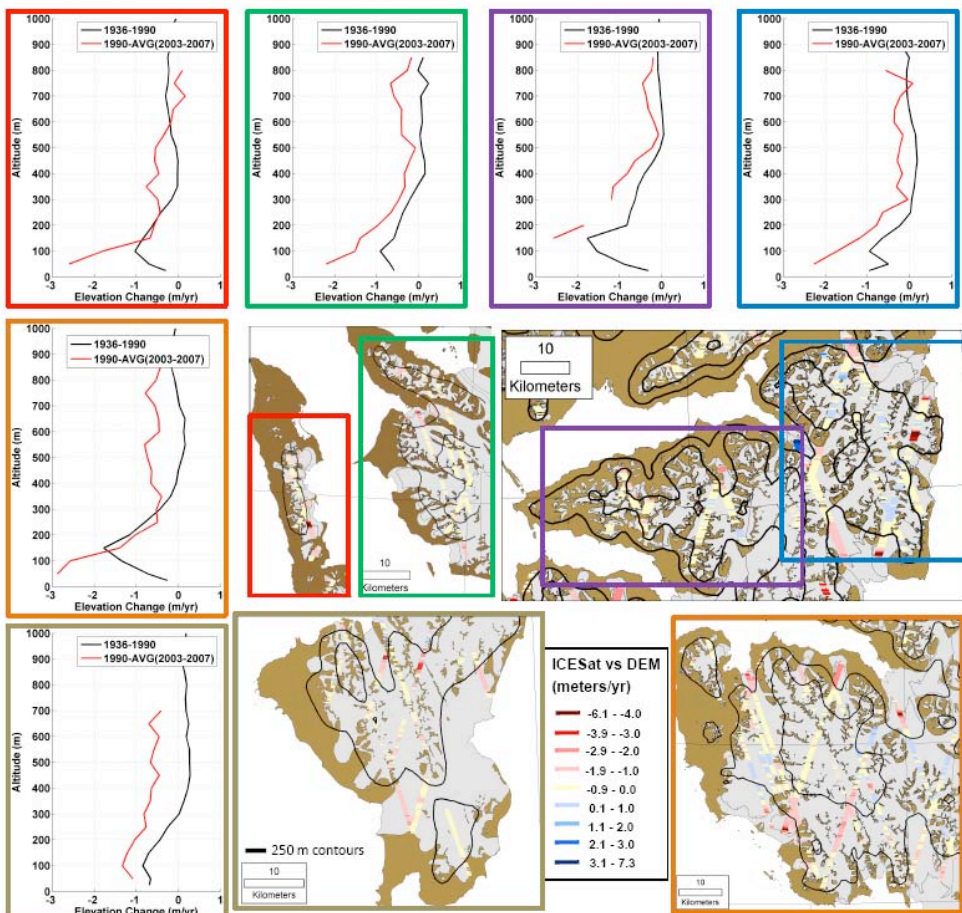

Figure 2. Annual elevation change curves for 6 regions in southern Spitsbergen.

References

Arendt A.A., K.A. Echelmeyer, W.D. Harrison, C.S. Lingle, V.B. Valentine. 2002. Rapid wastage of Alaska glaciers and their contribution to rising sea level. Science 297, 382-386.

Brenner A., DiMarzio J., and Zwally, J. 2007. Precisionand Accuracy of satellite radar and laser altimeter data over the continental ice sheets. IEEE Tran.Geo.Rem. 45(2).

Krabill and 9 others. 2000. Greenland ice sheet: high-elevation balance and peripheral thinning. Science 289, 428 – 430.

Nuth C., J.Kohler, H.F.Aas,O.Brandt.,J.O.Hagen. (2007).Glacier geometry and elevaiton changes on Svalbard. Ann.Glac 46: pp 106-116.

Wingham D. J., A.J. Ridout, R. Scharroo, R.J. Arthern, C. K. Shum. 1998. Antarctic elevation change from 1992-1996. Science 282 (5388): pp. 456-458.

Zwally and others(2002). ICESat's laser measurements of polar ice, atmosphere, ocean, and land. Journal of Geodynamics 34: pp 405-445.

Ice volume changes of Ariebreen, Spitsbergen, during 1936-1990-2007

M. Petlicki[1], J. Lapazaran[2], F. Navarro[2], P. Glowacki[1] and F. Machío[3]

[1] Institute of Geophysics, Polish Academy of Sciences, Poland,
[2] Dept. Matemática Aplicada, Universidad Politécnica de Madrid, Spain
[3] Dept. Electrónica y Comunicaciones, Facultad de Ingeniería Informática, Universidad Pontificia de Salamanca, Spain

Introduction

Ariebreen (77° 01' N, 15° 29' E) is a small valley glacier (ca. 0.36 km^2 in August 2007) located at Hornsund, Spitsbergen, Svalbard, ca. 2.5 km to the west of Hornsund Polish Polar Station. Many Svalbard glaciers have experienced a significant recession at least since the 1930s, and most likely since the end of Little Ice Age in the early 20th century (Werner, 1993). It has manifested as thinning and retreating of ice fronts, though a simultaneous thickening at the uppermost elevations in many locations has been reported (Bamber et al., 2004; Nuth et al., 2007). Moreover, the thinning rate of western Svalbard glaciers has shown an acceleration during the most recent decades (Kohler et al., 2007).

The main aims of this contribution are to determine whether Ariebreen follows such retreat pattern and to quantify the retreat it has experienced, in terms of area, thickness and volume changes, to estimate the average mass balance equivalent to the ice volume change during the period under investigation, and to estimate the volume of ice presently stored in Ariebreen. The main tools to accomplish this will be the analysis of digital terrain models (DTM) of the glacier surface corresponding to different dates, and the radio-echo sounding of the ice body to determine the present ice volume. The latter is described in a separate contribution to this workshop (Navarro et al., 2008).
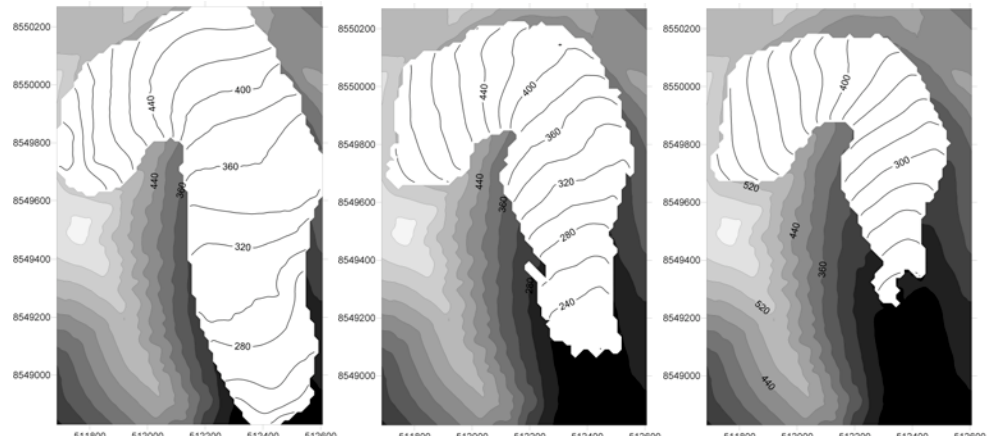

Figure 1. Surface topography of Ariebreen in 1936 (left), 1990 (centre) and 2007 (right).

Construction of DTMs and estimation of ice volume changes 1936-1990-2007 and total volume (2007)

The volume changes 1936-1990 and 1990-2007 were estimated by subtracting the DTMs for the corresponding years, constructed on a common (for each pair) grid 5 m x 5 m. The total volume in 2007 was estimated from the ice thickness map constructed from the radar data.

The DTM for 1936 (Figure 1, left) was constructed from the sheet B12 (Torellbreen, Spitsbergen) of the 1:100 000 Svalbard topographic map (Norsk Polarinstitutt 1953), which is a photogrammetric compilation from aerial photographs taken in 1936. The errors in the DTM for 1936 are the most prominent ones, because of the uncertainties inherent to the original map and the poor coverage of the source data, limited to the glacier boundary and a few contour levels. We have taken as an estimate of the vertical accuracy of the individual data points the value of ±12.49 m for Wedel Jarlberg Land (where Ariebreen is located) obtained by Nuth et al. (2007).

The DTM of the glacier surface in 1990 (Figure 1, centre) was extracted from the DTM of Werenskiold area constructed by Kolondra (2002) from infrared false colour aerial photographs taken in August 1990. The vertical accuracy for the original 1990 DTM was estimated by its author as ±0.5 m. However, for our reconstruction of the glacier surface on the same common grid 5 m x 5 m as 1936 DTM, a standard deviation of ±2.08 m resulted for the interpolation error of the vertical coordinates by kriging.

The DTM of Ariebreen for 2007 (Figure 1, right) was based on our own geodetic measurements made in August 2007 with a Leica TCR-1105 total station. A total of 646 points were measured, of which 192 corresponded to the glacier boundary. The resulting DTM for 2007, with the same regular grid 5 m x 5 m as the 1990 DTM, showed a standard deviation of ±2.42 m for the interpolation error of the vertical coordinates by the kriging method.

The volume changes between any two years were estimated computing, by Simpson's method, the volume resulting from the subtraction of the DTMs for the corresponding years, constructed on a common grid. The total ice volume in 2007 was estimated from the ice thickness map retrieved from the radar data. The ice thickness data were also subtracted from the 2007 glacier surface DTM, constructed on the same grid, in order to determine the subglacial bedrock map. The ice thickness and subglacial relief maps are shown in another contribution to this workshop (see Figure 2 in Navarro et al., 2008).

Results, discussion and conclusions

The area, average ice thickness and ice volume of Ariebreen in 1936, 1990 and 2007, together with their changes during the periods 1936-1990, 1990-2007 and 1936-2007, are shown in tables 1 and 2, while Figure 2 shows the ice thickness changes experienced by the glacier during the mentioned periods.
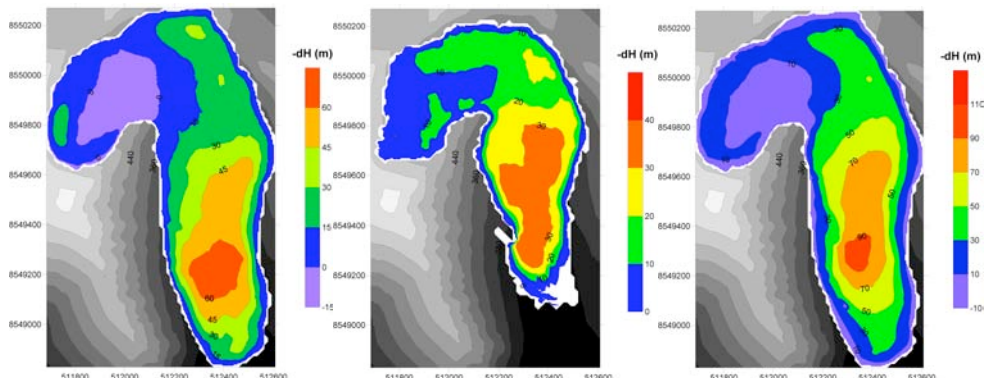
Figure 2. Thickness change of Ariebreen 1936-1990 (left), 1990-2007 (centre) and 1936-2007 (right).

Notice the distinction between the change in average thickness (Table 1) and the average thickness change (Table 2), resulting from the computation over different areas, the latter being that of the start of the period, which is larger and then results a smaller average.

Quite remarkable changes are observed for all parameters in Table 1 and 2. The largest percent change corresponds to the ice volume (that has decreased by 69±29% during the full period analysed), as this figure combines the effects of both changes in area –mainly due to ice front retreat– and changes in ice thickness. The changes in ice volume during the periods 1936-1990, 1990-2007 and 1936-2007 are equivalent to average annual mass balances of –0.44±0.27, –1.00±0.27 and –0.57±0.24 m/y w.e., respectively, computed considering an ice density of 900 kg/m3 and an average area for each period.

Table 1. Glacier area, average ice thickness and ice volume of Ariebreen in 1936, 1990 and 2007, and changes for the periods 1936-1990, 1990-2007 and 1936-2007.

	1936	1990	2007	Change 1936-1990	Change 1990-2007	Change 1936-2007	% Change 2007/1936
Area (km^2)	0.689 ±0.040	0.504 ±0.038	0.363 ±0.009	–0.185 ±0.055	–0.141 ±0.039	–0.325 ±0.041	–53 ± 6
Average thickness (m)	50.22 ±12.83	37.70 ±3.61	22.29 ±1.68	–12.52 ±12.82	–15.41 ±3.98	–27.93 ±12.94	–56 ± 26
Volume (km^3)	0.0346 ±0.0098	0.0190 ±0.0024	0.0108 ±0.0008	–0.0156 ±0.0096	–0.0082 ±0.0022	–0.0238 ±0.0100	–69 ± 29

Table 2. Average thickness change of Ariebreen for the periods 1936-1990, 1990-2007 and 1936-2007.

	1936-1990	1990-2007	1936-2007
Average thickness change (m)	–22.65 ±12.66	–16.22 ±3.19	–34.52 ±12.72

The above data show that Ariebreen has followed the general recession pattern observed in Svalbard, manifested as thinning and retreating of ice fronts, though a simultaneous thickening at the uppermost elevations, an also shows the acceleration in thinning rate observed in western Svalbard glaciers during the most recent decades.

References

Bamber J., Krabill W., Raper V., Dowdeswell J. 2004. Anomalous recent growth of part of a large Arctic ice cap: Austfonna, Svalbard. Geophysical Research Letters 31, L12402, doi: 10.1029/2004GL019667.

Kohler J., James T.D., Murray T., Nuth C., Brandt O., Barrand N.E., Aas H.F, Luckman A. 2007. Acceleration inthinning rate on western Svalbard glaciers, Geophysical Research Letters 34, L18502, doi: 10.1029/2007GL030681.

Kolondra L. 2002. Werenskioldbreen and surrounding areas, Spitsbergen, Svalbard, Norway. Orthophotomap 1:25000. Published by Silesia University, Sosnowiec, and Norsk Polarinstitutt, Tromso.

Navarro F., Grabiec M., Puczco D., Jonsell U., Nawrot A. 2008. Internal Structure of Ariebreen, Spitsbergen, from radio-echo sounding data. Workshop on the dynamics and mass budget of Arctic glaciers/ Glaciodyn (IPY) meeting, Obergurgl, Austria, January 2008.

Nuth C., Kohler J., Aas H.F., Brandt O., Hagen, J.O. 2007. Glacier geometry and elevation changes on Svalbard (1936-90): a baseline dataset. Annals of Glaciology 46, 106-116.

Werner A. 1993. Holocene moraine chronology, Spitsbergen, Svalbard: lichenometric evidence for multiple Neoglacial advances in the Arctic, The Holocene 3, 128-137.

Altimetry of Nordenskiöldbreen and Vestfonna 1991 - 2007 - Preliminary Results

Veijo Pohjola[1], Jim Hedfors[1], John Moore[2], Björn Sjögren[1], Leszek Kolondra[3], Carleen Reijmer[4], Elisabeth Isaksson[5], and Jon Ove Hagen[6]

[1] Department of Earth Sciences, Uppsala university, Sweden.
[2] Arctic Centre, University of Lapland, Finland.
[3] University of Silesia, Poland.
[4] IMAU, University of Utrecht, The Netherlands.
[5] Norwegian Polar Institute, Norway.
[6] University of Oslo, Norway.

Introduction

Regional modelling of the future of the Arctic finds the average warming over the High Arctic may likely be in the range of 5-7˚C during the present century (*1,2*). The current rate of sea level increase is 3.2 mm yr^{-1} (*3*), to a large part as a product of melting ice caps (*4*). Recent compilations points to that the Antarctic ice sheets are more or less in balance within the present error bars, and that Greenland delivers ca 10% of this increase (*5,6*), suggesting that most of the contribution to the current sea level increase may be from ice outside these large ice sheets. With the projected large warming of the Arctic, areas closer to the advection pathways of heat will initially be more affected than areas more isolated to exchange of heat. Svalbard is such a sensitive area, due to the proximity to the North Atlantic drift, and may be expected to show large changes with future warming.

Figure 1. Svalbard and the ice fields Lomonosovfonna and Vestfonna. © Norskt Polarinstitutt.

Svalbard is ~60% glaciated, and the amount of glaciation increases towards the north-eastern part of the archipelago (Figure 1), due to predominant easterly airflow during precipitation events. The total ice coverage of Svalbard is two times the ice coverage on the rest of Europe (including Iceland) (7). This suggests the state and the fate of the large ice fields and ice caps on Svalbard should have a high attention in a European perspective, since they encompass an area of high expected warming and are the largest ice volumes in Europe.

Previous altimetry on Lomonosov- and Vestfonna

Earlier campaigns on the two ice fields by surface DGPS altimetry (8) did not show any conclusive changes in altimetry on Lomonosovfonna / Nordenskiöldbreen during the period 1991-1997. This picture was changed for the period 1996-2002 when aerial laser altimetry was flown by NASA (9). The results from the NASA fligths show a subsidence of more than 0.5 m a^{-1} below 600 m elevation, but a general growth above 1000 m elevation (9). The NASA altimetry flown over Vestfonna the same years show a general subsidence of Vestfonna of the order of 0.0 - 0.6 m a^{-1} along the flight line. A general conclusion, adding the altimetric observation over Austfonna in the same NASA missions (10), is a growth in elevation on the highest parts of these ice fields, but a general subsidence at least below 600 m a. sl.
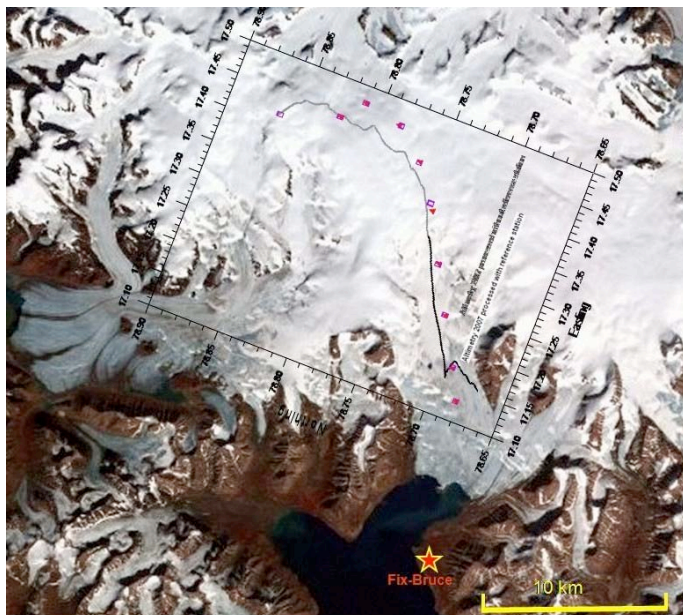

Figure 2. Lomonosovfonna and the outlet Nordenskiöldbreen. The altimetry measured by (8) are marked by purple dots. The geometrical symbols, and the DGPS line driven in 2007 by the black track. The background is a LANDSAT image.

Altimetry campaigns on Lomonosov- and Vestfonna spring 2007

The years after 1997 have been anomalously warm on Svalbard, with longer melt periods, and also years with high precipitation. This may explain the subsidence of the lower elevations, and the growth on higher altitudes found by the NASA missions. This trend of warmer temperatures and higher precipitation has continued over the decade. This motivated our mission to re-measure the altimetry of the two ice fields by driving surface borne DGPS over parts of the two ice fields.

The mission accomplished in 2007 is only a first campaign of three consecutive years of planned surface borne profiling. This gives all data is incomplete and only preliminary at this stage. Figure 2 shows the profiles driven on Lomonosovfonna 2007, and Figure 3 shows the changes over the different measurements periods from (*8,9*) and the 2007 campaign. This preliminary data suggest that the trends found by (*9*) prevail into the five year period between 2002 and 2007.
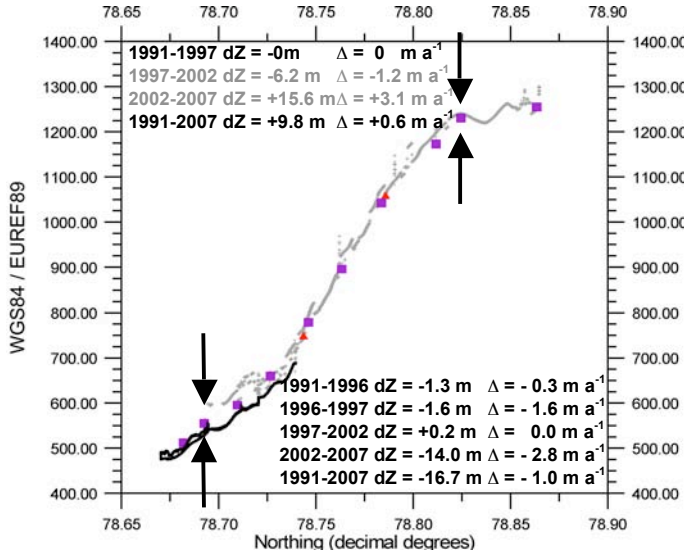

Figure 3. Changes in surface level (dZ) between the different campaigns on Lomonosonfonna. Δ is the rate of change per year. The gray numbers distributions indicate less certain values. Squares and triangles is measurements by (*8*). The lines are measurements 2007.
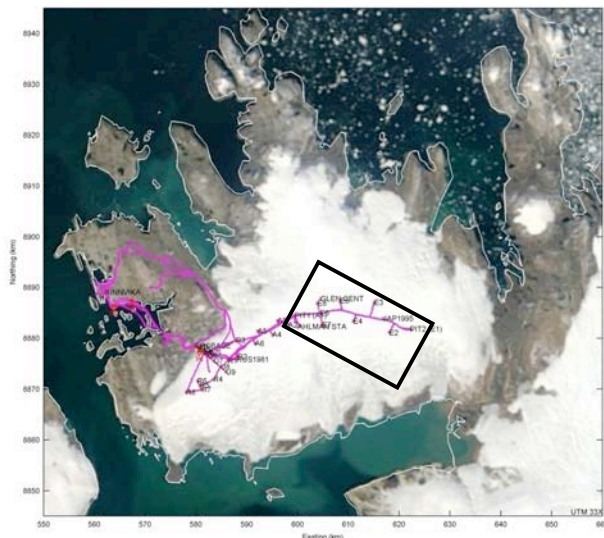

Figure 4. Vestfonna and the altimetry driven 2007 shown as the purple track on the ice cap. The background is a LANDSAT image. The black rectangle is the approximate area covered in Figure 5.

On Vestfonna no ground based campaigns have been accomplished up to date. The only data is the NASA flight lines (*9*), and the altimetry flown by Scott Polar Research Institute in the 1980s (*11*). Figure 4 shows the DGPS profiling done 2007, and Figure 5 show the trends between 2002 and 2007 over these few points

the NASA flight lines crosses our ground based profiling. In all three cases our preliminary results points at a continued lowering rate throughout the last ten years.
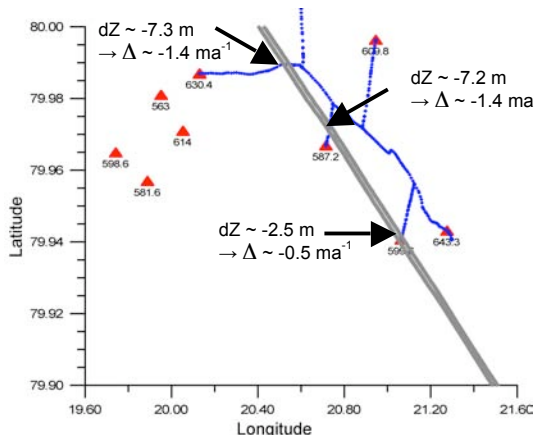

Figure 5. Changes in surface level (dZ) between the different campaigns on Vestfonna. Δ is the rate of change per year. The triangles are heights on position markers for DGPS, and the blue track is kinematic GPS from 2007. The gray lines are airborne altimetry flown 2002. All heights are over WGS84.

Acknowledgements.

References

1. ACIA scientific report. 2004. http://www.acia.uaf.edu/.
2. IPCC. 2007. Global Change 2007 - the 4th assessment report. http://www.ipcc.ch/
3. Cabanes, C., A.Cazenave and C.LeProvost. 2001. Sea level rise during past 40 years determined from satellite and in situ observations. Science, 294, 840-842.
4. Alley, R.B., P.U.Clark, P.Huybrechts and I.Joughin. 2005. Ice-sheet and sea-level changes. Science, 310, 456-460.
5. Raper, S.C. and R.J.Braithwaite. 2006. Low sea level rise projections from mountain glaciers and icecaps under global warming. Nature, 439(19 jan), 311-313.
6. Luthcke, S.B. and 8 others. 2006. Recent Greenland ice mass loss by drainage system from satellite gravity observations. Science, 314(24 nov), 1286-1289.
7. Meier, M.F., and 7 others. 2007. Glaciers dominate eustatic sea-level rise in the 21st century. Science, 317(24 Aug), 1064-1066.
8. Hagen, J.O., T.Eiken, J.Kohler and K.Melvold. 2005. Geometry changes on Svalbard glaciers: mass-balance or dynamic response? Ann.Glaciol., 42, 255-261.
9. Bamber, J.L., W.Krabill, V.Raper, J.A.Dowdeswell and J.Oerlemans. 2005. Elevation changes measured on Svalbard glaciers and ice caps from airborne laser data. Ann.Glaciol., 42, 202-208.
10. Bamber, J., W.Krabill, V.Raper and J.Dowdeswell. 2004. Anomalous recent growth of part of a large Arctic ice cap: Austfonna, Svalbard. Geophys.Res.Let., 31(L12402, doi:10.1029/2004GL019667).
11. Dowdeswell, J.A., D.J.Drewry, A.P.R.Cooper, M.R.Gorman, O.Liestøl and O.Orheim. 1986. Digital mapping of the Northaustlandet ice caps from airborne geophysical investigations. Ann.Glaciol., 8, 51-58.

MASS BALANCE AND VELOCITY OBSERVATIONS ON NORDENSKIÖLDBREEN, SVALBARD

CARLEEN REIJMER[1], MARIANNE DEN OUDEN[1], VEIJO POHJOLA[2] BJÖRN SJÖGREN[2] AND HANS OERLEMANS[1]

[1] Institute for Marine and Atmospheric Research, Utrecht University, The Netherlands
[2] Department of Earth Sciences, Uppsala University, Sweden.

Introduction

Recent studies suggest that in a warming climate, increasing supply of (melt)water to the drainage system of a glacier may lead to higher ice velocities, at least temporarily (Zwally et al., 2002). In order to study the relation between (melt)water input and ice velocities, and focusing on seasonal and inter-annual variability, mass balance and continuous ice velocity measurements are carried out on Nordenskiöldbreen (Svalbard) (Figure 1a). The ice velocity measurements are performed using relatively low cost stand alone GPSs (Figure 1b). These GPSs record their position every hour, from which flow velocities are calculated. The mass balance is determined by traditional stake measurements and by means of a sonic height ranger. The locations of the stakes and GPSs are marked in Figure 1. Here we report first results for the period March 2006 - March 2007.
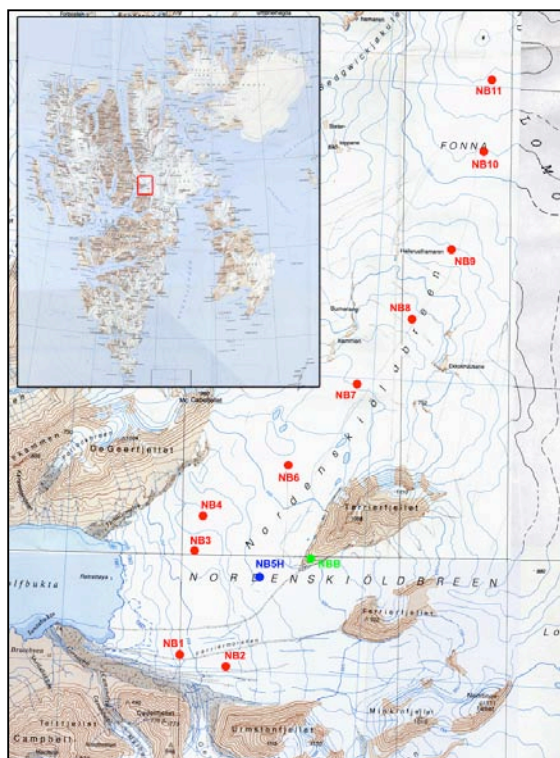
Figure 1. Left: Nordenskiöldbreen, Svalbard. Red dots are GPS and mass balance stake locations on the glacier, green dot marks the location of the GPS reference station, NBB. Location marked NB5H is the location of the sonic altimeter. Locations NB1, 2, 4-8 and B were established in March 2006, NB3 and 9-11 were placed in March 2007. Inset: map of Svalbard with the location of the glacier marked by a red box. Top: Stand alone GPS mounted on a mass balance stake on Nordenskiöldbreen.

Mass balance

Knowledge of the mass balance of Nordenskiöldbreen is limited to accumulation values for the higher parts of the glacier, the Lomonosovfonna ice field, based on ground penetrating radar observations and ice cores. Estimates range from 0.41 m w.e. (Pohjola et al. 2002) to 0.52 m w.e. (Pälli et al., 2002). For the lower parts of the glacier estimates are thus far based on the average mass balance gradient presented by Hagen et al. (2003) in combination with the values presented by Pälli et al. (2002) and an average value of the equilibrium line of 600 m a.s.l. The measurements presented in figure 2 are the first available for the lower part of Nordenskiöldbreen. The values in Figure 2a are based on stake readings using an ice density of 900 kg/m^3 and snow density of 400 kg/m^3. They show an increase in mass balance from an ablation of ±2 m w.e. at ±100 m a.s.l. to 0.2 m w.e. of accumulation at ±700 m a.s.l. The equilibrium line altitude (ELA) was at ±660 m a.s.l., between sites 7 and 8. Compared to the gradient estimated by Hagen et al. (2003), the observed gradient is smaller, -0.43 m w.e. and -0.46 m w.e. per 100 m altitude increase, respectively. Note however that we present only one year of data.
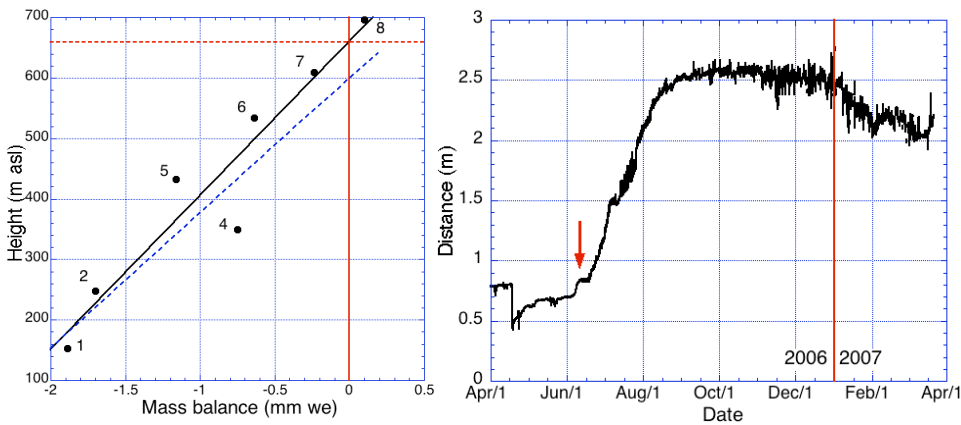

Figure 2. Left: Annual mass balance (April 2006 - March 2007). Numbers denote the stake locations in Figure 1. The red dotted line indicates the equilibrium line altitude. The blue dotted line indicates the estimated mass balance gradient from Hagen et al. (2003). Right: Time series of distance to the surface as measured with the sonic height ranger (site NB5H in figure 1).

The temporal variations in the mass balance are measured using a sonic height ranger (Figure 2b). The data are corrected for the effect of changes in air temperature on the speed of sound. Several features can be noted in this record. A snowfall event resulted in a decrease of 0.3 m in distance between sensor and surface at the end of March. After this event, the distance increased from May till August, showing about 2 m of snow/ice melt. Furthermore, the autumn of 2006 was very dry, no melt took place and accumulation only started in January 2007. Note also the variability in the record from July onwards, which is caused by the sensor hanging loose on its pole, moving in the wind. From the record we guess that the sensor came loose on 14 June.

Ice velocity

The GPSs record their position every hour. The accuracy of the sampled locations can be estimated from the time series obtained at the reference site NBB. Figure 3a shows for every sample recorded at NBB the displacement with respect to the average location of NBB. Maximum displacement is 5.1 m and the standard deviation is 1.8 m, which is a measure for the annual accuracy in the displacement. Time series of velocities are determined by applying a Gaussian weighted running average of 360 hours over the recorded locations, then calculating velocity from the resulting hourly displacements and applying a Gaussian weighted running average of 360 hours over the resulting velocities. The results for NB4, 6 and 7 are plotted in Figure 3b. The figure shows large variations in flow velocity throughout the year with a clear maximum around 10 July 2007, about 3 weeks after the onset of the melting season in June. There is no clear lead or lag in timing of the maximum in flow speed. This is partly explained by the limited distance between the locations (order of km). After this peak in velocities, velocities decrease to on average lower values in winter. The records also exhibit variability on time scales of 2-3 weeks, for which at present we do not have an explanation. We do not show NB1, 2, 5 and 8. NB1 and 2 are not on the main flow line of Nordenskiöldbreen (see Figure 1) and NB5 and 8 did not work properly due to technical problems.
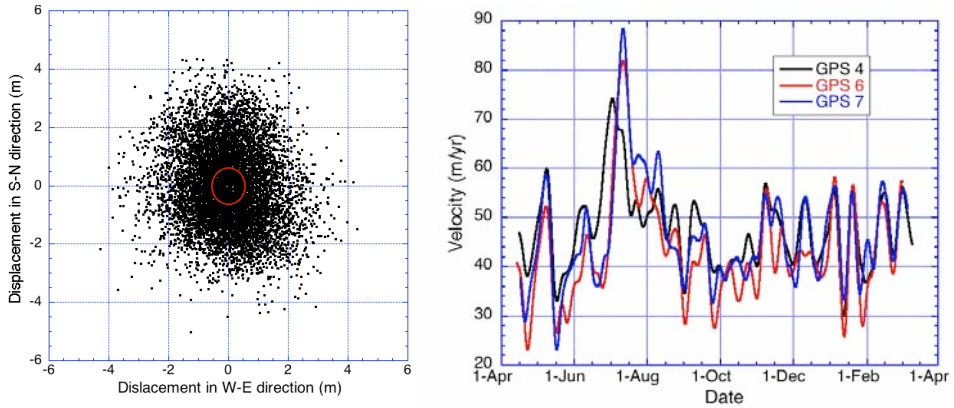

Figure 3. Left: Displacement at NBB with respect to its mean location. The red circle denotes the standard deviation in the average displacement. Right: Flow velocity record at NB4, 6 and 7.

We use the GPS data also to determine annual flow velocities at all sites. Results are given in Table 1. The table presents annual mean velocities determined using three methods, two based on the stand alone GPS records and one based on traditional DGPS observations. The flow velocities are clearly much lower on NB1 and 2 compared to the sites on the main flow line. Flow velocities at the lower part of the glacier are on the order of 45 m/yr. Compared to the DGPS observations, which have an accuracy of 0.1 m, the stand alone GPSs show similar values within their uncertainty range of 3.7 m/yr.

Table 1. Annual ice velocities. Av refers to values based on velocity averages as presented in figure 3b, E-S refers to values based on first and last location in the time series. The DGPS values are based on traditional DGPS measurements. Given percentages refer to amount of available data on which the velocity value is based when smaller than 99%.

Station	GPS (m/yr) (Av)	GPS (m/yr) (E-S)	Max (m/yr)	DGPS (m/yr)
NB1	9.2	4.0	36.2	
NB2	7.9	5.6	18.2	
NB4	47.8	47.2	74.3	46.3
NB5H	*27.1 (32%)*	*28.6*	*48.7*	
NB6	43.2	46.0	81.9	40.2
NB7	46.5	45.7	88.5	50.2
NB8	*39.6 (90%)*	*39.0*	*52.5*	36.6

Outlook

The stand alone GPS have provided us with mass balance and velocity records at 7 locations on Nordenskiöldbreen. In 2008, data from 4 more locations will become available. The data will be used for tuning and validation of mass balance and dynamical models, the latter including the effect of (melt)water on the flow velocities. On the technical site, the GPSs are developed further in order to increase their accuracy.

References

Pälli, A., J. Kohler, E. Isaksson, J.C. Moore, J.F. Pinlgot, V.A. Pohloja and H. Samuelsson, 2002. Spatial and temporal variability of snow accumulation using ground-penetrating radar and ice cores on a Svalbard glacier. J. Glaciol., 48(162), 417-424

Pohjola, V.A. , T.A. Martma, H.A.J. Meijer, J.C. Moore, E. Isaksson, R. Vaikmäe and R.S.W. van de Wal, 2002. Reconstruction of three centuries of annual accumulation rates based on the record of stable isotopes of water from Lomonosovfonna, Svalbard. Ann. Glaciol., 35, 57-62.

Hagen, J.O., J. Kohler, K. Melvold and J.G. Winther, 2003. Glaciers in Svalbard: mass balance, runoff and freshwater flux. Polar Research, 22(2), 145-159.

Zwally, H. J., W. Abdalati, T. Herring, K. Larson, J. Saba and K. Steffen, 2002. Surface Melt-Induced Acceleration of Greenland Ice-Sheet Flow. Science, 297, 218-222.

Spatio-temporal variability of snow melt on Svalbard derived from spaceborne scatterometer data (Qscat)

Gerit Rotschky, Jack Kohler, Elisabeth Isaksson

Norwegian Polar Institute, Tromsø, Norway

Introduction

Evidence for ongoing large changes in the Arctic climate has been accumulating during the last decade, particularly with regards to sea ice, permafrost and glacier mass balance. Due to the effect of global warming dramatic changes in the Arctic snow and ice coverage are currently observed, expressed by a reduction of 10% over the last 30 years associated with an extended and longer lasting melting season. Previous studies have demonstrated the capacities of active microwave instruments for the detection of surface melt and freeze-up due to the high sensitivity of radar backscatter to snow wetness (e.g. Wismann, 2000; Nghiem et al., 2001; Smith et al., 2003; Steffen et al., 2004; Wang et al., 2005). Spaceborne scatterometers provide data at low spatial but high temporal resolution allowing consistent observations on a daily time scale.

This study focuses on Svalbard characterized by a highly variable climate throughout the year due to its position within a zone that includes both the polar ocean and atmospheric fronts between the Arctic Ocean, Nordic Seas and Barents Sea. Nevertheless, over a long enough period of time we expect to see a general climatic trend by monitoring the spatio-temporal variability of snow distribution and melt all over Svalbard. For this we utilize microwave backscattering measurements continuously carried out by the Ku-band scatterometer QSCAT since fall 1999. Meteorological data from weather stations around Svalbard are available to investigate links between atmospheric circulation, moisture transport, near surface air temperature and corresponding deposition and melting of snow, respectively. The analysis demonstrates that coarse resolution scatterometer data can be usefully applied to trace consequences of a warming climate in the Arctic.
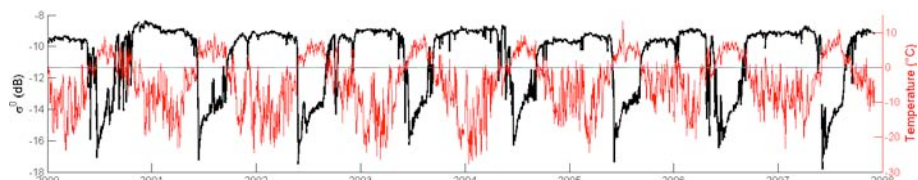

Figure 1. Qscat σ^0 measurements plotted against Ny-Ålesund temperature records.

Methodology

We utilized Qscat enhanced resolution products (Long et al., 1993) to detect spatio-temporal changes in microwave backscattering properties of Svalbard. For a given frequency the latter are mainly a function of surface wetness, temperature, and density. Due to high absorption of radar waves by liquid water within a snowpack the beginning of the melt season is clearly marked by a sudden drop of

the backscatter coefficient σ^0 linked to air temperatures rising to above-zero values (Figure 1). By taking advantage of this connection we mapped melt onset as well as number of melt days per year for all of Svalbard since 1999 based on a dynamic σ^0 threshold. Melt was thereby assumed when the backscattering within a specific Qscat resolution cell had lowered to 1.35 times its mean winter value. However, for some years this simple melt detection approach is easily obscured by single rainfall events that occur within the winter season visible as spike-like features within the σ^0 time series. Therefore, short-term backscatter reductions are removed from the analysis.

Results

The annual melt intensity, expressed as the number of melt days in each year, is found to be highest in the south and along the western coast of Svalbard. To compare spatio-temporal differences we calculate an average backscatter response (σ^0_{mean}) for 7 Svalbard regions. While there is pronounced regional and interannual variability in melt onset as well as number of melt days per year, there is nevertheless a trend of earlier melt onset and an increasing number of melt days per year apparent for the period of observation (Figure 2), as expected in a warming climate. Further, in some years striking synchronous melt onsets all over Svalbard can be observed, which are most likely the result of regional-scale rainfall events.
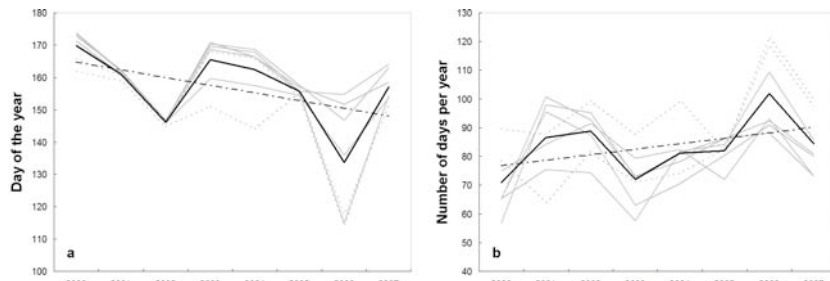

Figure 2. (a) Summer melt onset and (b) number of melt days per year for Svalbard (regional variability in gray).

References

Long, D.G., P.J. Hardin, P.T. Whiting, 1993. Resolution enhancement of spaceborne scatterometer data, IEEE Trans. Geosci. Remote Sens., 31(3):700-715.

Nghiem, S.V., K. Steffen, R. Kwok, W.-Y. Tsai, 2001, Detection of snowmelt regions on the Greenland ice sheet using diurnal backscatter change, J. Glaciol., 47(159), 539-547.

Smith L.C., Y. Sheng, R.R. Forster, K. Steffen, K.E. Frey, D.E. Alsdorf, 2003. Melting of small Arctic ice caps observed from ERS scatterometer time series, Geoph. Res. Lett., 30(20), 2034.

Steffen, K., S.V. Nghiem, R. Huff, G. Neumann, 2004. The melt anomaly of 2002 on the Greenland Ice Sheet from active and passive microwave satellite observations. Geoph. Res. Lett., 31, L20402, doi:10.1029/2004GL020444.

Wang L., M. J. Sharp, B. Rivard, S. Marshall, and D. Burgess, 2005. Melt season duration on Canadian Arctic ice caps, 2000–2004, Geoph. Res. Lett., 32, L19502.

Wismann, V., 2000. Monitoring of seasonal snowmelt on Greenland with ERS scatterometer data, IEEE Trans. Geosci. Remote Sens., 38(4), 1821-1826.

IPY Outreach, Education, and Polar Science Days

Rhian Salmon

IPY International Programme Office Education and Outreach Coordinator

Abstract

Scientists from a wide range of disciplines and countries are becoming involved in outreach activities that are unique to their project and reach a wide range of audiences. Quarterly IPY Science Days are also now being organised in order to develop easy ways for the IPY Community to raise awareness of the polar regions and their research. It is hoped that the Glaciodyn community will become involved with the March Polar Day that will focus on 'Changing Earth'. This talk and discussion hopes to expand on some of these ideas to develop and outreach strategy that works for the scientists involved.

A FIVE-YEAR RECORD OF SUMMER MELT ON EURASIAN ARCTIC ICE CAPS

MARTIN SHARP[1] AND LIBO WANG[2]

[1] Department of Earth and Atmospheric Sciences, University of Alberta, Canada
[2] Climate Research Division, Atmospheric Science and Technology Directorate, Environment Canada, Canada

Abstract

Five-year climatologies (2000-2004) and annual anomaly patterns of melt season duration and dates of melt onset and freeze-up were derived for major ice masses in Svalbard, Novaya Zemlya and Severnaya Zemlya using enhanced resolution backscatter data from QuikScat. Severnaya Zemlya has later melt onset, earlier freeze-up and shorter melt seasons than the other areas. Latitude (Svalbard) and longitude (Novaya Zemlya and Severnaya Zemlya) are stronger influences on the five-year mean melt duration than elevation. Melt duration is generally greatest in the west of each archipelago, likely due to the influence of warm ocean currents offshore. 2001 was the longest melt season in all 3 archipelagos, while 2000 was the shortest. Annual mean melt duration in each region was strongly correlated with the mean June + August air temperature at 850 hPa geopotential height (derived from the NCEP/NCAR Reanalysis). Integration of these results with previously published results from Greenland and the Canadian Arctic reveals that 2003 was the longest melt season in the 2000-2004 period across the Arctic as a whole, while 2002 was the shortest. Correlation of melt duration anomaly series for 19 discrete areas of the Arctic identifies 7 spatially coherent regions with common patterns of variability in annual melt duration, and suggests the possibility of teleconnections between some widely separated regions.

Regional distribution of snow accumulation on North-Western Spitsbergen glaciers, Svalbard

Ireneusz Sobota and Marek Grześ

Department of Cryology and Polar Research, Institute of Geography, N. Copernicus University, Poland

The studies of the snow cover were made on the glaciers of the Kaffiøyra region in the north-western Spitsbergen. The studies, carried out since 1996, are part of a programme which researches the mass balance of the selected glaciers of this region (Sobota 2003, 2005, 2007a, 2007b). The main goal of the research was to assess the water resources in snow and the accumulation part of their mass balance. The snow profiles were also used to analyse the selected physical and chemical properties of the snow cover. Spatial diversity of snow accumulation on the glaciers and its changes resulting from the altitude were analysed. The studies of the snow cover on the Waldemarbreen began in 1996, on the Irenebreen in 2001, while on the Elisebreen in 2005. In 2007 snow accumulation was also studied on Aavatsmarkbreen. All the studies carried out enabled the authors to assess the size and regional diversity of snow accumulation on the glaciers located in the north-western part of Spitsbergen.

The glaciers are located in the northern part of the Oscar II Land, Kaffiøyra, north−western Spitsbergen. Kaffiøyra is a coastal lowland situated on the Forlandsundet. Waldemarbreen is about 3.5 km long and has an area of 2.6 km^2. The ice originates in one cirque and flows from an elevation of more than 500 m to the present snout at 135 m a.s.l. Irenebreen, a valley glacier located to the south of Waldemarbreen, flows down towards the Kaffiøyra plain. The area of Irenebreen amounts to 4.1 km^2. Elisebreen area is 10.2 km^2. Its length is about 7 km, while its width is up to 1.8 km. To the north the glacier borders Agnorbreen which is often treated as part of Elisebreen. Aavatsmarkbreen is the largest of all the studied glaciers; its area is about 75 km^2. Its length is 15 km, while its width is from about 3 km in the mountain zone to 4 km in the ice cliff zone, which ends up in the sea.

The measurements were taken three times at every site, the accuracy of the readings being ±1 cm. The basis for calculations and graphic presentation of spatial variation of snow cover thickness resulted from 100 to 150 soundings. Snow pits were dug if a snow layer could not be penetrated through. The measurement sites were located with GPS and marked on the map. Snow density, structure, grain type and hardness values were recorded. The density of snow was measured in pits and at representative points.

The research has enabled the authors to determine the spatial diversity of snow accumulation on four glaciers located in the north-western part of Spitsbergen: Waldemarbreen, Irenebreen, Elisebreen and Aavatsmarkbreen. All those glaciers had a large spatial diversity of their snow cover thickness, and its distinct changeability with the changing altitude. Accumulation values observed on the

glaciers were related to their absolute altitude a.s.l. (Fig. 1). The largest accumulation gradient was recorded for the Elisebreen and the Aavatsmarkbreen. An important role in forming the spatial diversity of snow accumulation belongs to snow movement due to wind. The spatial distribution of the winter snow accumulation on the glaciers of this region shows some rules observed every winter season (Grabiec et al. 2006; Grześ and Sobota 2000, Sobota and Grześ 2006; Sobota 2003, 2005, 2007a).
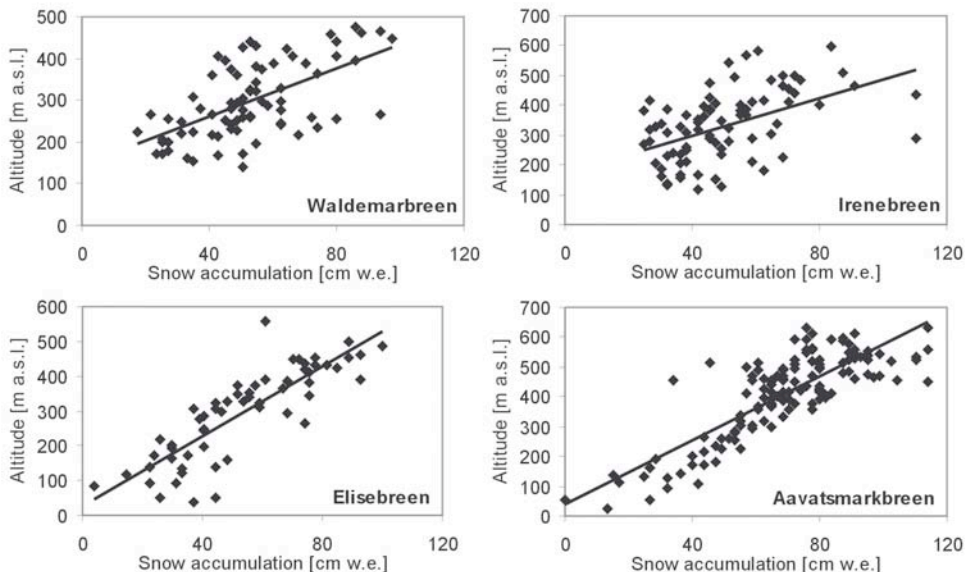

Figure 1. Relation between the snow accumulation and altitude in 2007 on selected glaciers.

The measurements of structure and graining of the snow cover were not undertaken during all of the analysed periods. Snow cover shows some specific physico-chemical properties. Its vertical profile shows a variety of snow types of diverse level of metamorphosis, hardness and wetting. Snow structure reflects prevailing weather conditions at the time when the snow cover formed. In the individual years the snow cover of the studied glaciers was dominated by fine-grained and medium-grained snow, while the layer above ice contained coarse-grained snow. Numerous ice layers were also found. Ice layers results prove seasonal warming above 0°C, which causes melting followed by freezing of snow during the formation of the snow cover. Such a phenomenon is an important factor that stops snow redeposition, as the frozen cover is resistant to wind and it protects the underlying layers. Moreover, such ice layers deteriorate the conditions for the deposition of fresh snow. The entire course of the phenomena, in general, is dependant on the weather conditions, and the frequency and the length of the warming.

During all the years of study, the snow density on the researched glaciers at the individual depths was similar, and it was directly proportional to the depth. During

most of the accumulation seasons a slight increase of mean snow density was observed with the decreasing altitude and the decreasing snow cover thickness.

In 2007 the spatial diversity of snow density of the uppermost layer on all the glaciers was analysed. Although is shows large changeability in individual places of the studied glaciers, an inverse proportion was recorded between the snow density, the altitude and the size of the snow accumulation in a given place. The snow density distribution is clearly related to the characteristic areas of the glacier: its snout and its accumulative zone (Fig. 2). The interrelation between the mean snow density on a glacier in a given year and the mean snow accumulation was not recorded.
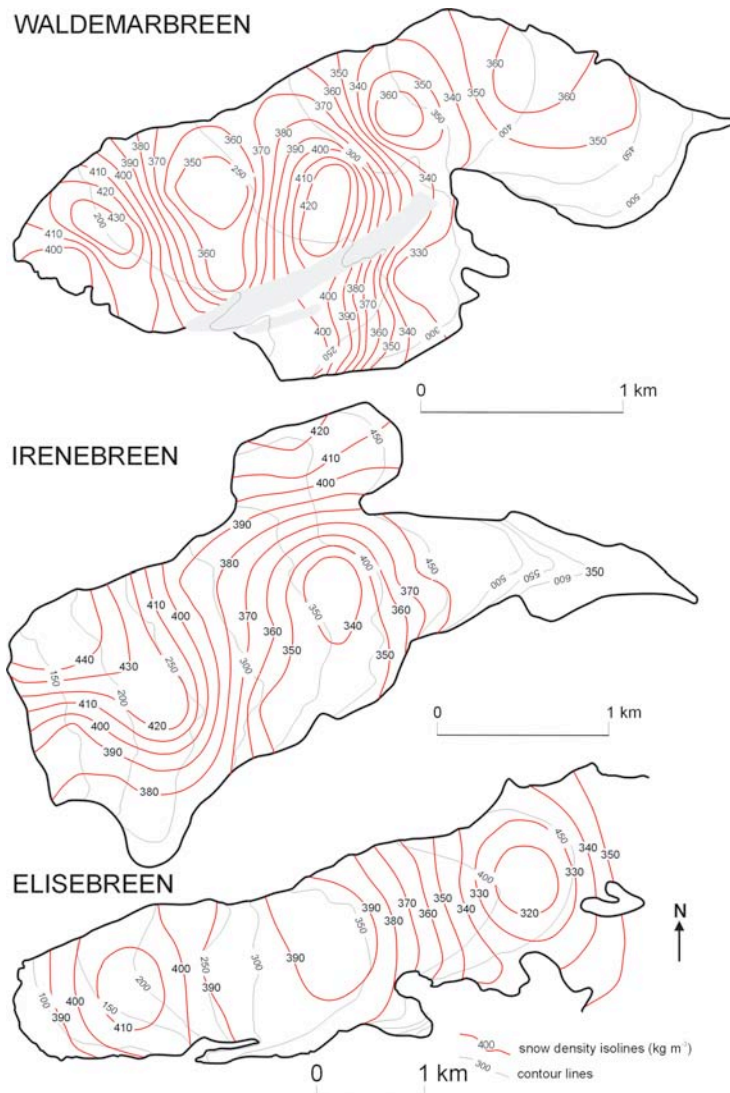

Figure 2. Maps of surface snow density on glaciers: Waldemarbreen, Irenebreen and Elisebreen in 2007.

The mean snow density on Waldemarbreen was 375 kgm^{-3} in the years 1996-2007, on Irenebreen it amounted to 360 kgm^{-3} in the years 2002-2007, while on Elisebreen it was 385 kgm^{-3} in the years 2005-2007. It was found out that the snow density on the studied glaciers at the individual depths was similar, and directly proportional to the depth.

It is characteristic that the regional diversity of snow accumulation on the researched glaciers is not large and the mean winter accumulation is similar. For instance, the mean snow accumulation on Waldemarbreen and Irenebreen was very similar in the years 2002-2007. However, all the analysed glaciers show a large spatial diversity of snow accumulation on their surface. It is connected with both the changing altitude and the local conditions on the glacier.

References:

Grabiec M., Leszkiewicz J., Głowacki P. and Jania J. 2006. Distribution of snow accumulation on some glaciers of Spitsbergen. Polish Polar Research, 27(4): 309-326.

Grześ M. and Sobota I. 2000. Winter snow accumulation and winter outflow from the Waldemar Glacier (NW Spitsbergen) between 1996 and 1998. Polish Polar Research 21(1): 19-32.

Sobota I. 2003. Warunki meteorologiczne i wybrane problemy akumulacji śniegu w regionie Kaffiøyry (NW Spitsbergen) w okresie od lipca 2001 roku do kwietnia 2002 roku, Problemy Klimatologii Polarnej 13: 239-249.

Sobota I. 2005. Struktura bilansu masy lodowców Kaffiøyry na tle lodowców Svalbardu. Kaffiøyra. Zarys środowiska geograficznego Kaffiøyry (NW Spitsbergen), 43-60.

Sobota I. 2007a. Mass balance monitoring of Kaffiøyra glaciers, Svalbard. The Dynamic and Mass Budget of Arctic Glaciers. Extended abstracts, Workshop and GLACIODYN (IPY) Meeting, IASC Working Group on Arctic Glaciology, Utrecht University, 108-111.

Sobota I. 2007b. Selected methods in mass balance estimation of Waldemar Glacier, Spitsbergen. Polish Polar Research, 28(4): 249-268.

Sobota I. and Grześ M. 2006. Charakterystyka pokrywy śnieżnej na lodowcach Kaffiøyry (NW Spitsbergen) w 2005 roku. Problemy Klimatologii Polarnej 16: 147-159.

Identifying causes of peripheral thinning of the Greenland Ice Sheet

Andrew Sole[1], Tony Payne[1], Jon Bamber[1], Peter Nienow[2] and William Krabill[3]

[1] Bristol Glaciology Centre, School of Geographical Sciences, Bristol, UK
[2] School of Geosciences, University of Edinburgh, Edinburgh, UK
[3] Cryospheric Sciences Branch, NASA Goddard Space Flight Centre

Introduction

Recent observations have shown that the periphery of the Greenland ice sheet is thinning rapidly and that this thinning is greatest around outlet glaciers. Two principal mechanisms for climate induced dynamic thinning have been presented in the literature.

The first suggests that enhanced ice melt caused by climatic warming is affecting ice dynamics directly (Zwally et al. 2002). Longer and more widespread surface melt may increase drainage to the bed through crevasses and moulins and thus enhance ice flow through basal lubrication. The second mechanism is related to the collapse of ice shelves and retreat of marine termini. Changes in flow of an outlet glacier occur in response to changes in its force balance – the sum of gravitational and resistive forces acting on the ice (Payne et al. 2004). As a floating ice shelf retreats, changes in longitudinal stresses within the ice may cause its velocity to increase and dynamic thinning to occur (Vieli et al. 2002). The initial perturbation could be due to accelerated calving rates (Thomas 2004) caused by increased basal melting of the ice shelf by warmer ocean water (Payne et al. 2005) or increased surface melting resulting from higher air temperatures (Alley et al. 2005).

Methodology

By using PARCA laser altimetry data to extract thinning rates (*dh/dt*) for many Greenlnad outlet glaciers, the relative importance of these mechanisms can be tested using several hypotheses:

1. *Thinning is not dynamic, but is related to local mass balance changes*. If this were the case we would expect thinning to vary only with local mass balance i.e. with altitude and between climatic regions. This is a null hypothesis which allows us to test whether 'inland ice' (slow flowing ice that is not obviously part of an outlet glacier) and outlet glaciers are thinning at different rates. To test this hypothesis we compare ice surface elevation change rates for inland ice (the control flight line) with that of nearby outlet glaciers for two areas in Southern Greenland.
2. *Thinning is principally caused by direct meltwater effects on ice flow*. In this case, *dh/dt* of land terminating and tidewater outlet glaciers should be statistically the same. We test this hypothesis by comparing mean *dh/dt* for a number of tidewater and land terminating outlet glaciers in Southern Greenland

(Figure 1). This region was chosen because there are more tidewater and land terminating outlet glaciers with good flight line coverage. However, tidewater outlet glaciers are likely to be more sensitive to meltwater input since their termini are already 'floating'. Thus, an identical increase in surface meltwater input to the bed would be more likely to raise subglacial water pressure to values approaching overburden pressure, with correspondingly greater ice acceleration and dynamic thinning.

3. *Thinning is principally caused by calving events of tidewater glaciers*. In this case land terminating outlet glaciers should either not be thinning at all, or thinning at a rate related to increases in the number of Positive Degree Days (PDDs), while thinning rates of tidewater outlet glaciers should be significantly greater than those expected from changes in air temperature. This hypothesis is tested by comparing observed *dh/dt* for land terminating and tidewater outlet glaciers with the melt expected from increases in air temperature using a Positive Degree Day (PDD) Model (Braithwaite 1995).
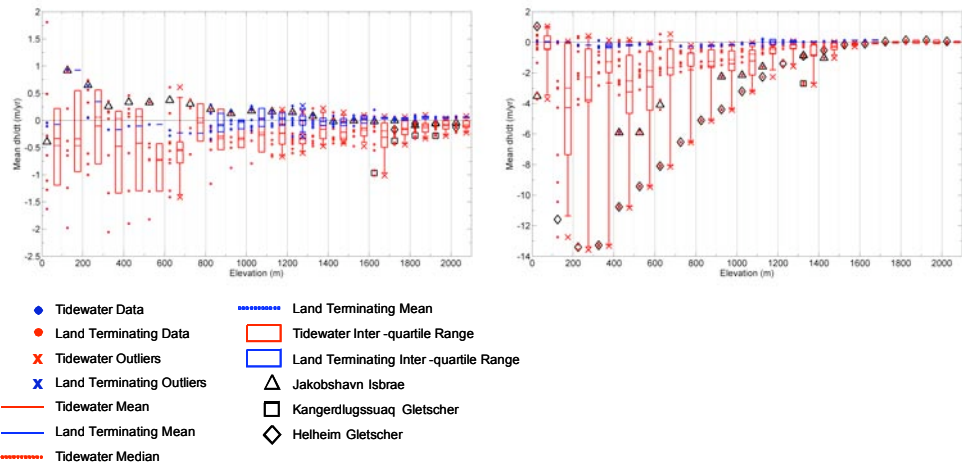

Figure 1. A comparison of surface elevation change rates for a) 11 tidewater and 6 land terminating glaciers for the period 1993 to 1998. Red refers to tidewater outlets, while blue refers to land terminating outlets. For each elevation band, both the actual data and a box plot representing the data are shown. Each solid dot represents the mean *dh/dt* value for the respective elevation band for a particular flight line. The closed boxes represent the inter-quartile range which includes 50 % of the data, and the whiskers are the 5th and 95th percentiles. Black, open shapes refer to specific outlet glaciers identified in the text; and b) 9 tidewater and 2 land terminating glaciers for the period 1998 to 2006.

Results and Discussion

Hypothesis 1: Thinning rates are significantly greater on outlet glaciers than on neighbouring areas of slow moving ice and suggest that ice dynamics does play an important role in the peripheral thinning of the ice sheet. This is in agreement with many other published results.

Hypothesis 2: Figure 1 shows that in general, tidewater outlet glaciers have thinned significantly more than their land terminating counterparts. Mean thinning rates for tidewater glaciers below ~1000 m are four times larger (significant at the 99 % confidence level) from 1998 to 2006 than from 1993 to 1998. Mean *dh/dt* values for land terminating outlets, however, remain statistically unchanged over the same time periods. This suggests that a change in a controlling mechanism specific to the thinning rates of tidewater outlets occurred in the late 1990s and that this change did not affect thinning of land terminating outlets. Moreover, the statistically significant differences between mean dh/dt values for tidewater and land terminating outlet glaciers suggest that they can be seen as separate populations.
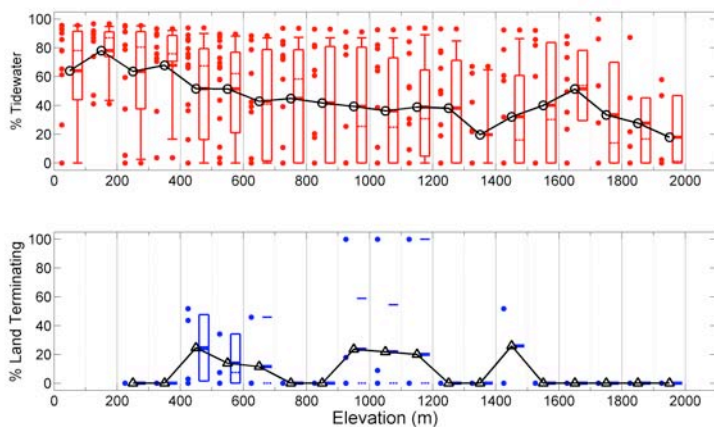

Figure 2. The percentage of observed thinning which cannot be explained by thinning calculated by a PDD model for all surveyed glaciers. A zero % value means that for all glaciers with data in that particular elevation band, the ablation anomaly thinning was greater than observed thinning. Hollow joined symbols are mean thinning rates, refer to Figure 1 caption for meaning of other symbols.

Hypothesis 3: The percentage difference between *dh/dt* values predicted by the PDD model and the observed dh/dt values are shown in Figure 2. For tidewater outlet glaciers, values increase towards the terminus, reaching ~70 %, while for land terminating outlet glaciers, values are low (mean of ~10 %) and show no relationship with elevation. It therefore seems likely that thinning of land terminating outlet glaciers is principally controlled by variations in local mass balance, while thinning of tidewater outlet glaciers is dependent on ice dynamics. The mechanism by which this dynamic thinning occurs is still not clear although a good correlation between calving front retreat and thinning rates (Joughin et al. 2008), as well as the association of dynamic thinning with tidewater outlet glaciers, suggests that perturbations at the termini of tidewater outlet glaciers are mainly responsible. It seems likely that sea surface temperatures, decadal scale surface air temperature increases and other factors such as glacier geometry, ice thickness and basal topography must be combined to understand a tidewater glacier's sensitivity to climate change (Box and Herrington 2007).

Dynamic thinning related to calving will cease once the ice sheet retreats beyond the direct influence of the ocean. These findings therefore have important

implications for the future mass balance of the ice sheet and predictions of sea level rise over the next few centuries.

References

Alley, R., Clark, P., Huybrechts, P., and Joughin, I., 2005. Ice-sheet and sea-level changes. Science, 310, 456-460.

Box, J., and Herrington, A. 2007, Was there a 1930's Meltdown of Greenland Glaciers? Eos Trans. AGU, 88(52), Fall Meet. Suppl., Abstract C11A-0077.

Braithwaite, R., 1995. Positive degree-day factors for ablation on the Greenland ice sheet studied by energy-balance modelling. Journal of Glaciology, 41, 153-160.

Joughin, I., Howat, I., Alley, R., Ekstrom, G., Fahenstock, M., Moon, T., Nettles, M., Truffer, M., and Tsai, V., 2008. Ice-Front Variation and Tidewater Behavior on Helheim and Kangerdlugssuaq Glaciers, Greenland. Journal of Geophysical Research, doi:10.1029/2007JF000837, doi:10.1029/2007JF000837.

Payne, A., Holland, P., Feltham, D., and Jenkins, A. 2005, Modelling the coupled evolution of the ice-shelf/stream flow system and the oceanic circulation in the ice-shelf cavity. European Geosciences Union, Vienna.

Payne, A., Vieli, A., Shepherd, A., Wingham, D., and Rignot, E., 2004. Recent dramatic thinning of largest West Antarctic ice stream triggered by oceans. Geophysical Research Letters, 31, doi:10.1029/2004GL021284.

Thomas, R., 2004. Force-perturbation analysis of recent thinning and acceleration of Jakobshavn Isbrae, Greenland. Journal of Glaciology, 50, 57-66.

Vieli, A., Jania, J., and Kolondra, L., 2002. The retreat of a tidewater glacier: observations and model calculations on Hansbreen, Spitsbergen. Journal of Glaciology, 48, 593-600.

Zwally, H., Abdalati, W., Herring, T., Larson, K., Saba, J., and Steffen, K., 2002. Surface melt-induced acceleration of Greenland ice sheet flow. Science, 297, 218-222.

Relations between horizontal strain and ice elevation change

Manfred Stober

Stuttgart University of Applied Sciences

Introduction

In a long-term project (1991 until 2006) two research areas, Swiss Camp and ST2, are surveyed by geodetic methods in order to determine elevation change, ice flow velocity and deformation of the ice surface. About elevation change and ice flow were reported in Stober (2007) and Stober and Hepperle (2007). This paper is focussed on deformation and strain and on the attempt in determination the net mass balance from geodetic ground measurements.

The research area at Swiss-Camp (ETH/CU-Camp), established in 1991, is situated 80 km east from the West Greenlandic coastal village of Ilulissat, latitude 69°34'N, longitude 49°20'W, elevation 1170 m a.s.l near the equilibrium line altitude. The network consists of 4 stakes, forming a triangle with a point in its centre. The side length of the network is about 1.5 km. The 3D-positions of the stakes are measured by GPS in relation to a fix point on solid rock at the coast. In 2004, the research area was extended by a new deformation network (ST2). ST2 is located in latitude 69°30'28"N; longitude 49°39'09"W, ellipsoidal height 1000 m.

In case of homogenous strain the distortion of the moving network between two campaigns can be calculated by a linear affine transformation with 6 unknowns a_i, b_i:

epoch 1 --- epoch 0

$$X = a_0 + a_1 \cdot x + a_2 \cdot y \tag{1}$$
$$Y = b_0 + b_1 \cdot x + b_2 \cdot y$$

Our network has 4 stakes, so the equation system is over-determined and a least squares adjustment is applied, which gives also standard deviations in order to calculate the significance level of the results.

With (1) the normal and shear strain respectively are calculated from

$$\begin{aligned} e_{xx} &= a_1 - 1 & [\text{ ppm }] \\ e_{yy} &= b_2 - 1 & [\text{ ppm }] \\ e_{xy} &= (a_2 + b_1)/2 & [\text{ ppm }] \end{aligned} \tag{2}$$

Amount and azimuth of the principal strains e_1, e_2 are derived by

$$e = \sqrt{(e_{xx} - e_{yy})^2 + 4 \cdot e_{xy}^2}$$

$$e_1 = \frac{e_{xx} + e_{yy} + e}{2} \tag{3}$$

$$e_2 = \frac{e_{xx} + e_{yy} - e}{2}$$

and

$$\Theta_1 = \frac{1}{2} \cdot \arctan \frac{2 \cdot e_{xy}}{e_{xx} - e_{yy}}, \tag{4}$$

$$\Theta_2 = \Theta_1 \pm 100^{gon}$$

Now we apply the incompressibility condition of ice:

$e_1 + e_2 + e_3 = 0$ (5)

and then the vertical strain component e_3 becomes:

$e_3 = - (e_1 + e_2)$.   (6)

Furthermore we normalize all values on one year and calculate time derivates to get strain rates, dimensions ppm/a. In the following part the same notation for strain is now used for strain rates, too.

Together with the vertical strain rate e_3 we can derive a strain induced elevation change by:

$\Delta He = e_3 H$,   (7)

where H = ice thickness .

In reality e_3 is not constant within the whole ice column, therefore modelling the vertical strain rate dependent on depth becomes necessary. Strain is caused by velocity differences, and we assume that e_3 is varying with depth in the same way as the horizontal flow velocity U_s. Based on Glen's flow law the horizontal velocity in different depths (U_h) becomes (Paterson, 1994):

$U_h = U_s - 2A/(n+1) \cdot (\rho \cdot g \cdot \sin \alpha)^n \cdot h^{n+1}$,   (8)

with:

U_s = horizontal velocity at surface, (Swiss Camp U_s = 115 m/a);

h = depth, counted from surface h=0 until bedrock h=H;

ρ = density = 900 kg/m^3 ;

g = acceleration due to gravity = 9,81 m/s^2

n = empirically determined constant, for ice sheet usually n = 3;

α = surface slope , Swiss Camp α = 1,14 °,   sin α = 0,02

A = flow parameter, depending on ice age and temperature,

    $A = 4,9 \cdot 10^{-16}$ [s^{-1} kPa^{-3}], for T = -10°C

    $A = 2,9 \cdot 10^{-16}$ [s^{-1} kPa^{-3}], for T = -15°C.

A special investigation has shown that the depth dependent flow velocity is varying only little from the velocity at the surface, and can be taken into account by a shape factor F, (assuming the ice temperature T = - 15 °C):

Swiss Camp   :   F = 0,930 ,

ST 2   :   F = 0,995 .   (9)

Applying (9) to (7) the vertical elevation change due to strain finally becomes

$\Delta H_e = F \cdot e_3 H$.   (10)

According to Patterson (1994), the ice thickness change follows from the mass balance equation and together with (6) and (10) becomes:

$\Delta H_{surface}$ = $b - F \cdot H \cdot (e_1 + e_2)$

              = $b + F \cdot H \cdot e_3$

              = $b + \Delta H_e$ (11)

with b = net mass balance (in ice equivalent) at the research area.

The surface elevation changes were directly measured by GPS at the same stake positions as in the former campaigns (Stober and Hepperle, 2007), therefore in

(11) a term due to terrain slope is not included. With $\Delta H_{surface} = \Delta H_{GPS}$ thus the net mass balance (b) follows by

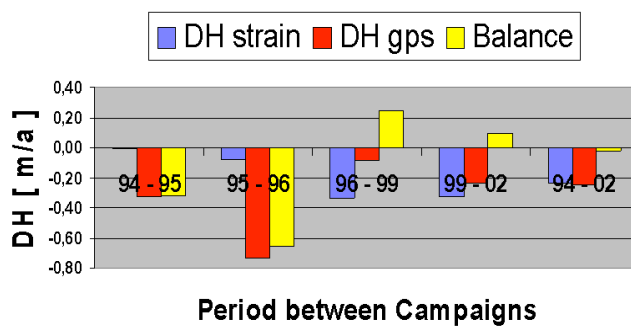$$b = \Delta H_{GPS} - \Delta h_e \ . \tag{12}$$

Results

Table 1 and figure 1 show the resulting strain rates for Swiss Camp. Except of the campaigns 1994-96, all strain rates are significant, indicating thinning due to ice outflow. The net mass balance (in ice equivalent, m/a) varies between campaigns, but is about zero for the long-term comparison 1994-2002.

Table 1. Strain rates and elevation/thickness changes at Swiss Camp 1994 – 2002.

Epochs	Azimuth Θ_1 for e_1 [gon]	Strain rates e_1 [ppm/a]	e_2 [ppm/a]	e_3 [ppm/a]	$\Delta H_e =$ $e_3 * F_{15} * H$ [m/a]	ΔH_{GPS} [m/a]	Net mass balance (b) [m/a]
1994 - 1995	29,1	927	-922	-5	-0,01	-0,33	- 0,32
1995 - 1996	25,0	924	-846	-78	-0,08	-0,74	- 0,66
1996 - 1999	20,7	1217	-890	-326	-0,33	-0,09	+ 0,25
1999 - 2002	13,5	1222	-904	-318	-0,33	-0,23	+ 0,09
1994 - 2002	19,3	1118	-894	-224	-0,23	-0,25	- 0,02

Figure 1. Net mass balance at Swiss Camp derived from GPS and strain

The results for the other research area ST2 are shown in table 2 and figure 2. This deformation network was established in 2004, so here we have only results from 2004, 2005 and 2006. Although the elevation changes by GPS are in the same magnitude as at Swiss Camp, the vertical strain rates are much larger. The resulting net mass balance (b) becomes positive with extreme high amount of +2,75 m/a ice equivalent.

Table 2. Strain rates and elevation/thickness changes at ST2 , 2004 - 2006.

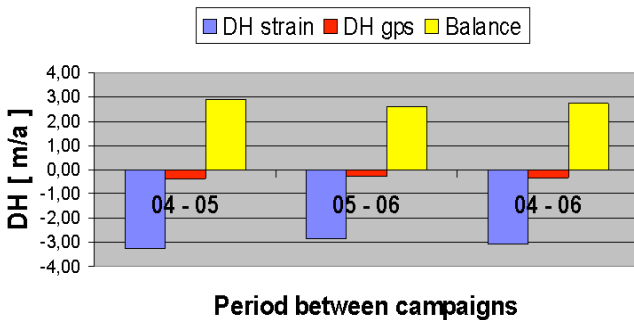| Epochs	Azimuth Θ_1 for e_1 [gon]	Strain rates e_1 [ppm/a]	e_2 [ppm/a]	e_3 [ppm/a]	$\Delta H_e =$ $e_3 * F_{15} * H$ [m/a]	ΔH_{GPS} [m/a]	Net mass balance (b) [m/a]
2004 - 2005	370,3	8548	-1951	-6597	-3,28	-0,39	2,89
2005 - 2006	369,8	8295	-2508	-5787	-2,88	-0,29	2,59
2004 - 2006	370,0	8445	-2243	-6202	-3,08	-0,34	2,75

Figure 2. Net mass balance at ST2 derived from GPS and strain.

Summary and acknowledgement

The combined evaluation of elevation changes measured by GPS and derived from horizontal strain rates seem to be an appropriate tool for the determination of the net mass balance at a certain area.

Modelling the vertical variability of flow velocity and strain rate show that at Swiss Camp the reduction in respect of the surface values does not exceed 7%.

The data of ice depth at Swiss Camp (H = 1100 m) and ST2 (H = 500 m) were kindly provided by the Alfred-Wegener-Institut, originally probably measured by the University of Kansas. The author thanks Dr. Andreas Ahlstrøm (GEUS/ Copenhagen) for intensive discussions into this topic.

References.

Paterson, W.S.B (1994): The Physics of Glaciers, 3. Edition, Pergamon Press, New York, 1994.

Stober, M. (2007): Geodetic investigations on dynamic parameters of the West Greenland inland ice. The Dynamic and Mass Budget of Arctic Glaciers. Workshop and GLACIODYN (IPY) meeting, IASC working group on Arctic Glaciology. Pontresina 15 – 18 January 2007, Institute for Marine and Atmospheric Research Utrecht, Utrecht University, 2007.

Stober, M. and Hepperle, J. (2007): Changes in Ice Elevation and Ice Flow-Velocity in the Swiss Camp Area (West Greenland) between 1991 and 2006. Polarforschung 76 (3), p. 109 – 118, 2006, released 2007.

RECENT SURGE ACTIVITY IN SOUTHERN SPITSBERGEN

MONICA SUND[1,2], TROND EIKEN[2], JON OVE HAGEN[2], ANDY KÄÄB[2], THOMAS VIKHAMAR SCHULER[2*], KARSTEN MÜLLER[2], GEIR MOHOLDT[2] AND CHRIS NUTH[2]

[1] University Centre in Svalbard
[2] Department of Geosciences, University of Oslo
[*] Now at the Norwegian Water Resources and Energy Directorate

Introduction
Surges are periods of extraordinarily enhanced glacier dynamics and show cyclic behaviour. Surges are believed to be related to internal changes in the glacier system rather than driven by external causes like changing climate (Meier and Post, 1969). However, the reoccurrence interval of surges is largely controlled by climate conditions (Harrison and Post, 2003). In Svalbard, surges constitute a common form of glacier advance (Liestøl, 1969). Glacier surges in this region are observed to have longer quiescent and active surge phases and relatively low surge velocities compared to other regions with surging glaciers. Surges in Svalbard typically have an active phase lasting up to several years and a quiescent phase of 30 to 500 years (Dowdeswell, et al., 1991). The surge mechanism itself is still object of investigation and several explanations have been proposed (Clarke, et al., 1984; Kamb, et al., 1985).

In particular, the initiation of surges is poorly studied and understood, due to the difficulty of recognizing a surge at an early stage when there is little visual evidence such as surface crevassing. The occurrence of crevasses in previously undisturbed areas is usually the first indication of a surge initiation (Hagen, et al., 1993). Currently there are indications that the initiation of surges on Svalbard may be a process lasting several years. In this contribution surface changes related to surge behaviour are presented for several glaciers in southern Spitsbergen. One of these, the ca. 9 km long valley glacier Kroppbreen in Kjellströmdalen is subject to a more detailed study.

Methods
Photos obtained on regular flights to and from Longyearbyen over several years are used in the visual search for changes of glacier surfaces. These photos and ASTER satellite images were compared to new and old maps and to 1990 aerial photos by the Norwegian Polar Institute (NPI) in order to detect new crevasses. Comparison of DTMs of 1990 by NPI, of 2003 from ASTER satellite stereo and of 2006 by Store Norske Spitsbergen Kullkompani (SNSK) is used to reveal large mass displacements. The ASTER-derived DTM was compiled using photogrammetric methods within the PCI Geomatica software (Kääb, 2002; Toutin 2002). For Kroppbreen the 2006 DTM is based on airborne LIDAR scanning, except for a small area near the front which is compiled from aerophotogrammetry for this purpose. ICESat data from 2003 – 2007 are also used for comparison to the 1990 DTM.

In April 2007 a kinematic Global Navigation Satellite System (GNSS) profile was measured along the centreline. Six stakes were also established along a longitudinal profile and measured with relative GNSS. These stakes were remeasured after 25 days and six additional stakes including a cross profile were drilled and surveyed as well. By middle of August 2007 all stakes were remeasured.

Ground Penetrating Radar (GPR) profiles were retrieved using a MALÅ 50 MHz antenna. The GPR data were sampled with a fixed time interval of 1s. The measurement interval along the transects was dependent on the snowmobile speed, ~10 km/h, and is in average about 3 m.

Results and discussion

Here we consider changes of the glaciers in the period 1990 – 2007. From the ASTER images it appears that Ingerbreen, confluencing with Richardbreen in the lower part, was in the initial stage of a surge in 2001 while the whole surface was heavily crevassed in 2005 and the surge was in the terminating phase. On several glaciers new crevasses are found on the photos taken from the scheduled flights, when compared with 1990 aerial photos.

- Mendelejevbreen showed a heavily crevassed surface from the ice divide in 2001. A drawdown of 40-50 m is found in the upper basin (Fig. 1).
- Skilfonna has a drawdown somewhat downglacier of the divide and marginal crevasses along the glacier, also transversal crevasses are observed. The major changes probably appeared during 2006.
- Zawadzkibreen experienced increased crevassing extending almost to the terminus. There are elevation losses of up to 20 m in the upper basin, with increases of ~5-10 m lower down (Fig. 1).
- On Polakkbreen there are some crevassed areas. A drawdown of up to 40 meters is experienced in the upper basin while slight thickening is seen at the confluence with Nathorstbreen (Fig. 1).
- Dobrowolskibreen has crevasses with enhanced marginal crevassing over the entire glacier, but not as heavy as that observed on Skobreen in 2005.
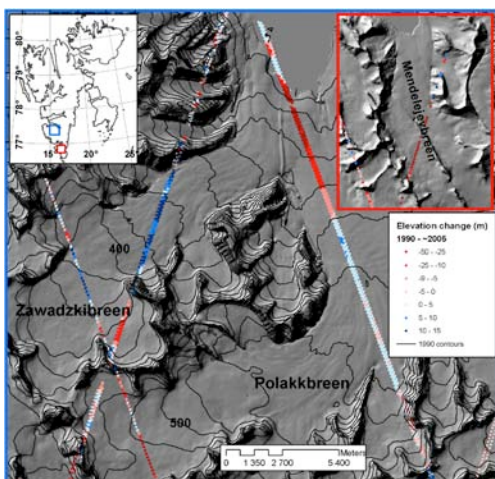

Figure 1. ICESat data (2003-2007) compared with the 1990 DTM. Both Zawadzkibreen and Polakkbreen experience elevation losses in the upper part, while an increasing elevation is observed in the lower part, especially on Zawadzkibreen. Mendelejevbreen shows elevation losses in the upper regions.

On Kroppbreen, we found a build up in the upper part and surface lowering of the lower part over the period 1936 – 1990. For the period 1990 – 2006 a surface lowering in upper part and thickening in central part is observed (Fig. 2a). This is similar to the development of Skobreen in the period 1990 – 2003 (Fig. 2b), which had proceeded to a fully developed surge (Sund, 2006). Similar changes have also been mapped on Hessbreen (Liestøl, 1976) prior to its surge (Sund and Eiken, 2004). Kroppbreen has developed large crevasses in the upper part since 1990, while smaller, and marginal crevasses characterize the surface of the lower part. Measurements of stake displacement indicate that currently the velocity magnitude are greatest where the ice has thickened and further indicate block flow across the transversal profile. GPR measurements on Kroppbreen strongly indicate that the lowermost part of the glacier consists of cold ice.

On Kroppbreen, Zawadzkibreen and Polakkbreen the changes cannot yet be observed at the terminus. This indicates that during the development of the surge the mass displacement is limited to a part of the glacier only

On Mendelejevbreen, Ingerbreen, Skobreen and Skilfonna the surge activities have reached all the way to the terminus. It is also observed that some glaciers, like Søkkbreen and Knoppbreen, previously only underwe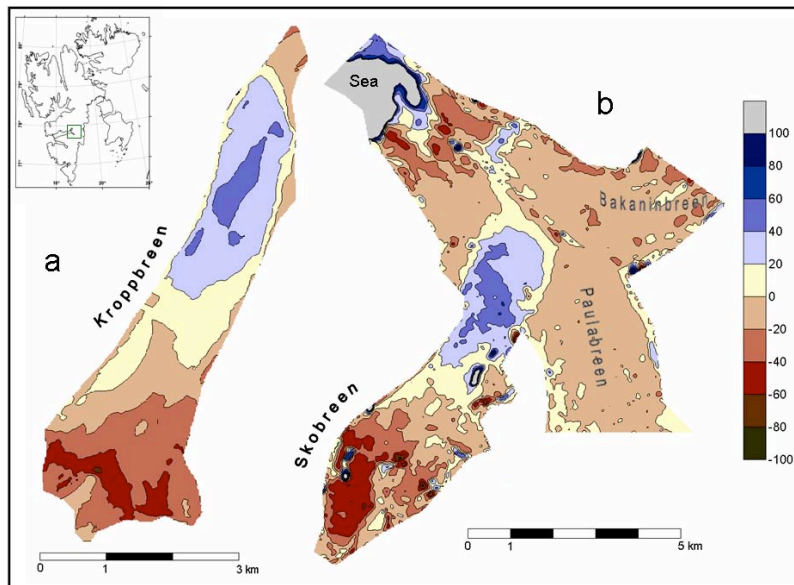nt a partial surge that declined downglacier. On Mendelejevbreen, Ingerbreen, Skobreen and Skilfonna the surge activities have reached all the way to the terminus. It is also observed that some glaciers, like Søkkbreen and Knoppbreen, previously only underwent a partial surge that declined downglacier.

Figure 2. a) Surface elevation changes of Kroppbreen over 1990-2006 showing a lowering in the upper part and increase of ice thickness in the central part. b) Surface elevation changes of Skobreen over 1990-2003 reveal a lowering of the upper part and a mass displacement to the lower part at the junction to Paulabreen.

Concurrent to enhanced crevassing, also a surface lowering in the upper part and thickening in the lower part is found at several of the glaciers. GPR and velocity data from Kroppbreen indicate that cold ice at the front is damming up the temperate ice upglacier. There may be also a possible effect on subglacial water drainage, such that thermal damming of water at the front eventually leads to increased subglacial water pressures in the area upglacier. Increased subglacial water pressure in turn lead to an enhanced sliding motion of the glacier (e.g. Iken and Bindschadler, 1986)

We have detected changes in the surface texture of several glaciers on Svalbard during recent years (since ~2000). A comparison of elevation data revealed considerable mass displacements downglacier on these glaciers relative to 1990. Recently enhanced crevassing of previously undisturbed areas indicates changes in the dynamics of the respective glaciers. The downglacier thickening in conjunction to thinning of the upglacier areas as observed at Kroppbreen, Zawadzkibreen and Polakkbreen are typical for geometry changes during a surge. Based on the experience from previous surges of Hessbreen and Skobreen, we interpret our observations at a number of glaciers as indicative of an early phase of a possible surge activity. Some glaciers have shown only a partial surge before the activity declined. We believe that not all surges have to be large and spectacular, but mass displacements still can have characteristics of a surge. This implies that there is a broad range of surge-like behaviour governing the dynamics of Svalbard glaciers.

Acknowledgement

References

Clarke, G. K. C. , Collins, S. G. and Thompson, D. E. 1984. Flow, thermal structure and subglacial conditions of a surge-type glacier. Canadian Journal of Earth Science. 21(2), 232-240.

Dowdeswell, J. A. Hamilton, G. S. and Hagen J. O. 1991. The duration of the active phase on surge-type glaciers: contrasts between Svalbard and other regions. Journal of Glaciology 37 (127), 388-400.

Hagen, J. O., Liestøl, O. Rolan, E. and Jørgensen, T. 1993. Glacier Atlas of Svalbard and Jan Mayen. Norsk Polarinstitutt Meddelelser 129.

Harrison, W. D. and Post, A. S. 2003. How much do we really know about glacier surging? Annals of Glaciology 36, 1-6.

Iken, A. and Bindschadler, R.A. 1986. Combined measurements of subglacial water pressure and surface velocity of Findelengletscher, Swizerland: conclusions about drainage system and sliding mechanism. Journal of Glaciology, 32(110): 101-119.

Kamb, B. and 7 others. 1985. Glacier surge mechanism: 1982-1983 surge of Variegated Glacier, Alaska. Science 227 (4686), 469-479.

Kääb, A. 2002. Monitoring high-mountain terrain deformation from repeated air- and spaceborne optical data: examples using digital aerial imagery and ASTER data. ISPRS Journal of Photogrammetry & Remote sensing 57(1-2), 39-52.

Liestøl, O. 1969. Glacier surges in West-Spitsbergen. Canadian Journal of Earth Science 6, 895-897.

Liestøl, O. 1976.Glaciological work in 1974. Norsk Polarinstitutt Årbok 1974. 191-193.

Meier, M. F. and Post, A. 1969. What are glacier surges? Canadian Journal of Earh Sciences 6, 8907-817.

Sund, M. 2006. A surge of Skobreen. Polar Research 25(2), 115-122.

Sund, M and Eiken, T. 2004. Quiescent –phase dynamics and surge history of a polythermal glacier: Hessbreen, Svalbard. Journal of Glaciology 50 (171), 547-555.

Toutin, T. 2002. Three-dimensional topographic mapping with ASTER stereo data in rugged topography. IEEE Transactions on geoscience and remote sensing 40(19), 2241-2247.

Glaciological and Meteorological observations in Suntar-Khayata Range, Eastern Siberia, in 2004-2007

Shuhei Takahashi[1], Konosuke Sugiura[2], Takao Kameda[1], Hiroyuki Enomoto[1], Yury Kononov[3] and Maria D. Ananicheva[3]

[1] Kitami Institute of Technology, Koencho 165, Kitami 165, Japan
[2] JAMSTEC, IORGC, Natsusima-cho, Yokosuka, Japan
[3] Geographical Institute, Russian Academy of Sciences, Moscow, Russia

IGY and IPY activities in Suntar-Khayata

In the IGY (International Geophysical Years: 1956/57), the Russian Academy has made extensively glaciological researches in Suntar-Khayata Range in Eastern Siberia, in which about 180 glaciers were numbered. Especially No. 31 Glacier was precisely studied; a meteorological station was constructed and lots of glaciological data were acquired through three whole years. After the IGY, however, almost no observations were done in this area except getting aerial-photo and satellite images.

In 2004-2005, meteorological observations were done in this area as an activity of IPY (International Polar Year). Meteorological instruments were installed at the former IGY station at the terminus of Glacier No. 31 in Suntar- Khayata Range and at several points around Oimiyakon area. In 2006-2007, also 13 thermometers were placed along Kolima Street from Magadan to Oimiyakon to study the temperature distribution around this area (Fig. 1).
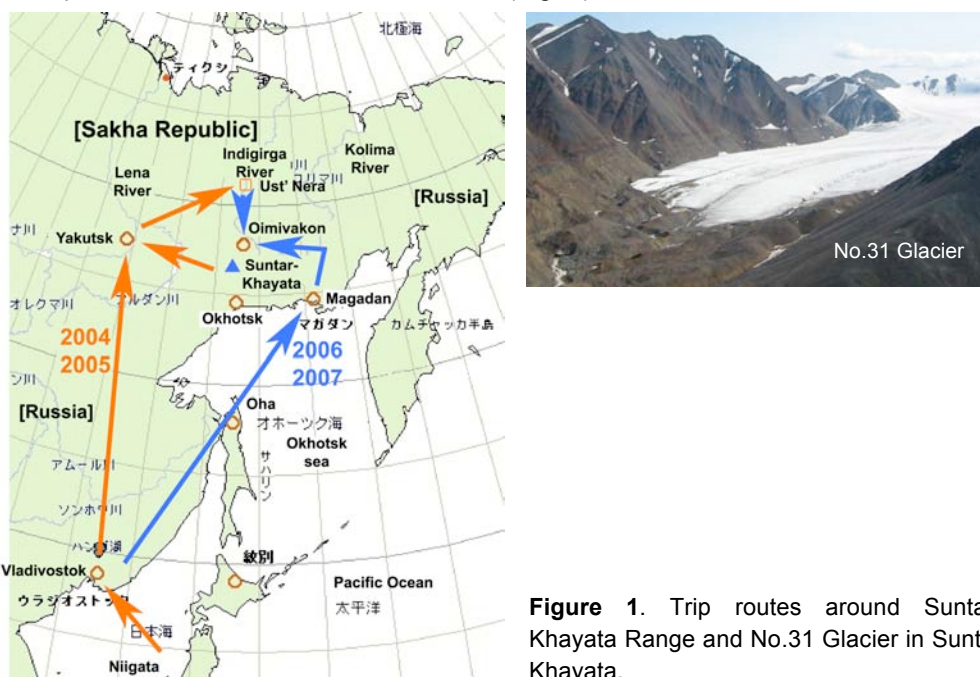

Figure 1. Trip routes around Suntar-Khayata Range and No.31 Glacier in Suntar Khayata.

2004-2005 Activities around Suntar-Khayata

In July to August, 2004, Meteorological instruments (temperature, wind speed, wind direction, solar radiation) were installed at Oimiyakon (Fig. 2), and at No. 31 Glacier in Suntar Khayata (Fig. 3). 13 thermometers were set along a road from Oimiyakon to Tomtor and around No. 31 Glacier to observe temperature distribution.

The meteorological instruments installed in 2004 were recovered in September 2005. Almost all instruments survived, though several thermometers along the road between Onimiyakon and Tomtor were lost.

Figure 2. Memorial tower of Coldness Pole in Oimiyakon The plate explains that -72 C was recorded in 1924.

Figure 3. Meteorological station at No.31 Glacier. Thermometer, anemometer, solar radiation meter and snow-depth camera were installed.

The minimum temperature over a year was -59°C at Oimiyakon (about 680 m a.s.l.), where it is called "Pole of Cold", and -45°C at Glacier No. 31 (about 2050 m a.s.l.) (Fig.4), which suggests there was strong temperature-inversion in this area in the period of Siberia high pressure in winter.
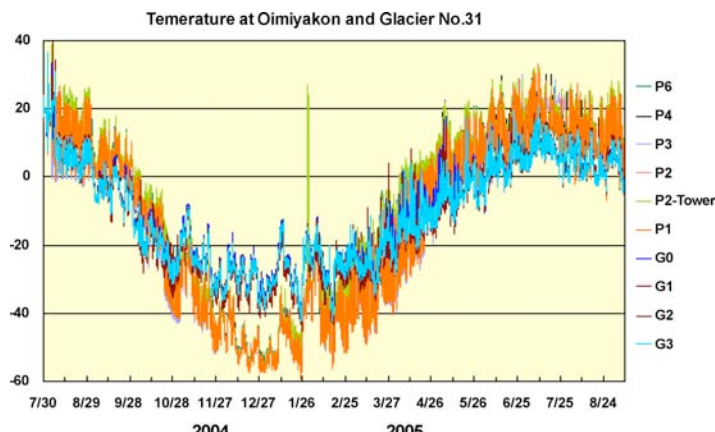

Figure 4. Temperature at Oimiyakon (P1-P6) and No.31 Glacier (G0-G3). The minimum temperature was -59.2°C (P1) in Oimiyakon area and -45.0°C (G1) at No.31 Glacier area.
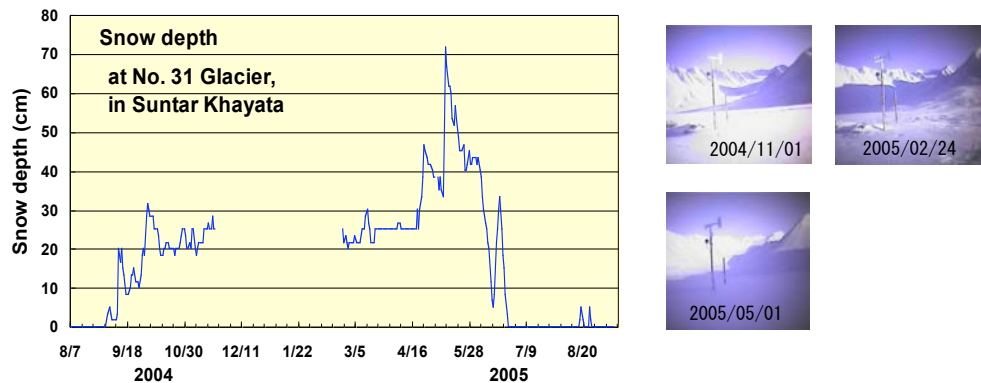
Figure 5. Snow accumulation by interval camera. Snow accumulation variation (left) and photos of a snow stake (right). Accumulation period was 2004/09/03- 2005/06/27 and the maximum depth was 72 cm on 2005/05/11.

Snow depth was observed at 3-hour interval digital images of snow stakes, by which the variation of snow accumulation was obtained (Fig. 5). By this data, snow accumulation period was 2004/09/03-2005/06/27 and the maximum snow accumulation was 72 cm on 2005/05/11.

A feature of the snow accumulation is that the snow depth increased in October, at the beginning of winter, was almost zero in winter, and increased again in the end of winter. It can be explained as water vapour could not be supplied during the Siberia high-pressure in winter but before/after the winter the atmosphere disturbance brought water vapour to this area.

2006-2007 Activities along Kolima Street

In September in 2006, thermometers and simple rain-gauges were set along a way from Magadan to Oimiyakon (Kolima Street) at interval of about 100 km (Fig. 6). To observe sea ice development at the north end of Okhotsk Sea, a interval camera was set at Magadan sea shore.

Figure 6. Boarder of Sakha Republic and Kolima aria on a way from Magadan to Oimiyakon
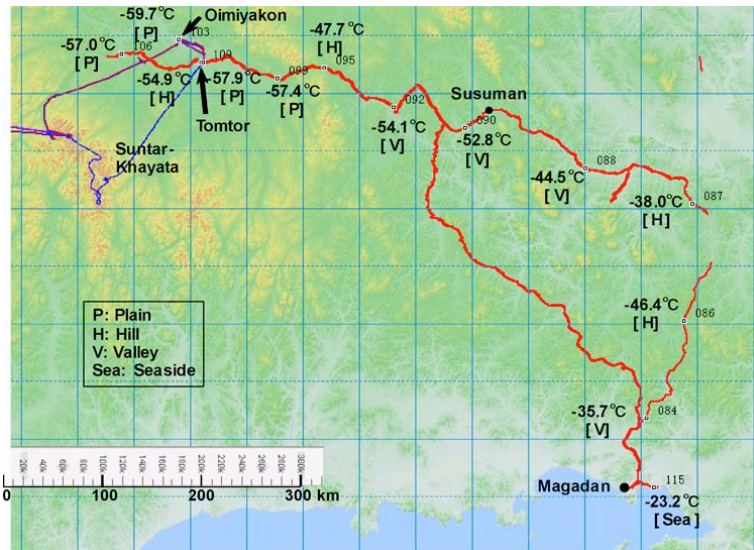
Figure 7. Location of thermometers and the minimum temperature of each place [P] means thermometer was set at plain, [H] at hill, [V] at valley and [Sea] at sea shore.

In Fig. 7 the location of thermometers and the minimum temperature of each place is shown. The minimum temperature in 2007 was below -50°C in inner region and -59.7°C at Oimiyakon, while higher at coastal region, -23.2°C at Magadan. From the records of temperature, the temperature at Oimiyakon was below -50°C from December to February, but higher than that of Magadan in summer.

Results

In Oimiyakon area, strong temperature inversion appears in winter. The minimum temperature was -59 oC at Oimiyakon (about 680 m a.s.l.) and -45 oC at Glacier No. 31 (about 2050 m a.s.l.). Along a route from Magadan to Oimiyakon, the coldest place was Oimiyakon. The minimum temperature was -59.7 oC at Oimiyakon, while -23.2 oC at Magadan.

125

PRELIMINARY RESULTS OF GIS-BASED SOLAR RADIATION MODEL FOR HORNSUND AREA, SW SPITSBERGEN

M. SZYMANOWSKI[1], M. KRYZA[1], K. MIGAŁA[1], P. SOBOLEWSKI[2] AND L. KOLONDRA[3]

[1] University of Wrocław
[2] Institute of Geophysics Polish Academy of Sciences
[3] Silesian University

Introduction
GIS-based, solar radiation model is a useful tool to evaluate diversity of glaciological, geomorphologic and biological processes. Results in elementary form allow to recognize the local climate diversity and its ranges or to identify cold/warm sub-areas formed by radiation balance and affected by relief. The model can also be applied to identify local surfaces with daily thaw/freeze cycles.

Model outlook
The "r.sun" model is applied here to calculate daily sums of direct, diffuse and total "clear-sky" solar radiation (direct + diffuse) (Hofierka 1997, Šuri and Hofierka 2004). The "r.sun" is one of the most developed solar models, which eliminates numerous drawbacks existed in the well-known commercial modules. The model is implemented in the GIS-GRASS system, that is Open Source GIS software used in the project.

The "r.sun" can be used in two modes: (1) to calculate the instantaneous radiation, and (b) to calculate daily/monthly sums of radiation. The first mode is used to validate the model against the measurements. The second mode is used here to calculate the spatial patterns of the solar radiation for the study area.

Input data
The model requires only a few mandatory input parameters:
- Digital elevation model (DEM; 10m resolution) based on the source data of the orthophotomap 1:25 000 „Werenskioldbreen and surrounding areas" (© Norsk Polarinstitutt and Silesian University). DEM, besides elevation, allows to calculate surface inclination, orientation and shadows;
- Astronomical factors (solar constant, declination, latitude, solar hour angle);
- Atmospheric attenuation (scattering, absorption) by gases in clear and dry (Rayleigh) atmosphere (relative optical air mass and optical thickness) and by solid and liquid particles (water vapour and aerosols) described by Linke turbidity factor (LTF). The LTF expresses a relation between the beam and diffuse radiation – the higher the LTF, the higher the diffuse component of the total radiation flux.

The obtained results (model) are planned to be validated against actinometrical data form the Polish Polar Station, Hornsund.

Results

As an example, few details can be introduced basing on the monthly mean total solar radiation in June (Figure 1):

- Not evident differentiation of solar energy income on the glaciers, ranges only between 300 and 350 W/m^2, e.g. Hans Glacier (H) and Werenskiold Glacier (W).
- Evidently colder slopes, predisposed for long lasting snow cover (NW – NE slopes with monthly mean total radiation < 250 W/ m^2)
- Evidently colder, southern-orientated, small and narrow valleys, e.g. Arie Valley with cold-ice glacier, with mean monthly total radiation flux: 200-300 W/m^2 (marked with white circle on the Figure 1).
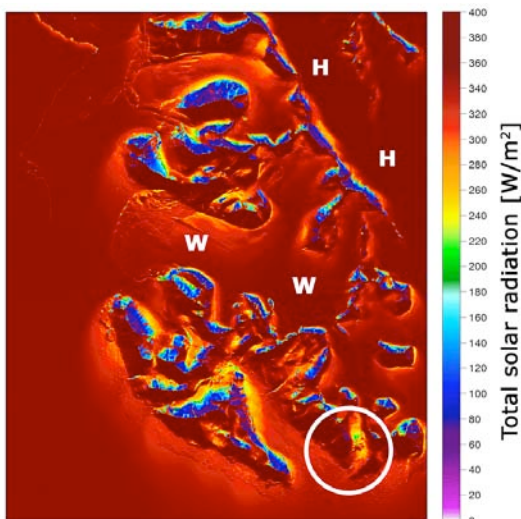
Figure 1. Mean monthly total solar radiation flux [W/m^2] under clear sky conditions in June (Wedel Jarlsberg Land, SW Spitsbergen): H – Hans Glacier, W – Werenskiold Glacier, white circle – Arie Valley.

Spatial distribution of solar energy income in the close vicinity of Polish Polar Station (Hornsund) modelled in hourly intervals for mid-August, leads to the conclusion that "r.sun" model gives a possibility to:

- Indicate thaw/freeze cycles zones and zones with more intensive weathering;
- Identify glacier's parts with different dynamics of daily outflow of ablation water and parts with decreased ablation;
- Simulate 24–hour cycle of water outflow intensity.

It should be stressed that multi-year daily mean of air temperature at the Polish Polar Station varies in the first half of August between 4,4°C and 5,2°C; with mean daily minimum between 0,3°C and 3,4°C (1988-2007). The analysis of hourly radiation indicates that freeze/thaw cycles on the southern slopes occur frequently (Figures 2 and 3). In the mid-day under clear sky conditions, southern slopes of the ridges (Ariekammen and Fugleberget) receive 50-100% more solar energy (650-750 W/m^2) if compared with the coastal areas (350-450 W/m^2). Outgoing radiation starts to dominate on the slopes after 18:00 LSoT, while the coastal plain still receives 150-200 W/m^2 (Figure 3). The process extends on all the area after 20:00 LSoT. It means that all processes concerned with heating, water flow from melting snow patches and from the melted active layer of permafrost etc. are reduced to

minimum. In consequence, a short-time freezing starts, in higher elevations mostly. Not before 04:00 LSoT solar radiation starts to warm the coastal plain with the intensity of c.a. 50 W/m^2.
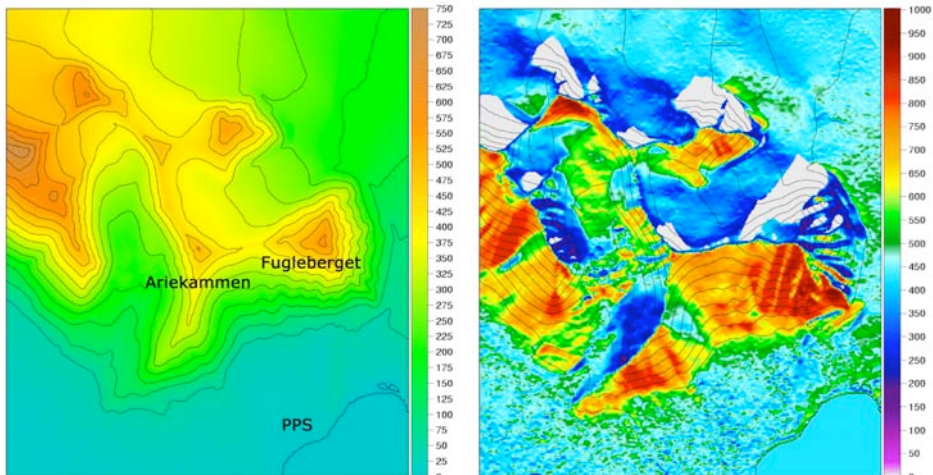

Figure 2. Orography in the vicinity of Polish Polar Station, Hornsund (left) and hourly mean values of beam solar radiation flux [W/m^2] under clear sky conditions at 13:00 LSoT,15 of August (right).
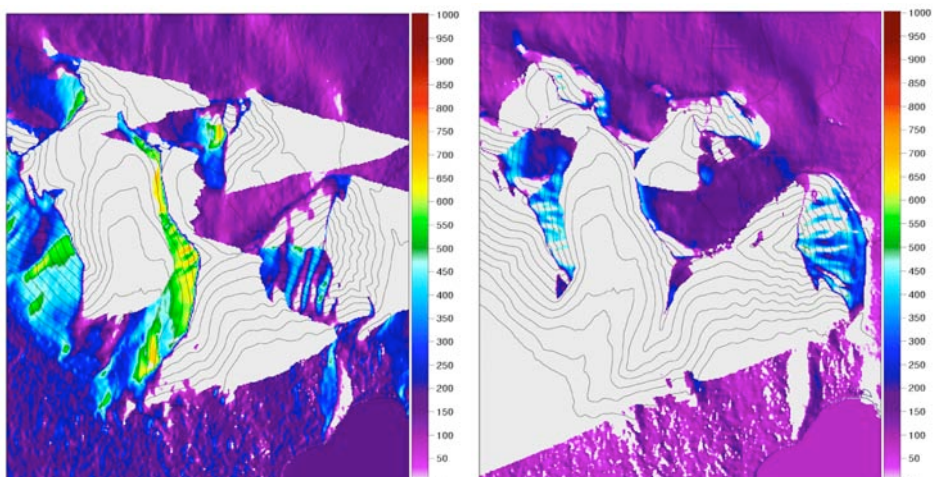

Figure 3. Hourly mean of beam solar radiation flux [W/m^2] under clear sky conditions at 18:00 LSoT (left) and at 04:00 LSoT (right), 15 of August.

References

Hofierka, J., 1997. Direct solar radiation modelling within an open GIS environment. Proceedings of JEC-GI'97 conference in Vienna, Austria, IOS Press Amsterdam: 575-584.

Šuri M, Hofierka J., 2004. A New GIS-based Solar Radiation. Model and Its pplication to Photovoltaic Assessments, Transactions in GIS 8 (2): 175-190

OBSERVATION AND MODELLING OF THE SURFACE ENERGY BALANCE IN THE ABLATION ZONE OF THE WEST GREENLAND ICE SHEET

MICHIEL VAN DEN BROEKE, PAUL SMEETS, JANNEKE ETTEMA, RODERIK VAN DE WAL, JOHANNES OERLEMANS

Institute for Marine and Atmospheric Research Utrecht, Utrecht University

The surface energy balance (SEB) determines the surface temperature T_s of any natural surface as well as the amount of melt of snow and ice surfaces, when T_s has reached the melting point. The SEB is given by:

$$M = R_{net} + SHF + LHF + G_s \tag{1}$$

In which M is the energy available for melting, $R_{net} = SW_{net} + LW_{net}$ is net absorbed radiation, i.e. the sum of net shortwave radiation and net longwave radiation, SHF and LHF are the turbulent fluxes of sensible and latent heat, respectively, and G_s is the subsurface heat flux evaluated at the surface.
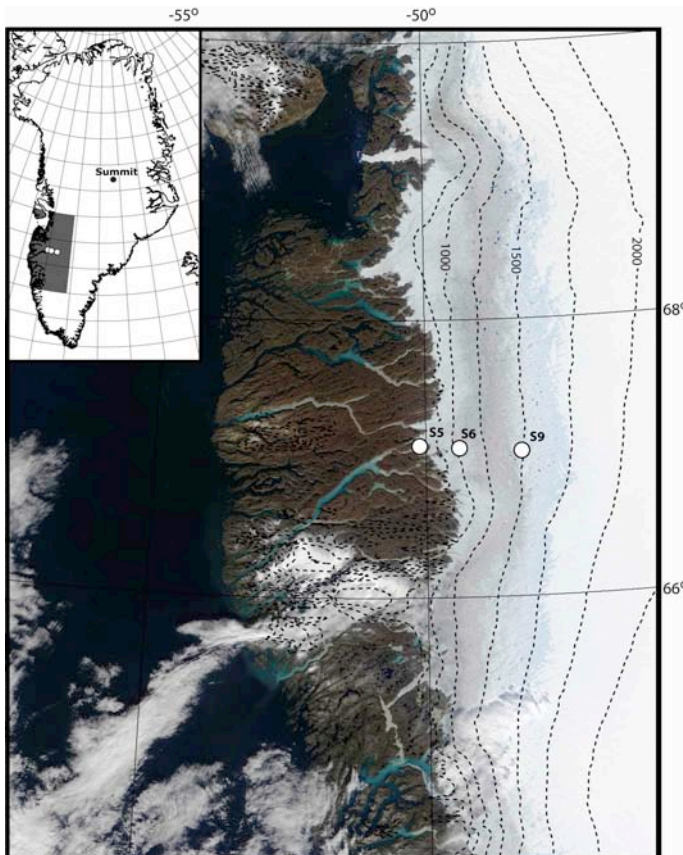

Figure 1. Locations of the AWS used in this study.

Four years (August 2003-August 2007) of meteorological observations along the K-transect, a mass balance stake array along the 67°N latitude circle in west Greenland, have been collected using three automatic weather stations (AWS). The AWS are located at 6, 38 and 88 km from the ice sheet margin at elevations of 490, 1020 and 1520 m asl (Fig. 1). This part of Greenland is characterized by an approximately 150 km wide tundra, an ablation zone that extends 100 km onto the ice sheet, and an equilibrium line at 1500 m asl. After elaborate data quality checks and corrections, the hourly AWS data are fed into a surface energy balance (SEB) model that iteratively solves for surface temperature T_s. If T_s rises above the melting point of ice, it is reset to 0°C and excess energy fluxes are invested in ice melting (M).
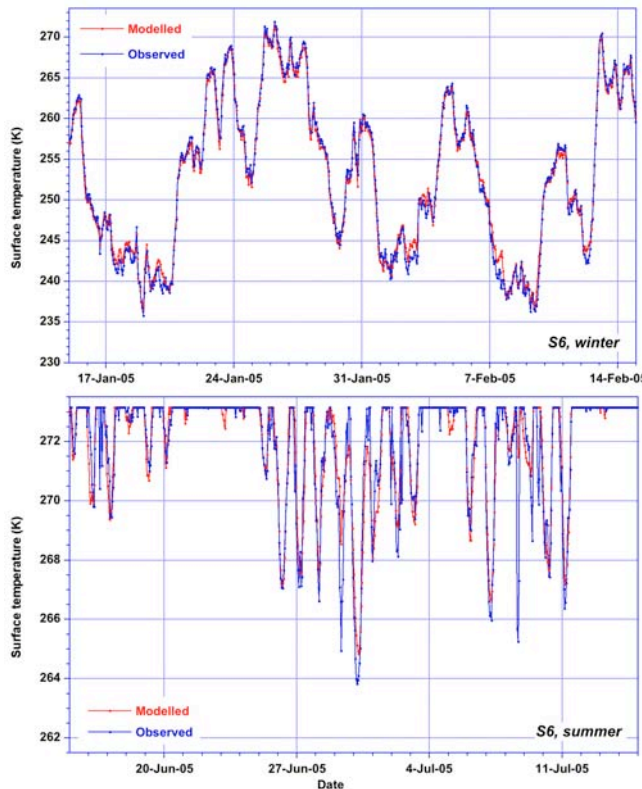

Figure 2. Observed and modelled surface temperature T_s for a 2005 winter month (top) and summer month (bottom) at S6.

To check model performance, modelled T_s is compared to an observed value derived from outgoing longwave radiation measurements, using Stefan Boltzmann's law and assuming the surface to have unit longwave emissivity. Figure 2a shows the good agreement that is found for a 2005 winter month at S6, with differences between observed and modelled Ts generally smaller than 1 °C, in spite of interdiurnal temperature changes in excess of 25 °C. In summer, nocturnal longwave radiative losses are almost always too great to sustain nocturnal melting

at S6, and surface refreezing occurs. Fig. 2b shows that this nocturnal refreezing of the surface is well captured by the SEB model, as is the daily melt duration at S6.

Now that the SEB has been validated, we can confidently study its various components. Figure 3 gives an example for a winter and summer month at S5. In the absence of shortwave radiation and melt, and with moisture concentrations and hence LHF generally small, the main wintertime SEB is a balance between negative LW_{net} and positive SHF, i.e. longwave cooling of the surface is compensated by a downward turbulent transport of sensible heat, heating the surface and cooling the air. Under clearsky, strong (katabatic) wind conditions, this sensible heat transport easily exceeds 100 W m^{-2}, remarkably large values under statically stable conditions that can only be maintained by surface radiative cooling in combination with strong wind shear.
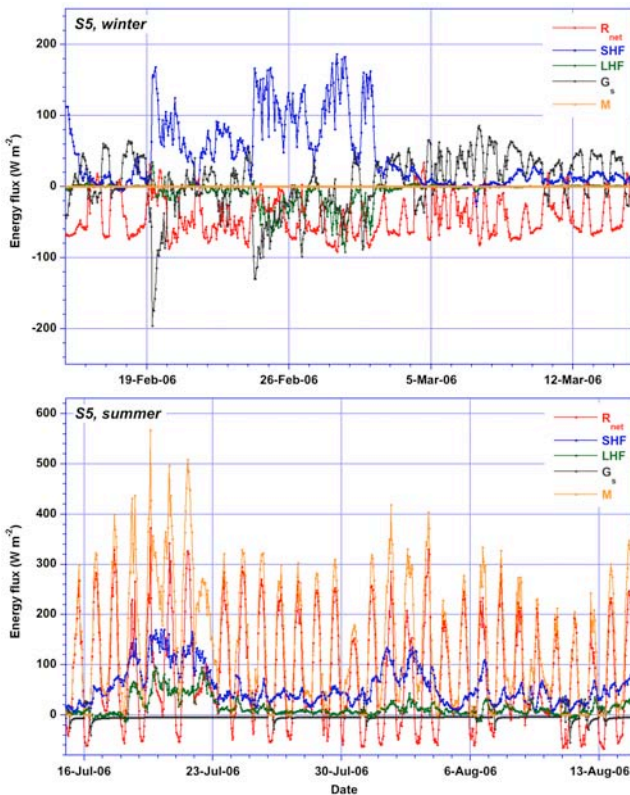

Figure 3. Modelled components of the surface energy balance (SEB) at S5 for a 2006 winter month (top) and summer month (bottom).

Under strongly non-stationary conditions, e.g. when cloudiness suddenly increases and longwave cooling ceases, the subsurface heat flux becomes important to transport heat away from the surface, as happens on 19 February 2006. When, on the other hand, under clearsky conditions the sensible heat flux ceases, for instance due to a lack of wind, the subsurface heat flux starts transporting heat towards the surface from the deeper ice/snow layers, to compensate the longwave cooling. Only when temperatures rise high enough, can sublimation (green line) become a significant surface heat loss in wintertime.

A very different SEB is calculated for the summer (Fig. 3b). SHF is still directed downwards, because the surface cannot further increase its temperature. Because the melting surface cannot further increase its water vapour pressure either, LHF is now also positive. Daytime R_{net} is dominated by absorption of shortwave radiation, longwave cooling occurs at night. The sub surface heat flux G_s is small, in reaction to small temperature gradients in the ice. The result is that the melt flux M attains considerable values in excess of 300-400 W m^{-2} at daytime, with a very pronounced daily cycle. For most of the nights, however, summertime melting at S5 continues. These results will be used to validate regional climate models. Once agreement is sufficient, these models will be used to calculate melt over the entire Greenland ice sheet.

LARGE AND RAPID VARIABILITY IN THE VELOCITY IN THE ABLATION ZONE OF THE GREENLAND ICE SHEET

R.S.W. V.D. WAL, W. BOOT, M.R. VAN DEN BROEKE, P. SMEETS, C.H. REIJMER, J.J.A. DONKER AND J. OERLEMANS

Institute for Marine and Atmospheric Research Utrecht, Utrecht University

Abstract

GPS observations show very rapid and large fluctuations along the K-transect in the ablation zone of the Greenland ice sheet. The velocity of the ice sheet nearly instantaneously reacts on increased production of melt water, and velocities increase with a factor four within days, which is much stronger and much faster than previously reported. The increase coincides with increased ablation rates indicating that surface water penetrates through ice layers of 500-1000 m thick within days, which is faster than expected from glaciological theory. At the bottom increased water pressure causes acceleration of the flow. On a longer time scale, 15 years, velocities decrease only slightly, implying that the englacial system adjusts very rapidly to the variable water input in the system maintaining a more or less constant ice flux. Here we show that despite the rapid fluctuations on short time scales, mean velocities are driven by slow changes in slope and thickness.